



MINISTÉRIO DA CIÊNCIA, TECNOLOGIA, INOVAÇÕES E COMUNICAÇÕES  
**INSTITUTO NACIONAL DE PESQUISAS ESPACIAIS**

sid.inpe.br/mtc-m21c/2018/06.19.19.59-TDI

## APPLICATIONS OF SOLAR RADIATION PRESSURE IN ORBITAL MANEUVERS

Geraldo Magela Couto Oliveira

Doctorate Thesis of the Graduate Course in Space Engineering and Technology, guided by Drs. Antonio Fernando Bertachini de Almeida Prado, and Diogo Merguizo Sanchez, approved in June 22, 2018.

URL of the original document:

<<http://urlib.net/8JMKD3MGP3W34R/3RATMEE>>

INPE  
São José dos Campos  
2018

**PUBLISHED BY:**

Instituto Nacional de Pesquisas Espaciais - INPE

Gabinete do Diretor (GBDIR)

Serviço de Informação e Documentação (SESID)

CEP 12.227-010

São José dos Campos - SP - Brasil

Tel.:(012) 3208-6923/7348

E-mail: pubtc@inpe.br

**COMMISSION OF BOARD OF PUBLISHING AND PRESERVATION  
OF INPE INTELLECTUAL PRODUCTION (DE/DIR-544):****Chairperson:**

Dr. Marley Cavalcante de Lima Moscati - Centro de Previsão de Tempo e Estudos Climáticos (CGCPT)

**Members:**

Dra. Carina Barros Mello - Coordenação de Laboratórios Associados (COCTE)

Dr. Alisson Dal Lago - Coordenação-Geral de Ciências Espaciais e Atmosféricas (CGCEA)

Dr. Evandro Albiach Branco - Centro de Ciência do Sistema Terrestre (COCST)

Dr. Evandro Marconi Rocco - Coordenação-Geral de Engenharia e Tecnologia Espacial (CGETE)

Dr. Hermann Johann Heinrich Kux - Coordenação-Geral de Observação da Terra (CGOBT)

Dra. Ieda Del Arco Sanches - Conselho de Pós-Graduação - (CPG)

Silvia Castro Marcelino - Serviço de Informação e Documentação (SESID)

**DIGITAL LIBRARY:**

Dr. Gerald Jean Francis Banon

Clayton Martins Pereira - Serviço de Informação e Documentação (SESID)

**DOCUMENT REVIEW:**

Simone Angélica Del Ducca Barbedo - Serviço de Informação e Documentação (SESID)

André Luis Dias Fernandes - Serviço de Informação e Documentação (SESID)

**ELECTRONIC EDITING:**

Marcelo de Castro Pazos - Serviço de Informação e Documentação (SESID)

Murilo Luiz Silva Gino - Serviço de Informação e Documentação (SESID)



MINISTÉRIO DA CIÊNCIA, TECNOLOGIA, INOVAÇÕES E COMUNICAÇÕES  
**INSTITUTO NACIONAL DE PESQUISAS ESPACIAIS**

sid.inpe.br/mtc-m21c/2018/06.19.19.59-TDI

## APPLICATIONS OF SOLAR RADIATION PRESSURE IN ORBITAL MANEUVERS

Geraldo Magela Couto Oliveira

Doctorate Thesis of the Graduate Course in Space Engineering and Technology, guided by Drs. Antonio Fernando Bertachini de Almeida Prado, and Diogo Merguizo Sanchez, approved in June 22, 2018.

URL of the original document:

<<http://urlib.net/8JMKD3MGP3W34R/3RATMEE>>

INPE  
São José dos Campos  
2018

Cataloging in Publication Data

---

Oliveira, Geraldo Magela Couto.

Ol4a Applications of solar radiation pressure in orbital maneuvers / Geraldo Magela Couto Oliveira. – São José dos Campos : INPE, 2018.

xxii + 133 p. ; (sid.inpe.br/mtc-m21c/2018/06.19.19.59-TDI)

Thesis (Doctorate in Space Engineering and Technology) – Instituto Nacional de Pesquisas Espaciais, São José dos Campos, 2018.

Guiding : Drs. Antonio Fernando Bertachini de Almeida Prado, and Diogo Merguizo Sanchez.

1. Astrodynamics. 2. Orbital maneuvers. 3. Solar radiation pressure. 4. Asteroid system. 5. Lagrange points. I.Title.

CDU 629.7.017.3:551.521.1

---



Esta obra foi licenciada sob uma Licença [Creative Commons Atribuição-NãoComercial 3.0 Não Adaptada](https://creativecommons.org/licenses/by-nc/3.0/).

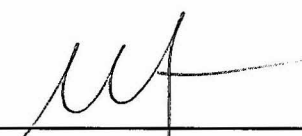
This work is licensed under a [Creative Commons Attribution-NonCommercial 3.0 Unported License](https://creativecommons.org/licenses/by-nc/3.0/).

Aluno (a): **Geraldo Magela Couto Oliveira**

Título: "APPLICATIONS OF SOLAR RADIATION PRESSURE IN ORBITAL MANEUVERS"

Aprovado (a) pela Banca Examinadora  
em cumprimento ao requisito exigido para  
obtenção do Título de **Doutor(a)** em  
**Engenharia e Tecnologia Espaciais/Mecânica  
Espacial e Controle**

Dr. Mario Cesar Ricci

  
\_\_\_\_\_  
Presidente / INPE / SJCampos - SP

( ) Participação por Vídeo - Conferência

Dr. Antonio Fernando Bertachini de  
Almeida Prado

  
\_\_\_\_\_  
Orientador(a) / INPE / SJCampos - SP

( ) Participação por Vídeo - Conferência

Dr. Diogo Merguizo Sanchez

  
\_\_\_\_\_  
Orientador(a) / INPE / São José dos Campos - SP

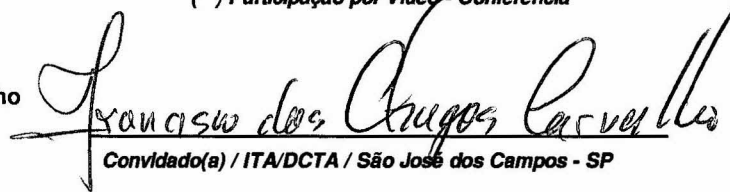
( ) Participação por Vídeo - Conferência

Dra. Vivian Martins Gomes

  
\_\_\_\_\_  
Orientador(a) / UNESP/FEG / Guaratinguetá - SP

( ) Participação por Vídeo - Conferência

Dr. Francisco das Chagas Carvalho

  
\_\_\_\_\_  
Convidado(a) / ITA/DCTA / São José dos Campos - SP

( ) Participação por Vídeo - Conferência

Este trabalho foi aprovado por:

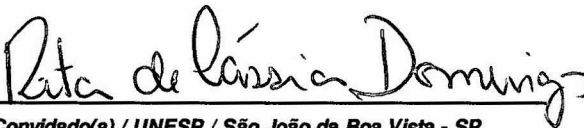
( ) maioria simples

unanimidade

São José dos Campos, 22 de junho de 2018

Aprovado (a) pela Banca Examinadora  
em cumprimento ao requisito exigido para  
obtenção do Título de **Doutor(a)** em  
**Engenharia e Tecnologia Espaciais/Mecânica  
Espacial e Controle**

Dra. Rita de Cássia Domingos



Convidado(a) / UNESP / São João da Boa Vista - SP

( ) Participação por Vídeo - Conferência

**Este trabalho foi aprovado por:**

( ) maioria simples

unanimidade

**São José dos Campos, 22 de junho de 2018**

*"Oh, the depth of the riches of the wisdom and knowledge of God!  
How unsearchable his judgments,  
and his paths beyond tracing out!  
Who has known the mind of the Lord?  
Or who has been his counselor?  
Who has ever given to God,  
that God should repay them?  
For from him and through him and for him are all things.  
To him be the glory forever! Amen."*

HOLY BIBLE  
Romans 11:33-36



*I dedicate this work to **God**  
to whom I owe everything I am.*



## ACKNOWLEDGEMENTS

I would like to thank:

**GOD** that gave me understanding to accomplish this work.

My advisors, **Bertachini, Diogo** and **Vivian** for the constant support and encouragement. Thank you for the guidance and advice given in difficult times and that made me feel more confident.

My wife **Fanny** for support and encouragement.

My daughter **Maria Julia** by his constant affection and smile.

My parents **Dirceu** and **Terezinha** who always supported me in my studies, allowing me to get where I arrived.

Allan with whom I studied at many times.

My family who always encouraged and supported me.

The friends of the INPE Astrodynamics group who contributed with their friendship and words of encouragement.

The Federal Center for Technological Education of Minas Gerais (CEFET-MG) for the resources made available to this work.

The National Institute for Space Research (INPE).



# APLICAÇÕES DA PRESSÃO DE RADIAÇÃO SOLAR EM MANOBRAS ORBITAIS

## RESUMO

São estudados os efeitos da pressão de radiação solar nas trajetórias de uma espaçonave em transferências orbitais. Em um sistema formado por pequenos corpos, a pressão de radiação solar tem influência significativa nos caminhos dessas transferências. Isso ocorre porque as forças gravitacionais nesses sistemas são menores se comparadas aos sistemas formados por corpos maiores. Soluções com menor e maior consumo de combustível podem ser encontradas adicionando a pressão de radiação solar. A pressão de radiação solar não é usada como controle, mas seus efeitos sobre as transferências são medidos e utilizados de forma natural para obter transferências mais econômicas. Para um sistema de primários com pouca massa, como asteroides, foi descoberto que é muito importante levar isso em conta para garantir que a espaçonave alcance os pontos desejados dentro dos respectivos sistemas.

Palavras-chave: Astrodinâmica. Manobras orbitais. Pressão de radiação solar. Sistema de asteroides. Pontos de Lagrange.



## ABSTRACT

The effects of the solar radiation pressure in the trajectories of a spacecraft in orbital transfers are studied. In a system formed by small bodies, the solar radiation pressure has a significant influence in the transfer paths. This occurs because the gravitational forces in these systems are smaller, if compared with systems formed by larger bodies. Solutions with lower and higher fuel consumption can be found by adding the solar radiation pressure. The solar radiation pressure is not used as a control but its effects over the transfers are measured and used in a natural form to get more economical transfers. For a small system of primaries such as an asteroid system, it was found that is very important to take into account this to make sure that the spacecraft will reach the desired points in the respective systems.

Keywords: Astrodynamics. Orbital maneuvers. Solar radiation pressure. Asteroid system. Lagrange points.



## LIST OF FIGURES

	<u>Page</u>
1.1 Artist rendering of the Genesis spacecraft during collection phase of mission. . . . .	3
1.2 Hayabusa final inspection. . . . .	4
1.3 Solar-sailing IKAROS in the interplanetary field, captured by a deployable camera on June 14th, 2010. . . . .	5
1.4 Solar sail deployment sequence. . . . .	6
1.5 IKAROS in the final assembly phase and one of the four petals of the sail flight model. . . . .	7
1.6 External view of the Hayabusa 2 spacecraft. . . . .	8
2.1 Bi-impulsive transfer between the Lagrange points $L_1$ and $L_3$ . . . . .	15
2.2 Schematic example of the shooting method. . . . .	17
2.3 Flight path angle ( $fpa$ ). . . . .	18
3.1 Location of the Lagrangian points and the primaries. . . . .	19
3.2 Reference frame in the planar circular restricted three-body problem. . . . .	21
3.3 Transfers from $L_1$ and $L_2$ . . . . .	24
3.4 Transfers from $L_1$ to $L_3$ . . . . .	25
3.5 Transfers from $L_2$ to $L_3$ . . . . .	26
3.6 Transfers from $L_3$ to $L_1$ . . . . .	27
3.7 Transfers from $L_1$ to the Earth. . . . .	28
3.8 Transfers from $L_2$ to the Earth. . . . .	29
3.9 Transfers from $L_3$ to the Earth. . . . .	30
3.10 Transfers from $L_4$ to the Earth. . . . .	31
3.11 Transfers from $L_5$ to the Earth. . . . .	32
3.12 Transfers from $L_1$ to $L_2$ . . . . .	34
3.13 Transfers from $L_2$ to $L_1$ . . . . .	35
3.14 Transfers from $L_1$ to $L_3$ . . . . .	36
3.15 Transfers from $L_3$ to $L_1$ . . . . .	37
3.16 Transfers from $L_1$ to the Earth. . . . .	38
3.17 Transfers from $L_2$ to the Earth. . . . .	39
3.18 Transfers from $L_3$ to the Earth. . . . .	40
3.19 Transfers from $L_4$ to the Earth. . . . .	41
3.20 Transfers from $L_5$ to the Earth. . . . .	42
3.21 Representation of the triple system 2001SN263. . . . .	43
3.22 Reference frame in the planar circular restricted three-body problem. . . . .	44

3.23	Transfers from $L_1$ to $L_2$ , asteroid at apoapsis. . . . .	46
3.24	Transfers from $L_1$ to $L_2$ , asteroid at periapsis. . . . .	47
3.25	Transfers from $L_2$ to $L_1$ , asteroid at apoapsis. . . . .	48
3.26	Transfers from $L_2$ to $L_1$ , asteroid at periapsis. . . . .	48
3.27	Trajectories between the collinear Lagrangian points, asteroid at periapsis.	49
3.28	Transfers from $L_1$ to Beta, asteroid at apoapsis. . . . .	50
3.29	Transfers from $L_1$ to Beta, asteroid at periapsis. . . . .	50
3.30	Transfers from $L_2$ to Beta, asteroid at apoapsis. . . . .	51
3.31	Transfers from $L_2$ to Beta, asteroid at periapsis. . . . .	52
3.32	Trajectories between the collinear Lagrangian points to Beta, asteroid at periapsis. . . . .	52
3.33	Transfers from $L_1$ to $L_3$ with the asteroid at periapsis and excluding the solar radiation pressure. . . . .	57
3.34	Trajectories from $L_1$ to $L_3$ for $\Delta v_{min}$ and $\Delta v_{max}$ . . . . .	58
3.35	$L_1$ to $L_3$ , $A/m = 0.02 \text{ m}^2/\text{kg}$ . . . . .	59
3.36	$L_1$ to $L_3$ , $A/m = 0.1 \text{ m}^2/\text{kg}$ . . . . .	60
3.37	$L_1$ to $L_3$ , $A/m = 0.5 \text{ m}^2/\text{kg}$ . . . . .	60
3.38	Transfer from $L_3$ to $L_1$ with the asteroid at periapsis and excluding the solar radiation pressure . . . . .	62
3.39	Trajectories from $L_3$ to $L_1$ for $\Delta v_{min}$ and $\Delta v_{max}$ . . . . .	63
3.40	$L_3$ to $L_1$ , $A/m = 0.02 \text{ m}^2/\text{kg}$ . . . . .	64
3.41	$L_3$ to $L_1$ , $A/m = 0.1 \text{ m}^2/\text{kg}$ . . . . .	64
3.42	$L_3$ to $L_1$ , $A/m = 0.5 \text{ m}^2/\text{kg}$ . . . . .	65
3.43	Transfers from $L_1$ to $L_3$ with the asteroid at periapsis of its orbit. . . . .	67
3.44	Transfers from $L_1$ to $L_3$ with the asteroid at periapsis of its orbit. . . . .	68
3.45	Transfers from $L_1$ to $L_3$ with the asteroid at periapsis of its orbit. . . . .	69
3.46	Transfers from $L_3$ to $L_1$ with the asteroid at periapsis of its orbit. . . . .	72
3.47	Transfers from $L_3$ to $L_1$ with the asteroid at periapsis of its orbit. . . . .	73
3.48	Transfers from $L_3$ to $L_1$ with the asteroid at periapsis of its orbit. . . . .	74
4.1	Reference frame in the circular restricted three-body problem. . . . .	79
4.2	Possible AEPs to place a stationary spacecraft around Ida in the Sun-Ida system above and below the ecliptic. . . . .	81
4.3	The AEPs around the Lagrange point $L_1$ . . . . .	84
4.4	The AEPs around the Lagrange point $L_2$ . . . . .	84
4.5	Trajectories from A to B. . . . .	89
4.6	Transfers from A to B. . . . .	90
4.7	Trajectories from C to D. . . . .	92
4.8	Transfers from C to D. . . . .	93
4.9	Trajectories from $L_1$ to A. . . . .	96

4.10	Transfers from $L_1$ to A. . . . .	97
4.11	Trajectories from $L_1$ to C. . . . .	99
4.12	Transfers from $L_1$ to C. . . . .	100
4.13	Trajectories from $L_2$ to A. . . . .	102
4.14	Transfers from $L_2$ to A. . . . .	103
4.15	Transfers from $L_2$ to C. . . . .	106
5.1	Asteroid and Earth orbits in a fixed inertial system fixed in the Sun. . .	111
5.2	Trajectories of the asteroid and the spacecraft for a 30 days transfer. . .	112
5.3	Trajectories of the asteroid and the spacecraft for a 60 days transfer. . .	113
5.4	Trajectories of the asteroid and the spacecraft for a 90 days transfer. . .	113
5.5	Trajectories of the asteroid and the spacecraft for a 120 days transfer. . .	114
5.6	Trajectories of the asteroid and the spacecraft for a 150 days transfer. . .	115
5.7	Trajectories of the asteroid and the spacecraft for a 180 days transfer. . .	116
5.8	Trajectories of the asteroid and the spacecraft for a 210 days transfer. . .	116
5.9	Trajectories of the asteroid and the spacecraft for a 240 days transfer. . .	117
5.10	Trajectories of the asteroid and the spacecraft for a 270 days transfer. . .	117
5.11	Trajectories of the asteroid and the spacecraft for a 300 days transfer. . .	118
5.12	Trajectories of the asteroid and the spacecraft for a 330 days transfer. . .	118
5.13	Trajectories of the asteroid and the spacecraft for a 360 days transfer. . .	119



## LIST OF TABLES

	<u>Page</u>
3.1 Parameters of the Earth-Moon system. . . . .	22
3.2 Canonical system of units for the Earth-Moon system. . . . .	22
3.3 Lagrange points and primaries of the Earth-Moon system. . . . .	22
3.4 Parameters for $L_1$ and $L_2$ . . . . .	23
3.5 Parameters for $L_1$ and $L_3$ . . . . .	24
3.6 Parameters for $L_2$ and $L_3$ . . . . .	25
3.7 Parameters for $L_3$ and $L_1$ . . . . .	26
3.8 Parameters for $L_1$ and the Earth. . . . .	27
3.9 Parameters for $L_2$ and the Earth. . . . .	28
3.10 Parameters for $L_3$ and the Earth. . . . .	29
3.11 Parameters for $L_4$ and the Earth. . . . .	30
3.12 Parameters for $L_5$ and the Earth. . . . .	31
3.13 Parameters of the Sun-Earth system. . . . .	33
3.14 Canonical system of units for the Sun-Earth system. . . . .	33
3.15 Lagrange points and primaries of the Sun-Earth system. . . . .	33
3.16 Parameters for $L_1$ and $L_2$ . . . . .	34
3.17 Parameters for $L_2$ and $L_1$ . . . . .	35
3.18 Parameters for $L_1$ and $L_3$ . . . . .	36
3.19 Parameters for $L_3$ and $L_1$ . . . . .	36
3.20 Parameters for $L_1$ and the Earth. . . . .	38
3.21 Parameters for $L_2$ and the Earth. . . . .	38
3.22 Parameters for $L_3$ and the Earth. . . . .	39
3.23 Parameters for $L_4$ and the Earth. . . . .	40
3.24 Parameters for $L_5$ and the Earth. . . . .	41
3.25 Parameters of the 2001SN263 system. . . . .	45
3.26 Canonical system of units for the 2001SN263 system. . . . .	45
3.27 Lagrange points and primaries of the 2001SN263 system. . . . .	45
3.28 Parameters for $L_1$ and $L_2$ . . . . .	46
3.29 Parameters for $L_2$ and $L_1$ . . . . .	47
3.30 Parameters for $L_1$ and Beta. . . . .	49
3.31 Parameters for $L_2$ and Beta. . . . .	51
3.32 Parameters of the 1996FG3 system. . . . .	54
3.33 Canonical system of units for the binary asteroid 1996FG3. . . . .	55
3.34 Lagrange points and primaries of the 1996FG3 system. . . . .	55
3.35 Minimum distances from $L_3$ . . . . .	61

3.36	Minimum distances from $L_1$ . . . . .	66
3.37	1996FG <sub>3</sub> at periapsis, $L_1$ to $L_3$ . . . . .	70
3.38	1996FG <sub>3</sub> at periapsis, $L_3$ to $L_1$ . . . . .	75
3.39	1996FG <sub>3</sub> at periapsis, $L_1$ to $L_2$ . . . . .	76
3.40	1996FG <sub>3</sub> at periapsis, $L_2$ to $L_1$ . . . . .	76
3.41	1996FG <sub>3</sub> at periapsis, $L_2$ to $L_3$ . . . . .	76
3.42	1996FG <sub>3</sub> at periapsis, $L_3$ to $L_2$ . . . . .	77
4.1	Parameters of the Sun-Ida system. . . . .	83
4.2	Canonical system of units for the Sun-Ida system. . . . .	83
4.3	Parameters for the equilibrium points . . . . .	86
4.4	Transfers from A to B . . . . .	91
4.5	Transfers from C to D . . . . .	94
4.6	Transfers from $L_1$ to A . . . . .	98
4.7	Transfers from $L_1$ to C . . . . .	101
4.8	Transfers from $L_2$ to A . . . . .	104
4.9	Transfers from $L_2$ to C . . . . .	105
5.1	Parameters of the Sun-Earth system. . . . .	109
5.2	Canonical system of units for the Sun-Earth system. . . . .	109
5.3	Distances between the Earth and the asteroid 1996FG <sub>3</sub> . . . . .	111
5.4	Initial and final $\Delta V$ with $A/m = 0 \text{ m}^2/kg$ for transfers between the Earth and the asteroid 1996FG <sub>3</sub> in the approach of 03-05-2022 . . . . .	120
5.5	Initial and final $\Delta V$ with $A/m = 0.1 \text{ m}^2/kg$ for transfers between the Earth and the asteroid 1996FG <sub>3</sub> in the approach of 03-05-2022 . . . . .	121
5.6	Initial and final $\Delta V$ with $A/m = 0.5 \text{ m}^2/kg$ for transfers between the Earth and the asteroid 1996FG <sub>3</sub> in the approach of 03-05-2022 . . . . .	121
5.7	Initial and final $\Delta V$ with $A/m = 5 \text{ m}^2/kg$ for transfers between the Earth and the asteroid 1996FG <sub>3</sub> in the approach of 03-05-2022 . . . . .	122
5.8	Initial and final $\Delta V$ with $A/m = 0 \text{ m}^2/kg$ for transfers between the Earth and the asteroid 1996FG <sub>3</sub> in the approach of 01-02-2024 . . . . .	122
5.9	Initial and final $\Delta V$ with $A/m = 0 \text{ m}^2/kg$ for transfers between the Earth and the asteroid 1996FG <sub>3</sub> in the approach of 01-04-2024 . . . . .	123
5.10	Initial and final $\Delta V$ with $A/m = 0 \text{ m}^2/kg$ for transfers between the Earth and the asteroid 1996FG <sub>3</sub> in the approach of 01-08-2029 . . . . .	123

# CONTENTS

	<u>Page</u>
<b>1 INTRODUCTION</b> . . . . .	<b>1</b>
1.1 Missions overview . . . . .	2
1.2 Organization of the present thesis . . . . .	9
<b>2 METHODOLOGY</b> . . . . .	<b>11</b>
2.1 Solar radiation pressure . . . . .	11
2.2 The circular restricted three-body problem . . . . .	13
2.3 Orbital maneuvers . . . . .	14
2.4 Two Point Boundary Value Problem . . . . .	16
<b>3 ORBITAL TRANSFERS BETWEEN THE LANGRANGE POINTS AND THE PRIMARIES</b> . . . . .	<b>19</b>
3.1 Earth-Moon system . . . . .	21
3.2 Sun-Earth system . . . . .	32
3.3 2001SN263 system . . . . .	42
3.4 1996FG3 system . . . . .	53
<b>4 LOCATING AND PERFORMING TRANSFERS FOR ARTIFI- CIAL EQUILIBRIUM POINTS IN A SUN-ASTEROID SYSTEM</b> <b>79</b>	
4.1 Methodology . . . . .	81
4.1.1 Artificial equilibrium points . . . . .	81
4.1.2 Transfers between the AEPs . . . . .	85
4.1.3 Solar sail configuration . . . . .	86
4.2 Results . . . . .	88
4.2.1 Transfer from <i>AEP A</i> to <i>B</i> . . . . .	88
4.2.2 Transfer from <i>AEP C</i> to <i>D</i> . . . . .	92
4.2.3 Transfer from $L_1$ to <i>AEP A</i> . . . . .	95
4.2.4 Transfer from $L_1$ to <i>AEP C</i> . . . . .	98
4.2.5 Transfer from $L_2$ to <i>AEP A</i> . . . . .	101
4.2.6 Transfer from $L_2$ to <i>AEP C</i> . . . . .	105
<b>5 MAPPING TRAJECTORIES FOR A SPACECRAFT TO HIT AN ASTEROID TO AVOID A COLLISION WITH THE EARTH</b> <b>107</b>	

5.1 Methodology . . . . .	108
5.2 Results . . . . .	110
<b>6 CONCLUSIONS . . . . .</b>	<b>125</b>
<b>REFERENCES . . . . .</b>	<b>127</b>

## 1 INTRODUCTION

In recent years, the interest in asteroids and comets has increased, since they are the direct remnants of the original building blocks of the Solar system. Knowledge of their nature is fundamental to understanding the early stage of solar system evolution, formation process of the planets and the origin of life. They are also a new frontier for space exploration, which can be used to demonstrate the key technologies for a round-trip mission with low cost. Furthermore, as there are many NEOs (Near Earth Objects), which are considered hazardous body against human civilization (CARUSI et al., 2002; IZZO, 2005) and, as a threat, it is important to understand their nature and establish new technologies to reach them. Another key point to its exploration is economical, the search for natural resources. A NEO could be a possible body for supplying natural resources in space, making it so important to develop methods to collect materials for future utilization.

It can be noticed that several missions have been proposed for these bodies in recent years, such as: NEAR Shoemaker (PROCKTER et al., 2002), Solar Power Sail (KAWAGUCHI, 2004), Dawn (RAYMAN et al., 2006), Hayabusa (KAWAGUCHI et al., 2006), Rosetta (GLASSMEIER et al., 2007), Aster mission (SUKHANOV et al., 2010), Hayabusa 2 (TSUDA et al., 2013a), ARM (MAZANEK et al., 2013; STRANGE et al., 2013), MarcoPolo-R (MICHEL et al., 2014) and OSIRIS-Rex (GAL-EDD; CHEUVRONT, 2015).

Because those bodies have high eccentricities, they have periapsis near the Sun and more distant apoapsis, so the influence of the solar radiation pressure on the probes of these missions may become relevant. In addition, with the wide range of asteroid-Sun distances covered during an orbital period, the dynamics become more complex.

In two of the missions mentioned above, Aster and MarcoPolo-R, the proposed target is a system of asteroids, which allows these missions to explore and study various bodies in a single mission. In order to extend the duration of the mission and to reduce the fuel consumed, it is important to study the behavior of the probe during the orbital maneuvers in such systems.

Previous works considered the problem of orbital maneuvers between the equilibrium Lagrange points of the Sun-Earth system (BROUCKE, 1979), the Earth-Moon system (PRADO, 1996; OLIVEIRA et al., 2016) and Sun-Earth-Moon system (CABETTE; PRADO, 2008). In a recent work Yang et al. (2015), the problem of orbital transfers connecting equilibrium points of irregular-shaped asteroids were studied. It was con-

sidered only the gravity of the asteroid in their dynamics. The perturbations from the gravity of the Sun and the planets were considered very small compared with the mass-point gravitational forces of the asteroids. It was not considered the case when the asteroid is very close to a planet.

Beyond the effects of the gravity that were used in previous publications, in this work the effects of the solar radiation pressure on such transfers is taken into account. The objective is to demonstrate that the solar radiation pressure must be considered when performing maneuvers under the conditions mentioned above, otherwise the spacecraft will not reach the desired points.

It is also suggested that, by changing the area/mass ratio of the spacecraft and the distance to the Sun, it is possible to observe the importance and the influence of this effect over the trajectories. In these missions the solar radiation pressure has a significant contribution to the dynamics and can not be neglected. These type of missions constitutes an important justification for the accomplishment of this work. Some missions with the characteristics mentioned above have already been carried out or are in progress. The next section discuss about some of these missions.

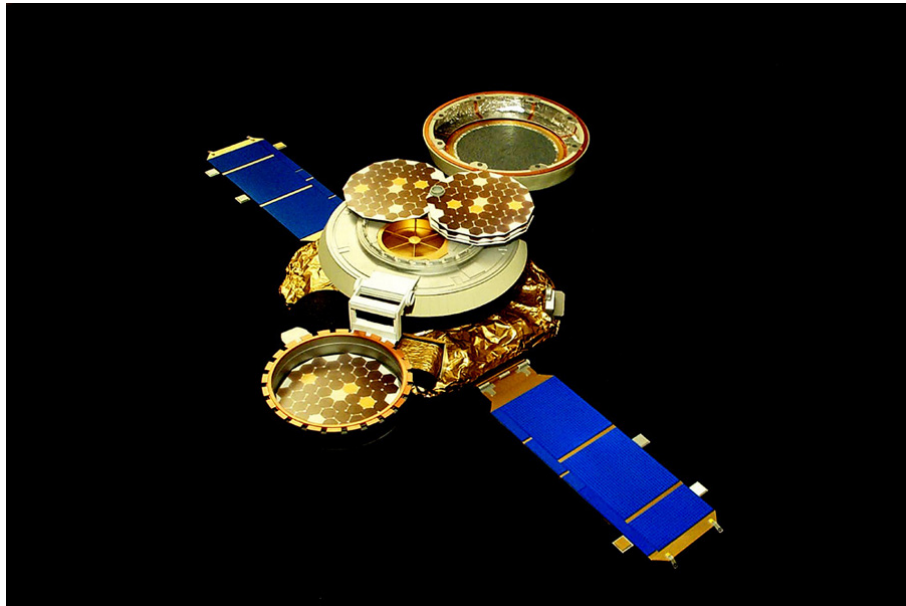
## 1.1 Missions overview

The American mission Genesis (LO et al., 1998) is an example of an accomplished mission for the collection of solar wind samples and return them to Earth for study. It was launched in August 2001 and returned to the Earth in September 2004 with particles from the Sun. It was the NASA's first sample return mission since the final Apollo lunar mission in 1972, and the first to collect material beyond the Moon. The type of spacecraft designed for this type of mission necessarily have a very high area/mass ratio due to the presence of the particle collector. Figure 1.1 shows an artist rendering of the Genesis spacecraft during collection phase of mission<sup>1</sup>.

---

<sup>1</sup><https://genesismission.jpl.nasa.gov/>

Figure 1.1 - Artist rendering of the Genesis spacecraft during collection phase of mission.



SOURCE: NASA/JPL-Caltech (2009)

Some missions have been also tested the application of the solar radiation pressure. The American mission Messenger (O'SHAUGHNESSY et al., 2014), launched in August 2004 to Mercury, used the solar radiation pressure on its solar panels to perform path corrections on the way to Mercury. The probe reached the planet in January 2008. By changing the angle of the solar panels relative to the Sun, several planned thruster firings en route to Mercury were unnecessary, because these fine course adjustments were performed using solar radiation pressure acting on Messenger's solar panels.

The Japanese mission Hayabusa (KAWAGUCHI et al., 2006; YOSHIKAWA et al., 2006), from the Japanese Aerospace Exploration Agency (JAXA), was launched in May 2003 to collect a surface sample of material from the small asteroid Itokawa (1998 SF36) and then return with samples to the Earth for analysis. In November 2005, it landed on the asteroid and collected samples in the form of tiny grains of asteroidal material, which were returned to Earth aboard the spacecraft on June 2010. This spacecraft had a box-shaped main body and two solar panel wings with a total array area of  $12 \text{ m}^2$ . The launched mass was 510 kg, which gives an area/mass ratio of  $0.023 \text{ m}^2/\text{kg}$ . Figure 1.2 shows the final inspection view of the spacecraft.

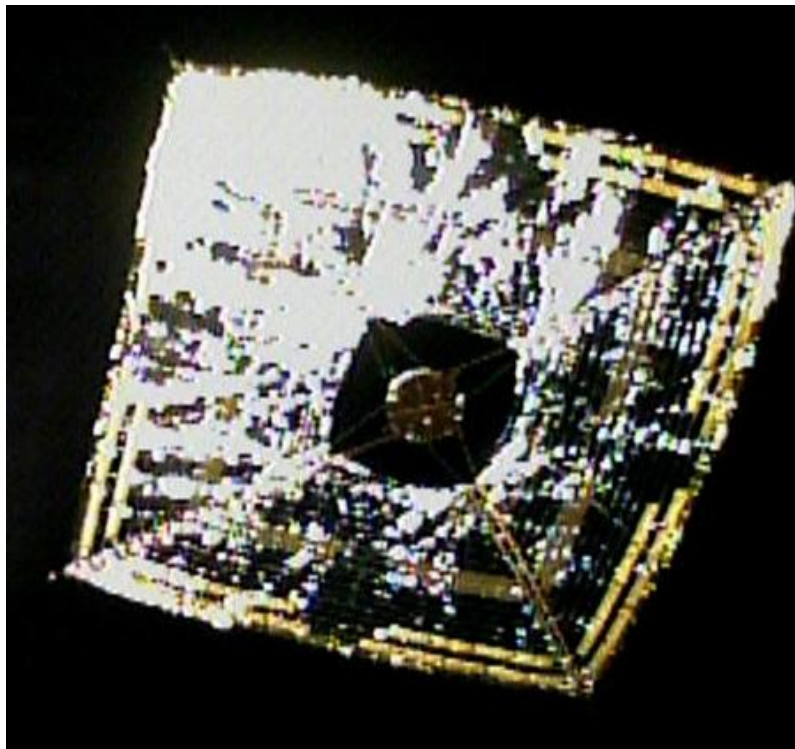
Figure 1.2 - Hayabusa final inspection.



SOURCE: Kawaguchi et al. (2006)

In addition to the first Hayabusa mission, JAXA has sent, in May 2010, the IKAROS (Interplanetary Kite-craft Accelerated by Radiation Of the Sun) (TSUDA et al., 2013a) probe to Venus and tested, for the first time, the concept of solar sail in an interplanetary mission. Figure 1.3 shows IKAROS in the interplanetary field. The image was acquired by a tiny camera ejected from the central hub of IKAROS.

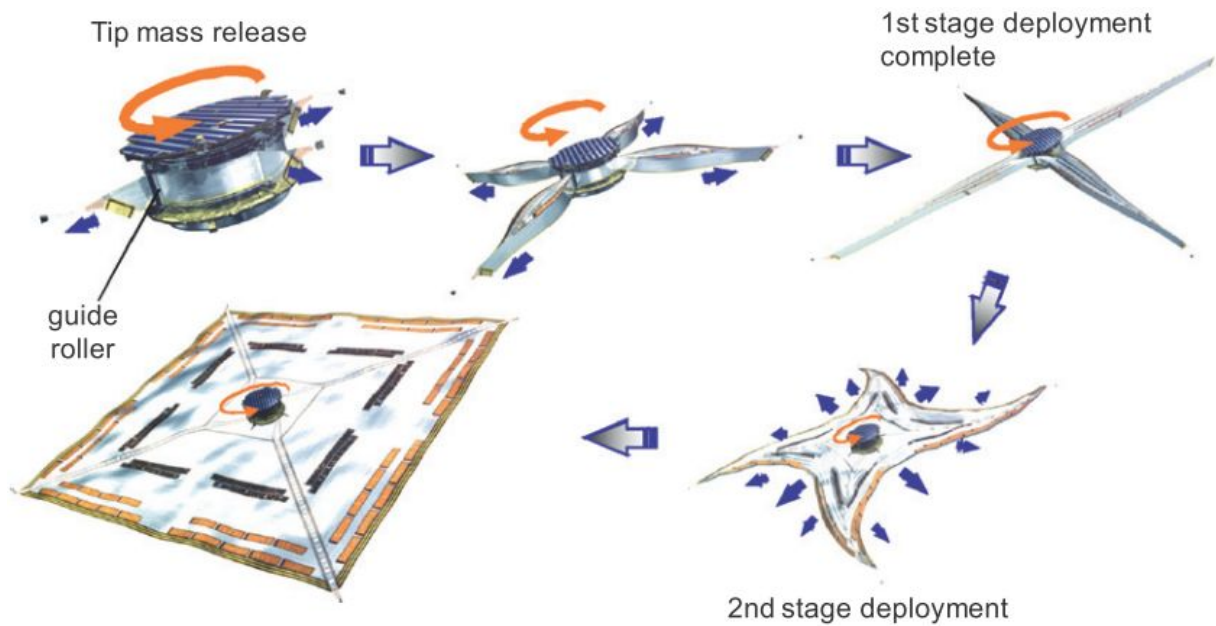
Figure 1.3 - Solar-sailing IKAROS in the interplanetary field, captured by a deployable camera on June 14th, 2010.



SOURCE: Tsuda et al. (2013a)

Its main body is a spinner and the shape is simply cylindrical, and taking advantage of centrifugal force, the main body extends a square membrane sail. Figure 1.4 summarizes the solar sail deployment sequence.

Figure 1.4 - Solar sail deployment sequence.



SOURCE: Tsuda et al. (2013a)

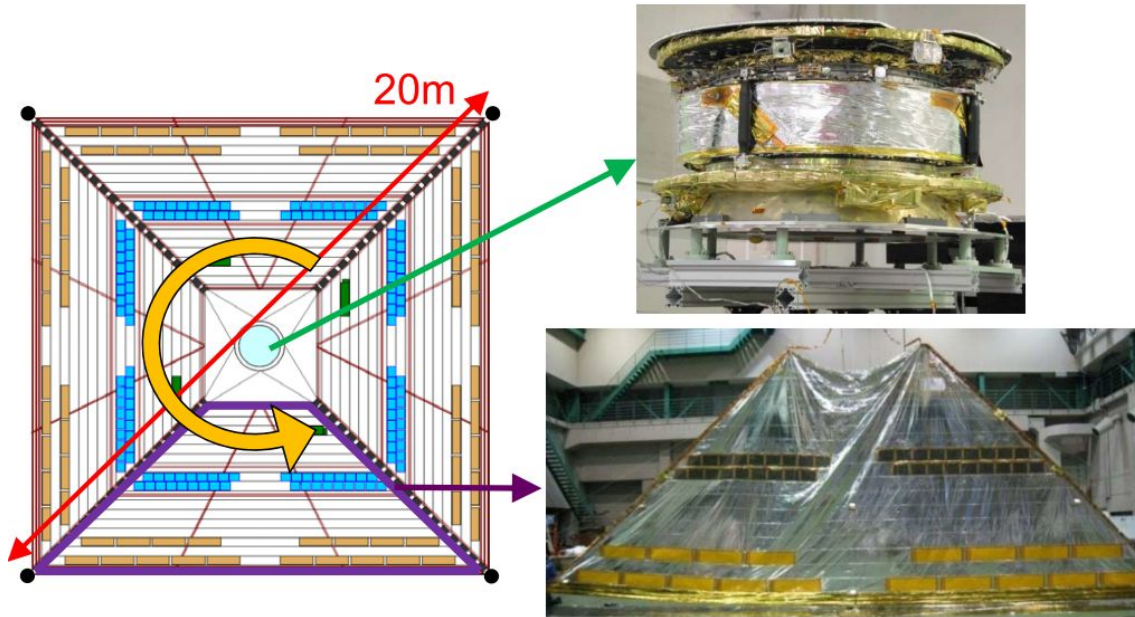
According to Tsuda et al. (2013a), the deployment sequence is divided into two phases:

- (1) The first stage deployment is to extend the sail to a cross-shape:  
The extension speed in this phase is controlled by four guide rollers moving around the spacecraft hub. Thus the extension is done in completely quasi-static manner so that the flexibility of the sail is suppressed as much as possible.
- (2) The second stage deployment is to extend the sail to the final flat rectangular shape:  
This is done by unlatching the four guide rollers. By this action, the sail is extended dynamically in a few seconds by the centrifugal force. The spin rate before initiating the first stage is 25 rpm, and the final spin rate after the complete extension is reduced to 2.5 rpm just due to the law of conservation of angular momentum.

After deployed, the solar sail was a huge square which sides of 14 meters, whose tip-to-tip length is 20 meters long in a diagonal line. Therefore, with a panel measuring

14 meters x 14 meters, totaling  $196 \text{ m}^2$  of area and an initial wet mass of 307 kg and equipped with a rectangular solar sail of 16 kg, it had an area/mass ratio of approximately  $0.61 \text{ m}^2/\text{kg}$ . The overall configuration is shown in Figure 1.5.

Figure 1.5 - IKAROS in the final assembly phase and one of the four petals of the sail flight model.



SOURCE: Adapted from Tsuda et al. (2013a)

Following the successful return back of Hayabusa from the asteroid Itokawa, the Japanese Aerospace Exploration Agency launched another asteroid sample return mission, Hayabusa 2 (TSUDA et al., 2013b) on December, 2014. It was designed to rendezvous with the asteroid Ryugu (1999 JU3) and return a sample. Hayabusa 2 is planned to reach Ryugu in the middle of 2018 and perform an asteroid proximity operation for 1.5 years. Three touch downs for sample collection and one crater forming by a high-speed kinetic impact are planned during the asteroid proximity operation. The sample is to be brought back to the Earth by a re-entry capsule in December 2020. This mission is similar in design to the first Hayabusa mission. It has the same  $12 \text{ m}^2$  solar panel wings, however it is 90 kg heavier and has increased redundancy and more scientific instruments for proximities observations. The launch mass was 600 kg, which gives an area/mass ratio of  $0.02 \text{ m}^2/\text{kg}$ . Figure 1.6 shows an external view of Hayabusa 2.

Figure 1.6 - External view of the Hayabusa 2 spacecraft.



SOURCE: Tsuda et al. (2013b)

The American mission OSIRIS-REx (Origins, Spectral Interpretation, Resource Identification, Security - Regolith Explorer) (GAL-EDD; CHEUVRONT, 2015), is a NASA asteroid study and sample return mission. It was launched on September 2016 and its objective is study the asteroid Bennu (1999 RQ36) for up to 505 days, globally mapping the surface from a distance of 5 km to a distance of 0.7 km. It also aims to obtain at least 60 grams of surface material, and return it to the Earth probably on September 2023 for detailed analysis. If successful, OSIRIS-REx will be the first American spacecraft to return samples from an asteroid.

NASA is also developing a new mission, the Asteroid Redirect Mission (ARM) (MAZANEK et al., 2013; STRANGE et al., 2013), to visit a large near Earth asteroid, collect a multi-ton boulder from its surface, and redirect it into a stable orbit around the Moon. Once it is there, astronauts will explore it and return with samples back to the Earth. It is part of NASA's plan to advance in new technologies and spaceflight experience. It is proposed to be launched in the 2020's.

The Japan Aerospace Exploration Agency has been proposing a new concept of propulsion, the Solar Power Sail (KAWAGUCHI, 2004; MORI et al., 2009), for a future exploration of the Jupiter Trojan asteroids. The Solar Power Sail is an original Japanese concept in which electrical power is generated by thin-film solar cells on the sail membrane. This solar power sail-craft would be composed of an ion engine and a large solar sail which have been successfully demonstrated by Hayabusa and IKAROS respectively. The area of this solar sail would be 2500  $m^2$  to 3000  $m^2$ , 10 to 15 times larger than that of IKAROS. After arriving at the Trojan asteroid, a lander is separated from sail-craft to collect surface and subsurface samples and perform in-situ analysis. The solar power sail-craft would perform cruise science observations as well as IKAROS did. After collecting samples, the lander would deliver the material to the sail-craft and will come back to the Earth. The planned solar power sail-craft, with a mass of about 1.3 tons would be able to transport a 100 kg lander to the Trojan asteroid and come back to the Earth, meanwhile, the Rosetta mission (GLASSMEIER et al., 2007), with its mass of 3 tons transported the Philae lander of the same 100 kg mass to the 67P/Churyumov-Gerasimenko comet, which was located closer than the Trojan asteroids. This difference indicates the superiority of the Solar Power Sail proposed by JAXA.

## 1.2 Organization of the present thesis

The remaining chapters of this thesis are organized as follows:

- Chapter 2: The purpose of this chapter is to provide the methodology that will take in carrying out this work.
- Chapter 3: This chapter presents the problem of orbital transfers in the restricted three-body problem considering the effects of the solar radiation pressure in the trajectory of the spacecraft. The follow systems of primaries are used: Earth-Moon, Sun-Earth and systems of asteroids. Transfers among the Lagrangian points and between the Lagrangian points and the primaries are considered. The results show that the solar radiation pressure has a significant participation in the process, in particular in the system formed by asteroids. This occurs because the gravitational forces in these systems are smaller if compared with systems formed by larger bodies. The effects of the solar radiation pressure in the trajectories of a spacecraft in orbital transfers between the collinear Lagrange points of a double asteroid system is also studied in this chapter. Solutions with lower and higher fuel consumption can be found by adding the solar radiation

pressure. For a small system of primaries such as an asteroid system, it is very important to take into account this force to make sure that the spacecraft will reach the desired point.

- Chapter 4: In the absence of a solar sail or any other forces, the traditional Lagrange points  $L_1$  and  $L_2$  are the only equilibrium points near the asteroid Ida, which is a celestial body located in the asteroid belt. The use of a solar sail in the spacecraft gives new configurations for the equilibrium points, which depend on the position and inclination of the vector normal to the solar sail with respect to the  $x$  axis. These new configurations of equilibrium points are the so called artificial equilibrium points (AEPs). The use of a solar sail is interesting because it allows a spacecraft to park close to the body that is the object of study. Besides that, new perspectives for viewing above or below the ecliptic plane can be reached through the use of a solar sail to observe the body from a stationary condition. The main idea of this chapter is to obtain the new locations of those points and to calculate the costs to transfer a spacecraft between those points, in particular showing some options to minimize the costs involved in these transfers.
- Chapter 5: The study of asteroids has revealed much about these small rock-formed bodies compared to the planets, which, like them, also orbit the Sun. But, although these bodies have masses smaller than the Moon, they present serious dangers, given the fact that many of them have already collided with the Earth in the past, and many others have the probability to collide in the future. Therefore, these are the reasons that lead scientists to promote the study of such celestial bodies, from the point of view of their physical characteristics and the point of view of its dynamics, which can provide the information of how many and when they will collide with the Earth. In recent years, several missions have been proposed to reach asteroids and comets in the Solar System, such as Aster, Dawn, Marco Polo-R, NEAR Shoemaker, Osiris-Rex and Rosetta. The bodies that are target of these missions are very important in terms of science, because they may keep information related to the origin of the Solar System. Another key point is that there is a growing interest in the problem of collision avoidance between an asteroid and the Earth. It means that it is very important to find trajectories to those bodies, which is the main objective of this work. Such trajectories can be used to collision avoidance missions.

## 2 METHODOLOGY

### 2.1 Solar radiation pressure

The solar radiation is composed by photons, which are elementary particles without mass traveling at the speed of light. Even if the mass of a photon is zero, its energy and momentum are not.

The energy of a photon is  $E = h\nu$ , where  $\nu$  is the frequency of the electromagnetic wave and  $h$  is the Planck constant.

The linear momentum of a photon is:

$$p = \frac{E}{c} = \frac{h\nu}{c}, \quad (2.1)$$

It is possible to exert a pressure over an object when radiating light on it, however, the forces generated are very small. A beam of radiation incident on an object during a time interval  $\Delta t$  produces a variation in the modulus of linear momentum  $p_r$ , given by:

$$\Delta p_r = \frac{\Delta E}{c} \quad (2.2)$$

If the radiation is fully absorbed, i.e. an inelastic collision, the variation in the modulus of  $p_r$  is given by Equation 2.2. When the radiation is fully reflected, i.e. an elastic collision, the variation in the modulus of  $p_r$  is doubled.

The energy, absorbed from a radiation source of intensity  $S$ , by a surface body  $A$ , in a time interval  $\Delta t$ , is given by:

$$\Delta E = SA\Delta t \quad (2.3)$$

where  $S$  is the energy flux, the energy per unit time per unit area.

The force,  $F_r$ , on an object due to the radiation is given by:

$$F_r = \frac{dp_r}{dt}, \quad (2.4)$$
$$F_r = \frac{S}{c}A.$$

The magnitude of the force, per unit area, exerted by the radiation is the radiation

pressure,  $rp$ . It is given by:

$$rp = \frac{S}{c} \quad (2.5)$$

The visible surface of the Sun, the photosphere, acts like a blackbody emitting radiation. According to Stefan-Boltzmann's law, the intensity of the radiated power is  $S_0 = \sigma T^4$ , where  $T$  is the absolute temperature of the blackbody and  $\sigma$  is the Stefan-Boltzmann constant.

The electromagnetic radiation follows the law of the inverse of the square, that is, if  $R_0$  is the radius of the photosphere, then the intensity of the solar radiation  $S_r$  at a distance  $R$  from the center of the Sun is:

$$S_r = S_0 \left(\frac{R_0}{R}\right)^2. \quad (2.6)$$

This is the energy flux carried by the photons through a surface normal to the direction of the solar radiation. As shown in Equation 2.5, the solar radiation pressure at Earth's orbit is given by  $S_r/c$ .

The acceleration acting on a spacecraft due to the solar radiation pressure is given by (VALLADO, 2001):

$$\vec{a}_{srp} = -C_r \frac{S_r}{c} \frac{A}{m} \left(\frac{1}{r_s}\right)^2 \hat{r} \quad (2.7)$$

where:

- the negative sign indicates that the radiation force is directed in the opposite direction to the Sun;
- $C_r$  is the reflectivity coefficient of the surface, which vary from 1 to 2:  
 $C_r = 1$ , if the surface is a black body, absorbing all the moment of the incident photons;  
 $C_r = 2$ , if all incident radiation is reflected, which doubles the applied force on the spacecraft.
- $S_r$  is the energy flux, equals to  $1365 \text{ W/m}^2$  (KOPP; LEAN, 2011) at one au (where au is the Astronomical unit, the average Sun-Earth distance (LUZUM et al., 2011));
- $c$  is the speed of light (LUZUM et al., 2011);
- $A$  is the area of the spacecraft illuminated by the Sun;
- $m$  is the mass of the spacecraft;

- $r_s$  is the distance Sun-spacecraft in au;
- $\hat{r}$  is the unit vector that represents the direction of the acceleration, which is assumed to be the Sun-spacecraft line.

## 2.2 The circular restricted three-body problem

The planar circular restricted three-body problem with the addition of the solar radiation pressure is used as the mathematical model. It is assumed that two bodies  $M_1$  and  $M_2$  are orbiting their common center of mass in circular Keplerian orbits and a third body  $M_3$ , with negligible mass, is orbiting these two main bodies, called primaries. The motion of the third body,  $M_3$ , is affected by the two main bodies  $M_1$  and  $M_2$ , but it does not affect their motion (SZEBEHELY, 1967).

In this work, the planar circular restricted three-body problem is combined with the forces coming from the solar radiation pressure to find different orbital trajectories necessary to move the spacecraft between the collinear Lagrange points of the asteroid system 1996FG<sub>3</sub>. The primaries  $M_1$  (the main asteroid) and  $M_2$  (the smaller asteroid) orbit the common center of mass of the system in circular Keplerian orbit, and the third body  $M_3$  (the spacecraft), considered to have a negligible mass, orbits the main bodies. The motion of  $M_3$  does not affect the motion of the main bodies  $M_1$  and  $M_2$ , but it is affected by them (SZEBEHELY, 1967).

The equations of motion can be written in a system of non-dimensional units, also known as a canonical system of units. In this system:

- The unit of distance is assumed as the distance between the two primaries (the semi-major axis of their orbits);
- The angular velocity of the motion of the primaries is considered one;
- The mass of the primaries are given by the mass ratio. The primary  $M_2$  has a given mass of  $\mu = M_2/(M_1+M_2)$ , and the primary  $M_1$  has a given mass of  $(1-\mu)$ . It makes the total mass one;
- The unit of time is defined such that the period of the motion of the primaries is  $2\pi$ ;
- The gravitational constant,  $G$ , is considered one.

The equations of motion of  $M_3$ , which is represented in the rotating coordinate system, are given by (SZEBEHELY, 1967):

$$\begin{aligned}\ddot{x} - 2\dot{y} &= \frac{\partial\Omega}{\partial x} + a_{srp,x}, \\ \ddot{y} + 2\dot{x} &= \frac{\partial\Omega}{\partial y} + a_{srp,y},\end{aligned}\tag{2.8}$$

where  $\Omega$  is the pseudo-potential given by:

$$\Omega = \frac{1}{2}(x^2 + y^2) + \frac{1 - \mu}{r_1} + \frac{\mu}{r_2},\tag{2.9}$$

where:

$$\begin{aligned}r_1^2 &= (x + \mu)^2 + y^2, \\ r_2^2 &= (x - 1 + \mu)^2 + y^2,\end{aligned}\tag{2.10}$$

and  $a_{srp,x}$  and  $a_{srp,y}$  are the components of the solar radiation pressure that is now added as another force. The magnitude of the acceleration due to the solar radiation pressure is given by Equation 2.7.

### 2.3 Orbital maneuvers

According to Curtis (2013), orbital maneuvers are defined as a change in the position and velocity of a spacecraft. They are used to transfer a spacecraft from one orbit to another, what requires the firing of rocket engines. There are two ways to model the thrust applied to a spacecraft: nonimpulsive and impulsive maneuvers.

The nonimpulsive maneuvers are those in which the thrust acts over a significant time interval and must be included in the equations of motion. The impulsive maneuvers are those in which brief firings of rocket change the magnitude and direction of the velocity instantaneously. Thus, during an impulsive maneuver, only the velocity changes and the spacecraft position remains unchanged.

The impulsive maneuver is the most applied model in the literature, due to its simplicity and reasonable precision. In this model, we can avoid solve the equations of motion with the rocket thrust included. It is satisfactory for those cases in which the position of the spacecraft changes only slightly during the time that the maneuvering rocket fire.

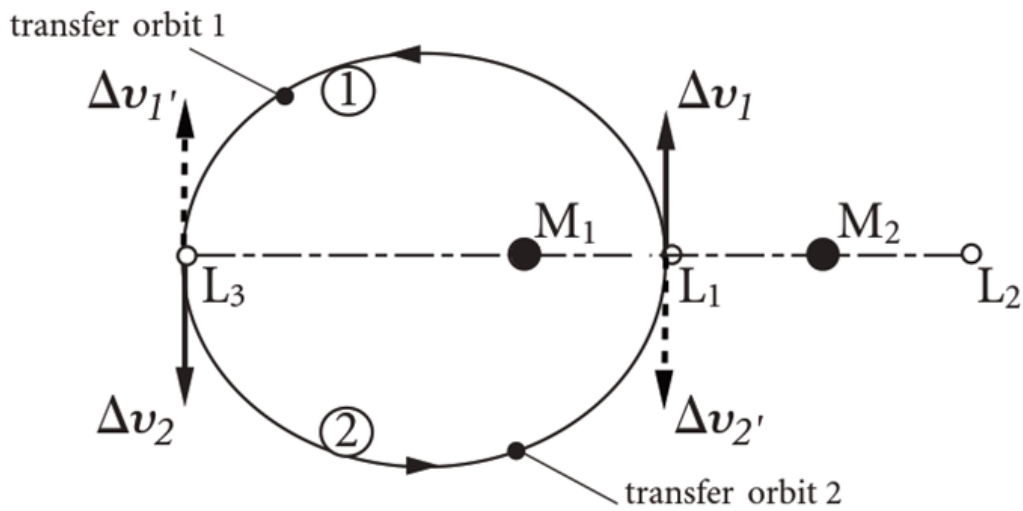
Thus, in this work, it will be used the approach of impulsive maneuvers, that take

place in zero time, producing the required velocity change,  $\Delta V$ , but leaving the position unchanged.

Figure 2.1 points how these transfers are simulated. It starts with the application of the first impulse at the initial position of the spacecraft, and ends with the application of the second impulse in the final desired position of the spacecraft.

Considering that the spacecraft is positioned on a Lagrange point of the system of primaries  $M_1$  and  $M_2$ , it can be required that the spacecraft changes its orbit during a mission, such that it may study and collect information about the bodies of this system. It may be also possible that the spacecraft can collect solar material when the mission approaches the closest point of its orbit around the Sun.

Figure 2.1 - Bi-impulsive transfer between the Lagrange points  $L_1$  and  $L_3$ .



SOURCE: Oliveira et al. (2017b).

An example for a transfer from the Lagrange point  $L_1$  to the Lagrange point  $L_3$  is shown in Figure 2.1. In this example, the spacecraft is situated at point  $L_1$  and must reach point  $L_3$ . In this way, an impulsive maneuver is applied at point  $L_1$ , giving the spacecraft the necessary variation of velocity  $\Delta v_1$  to start the transfer orbit 1, directed to point  $L_3$ . When the spacecraft reaches point  $L_3$ , another impulsive maneuver is applied, giving the spacecraft the necessary variation of velocity  $\Delta v_1'$ , in order to put the spacecraft in the desired final orbit of the Lagrange point  $L_3$ .

In our scenario, it is assumed that the spacecraft needs to return to  $L_1$ . Thus, by applying a variation of velocity  $\Delta v_2$  at point  $L_3$ , and a variation of velocity  $\Delta v_2'$ , at the end point  $L_1$ , the spacecraft will perform the transfer orbit 2, returning to the Lagrange point  $L_1$ .

The method used in this work to find the required  $\Delta V$  for each maneuver is called Two Point Boundary Value Problem (TPBVP) and is presented in the next section.

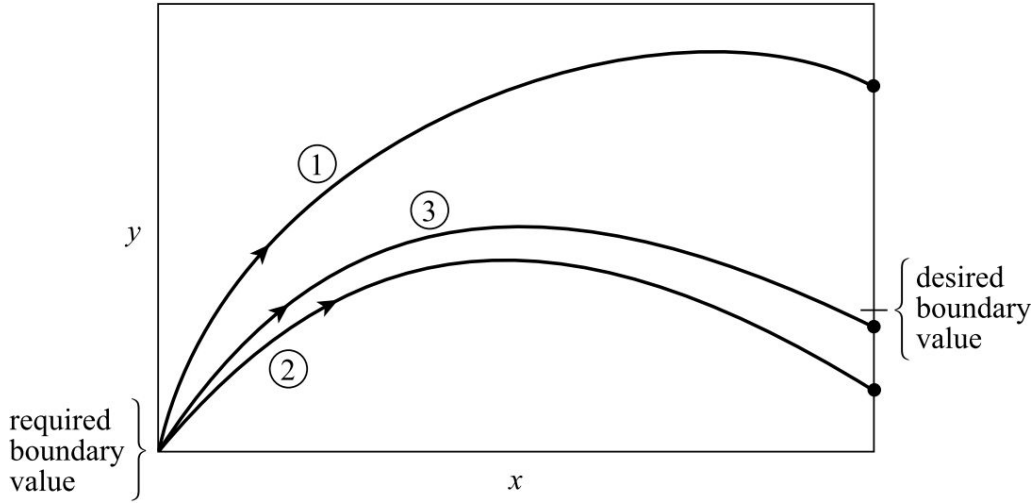
## 2.4 Two Point Boundary Value Problem

The main objective of this work is to find the trajectory of a spacecraft that leaves one given point to reach another given point. If the transfer time is free, there is an infinite number of solutions. Thus, it can be formulated as: "Find an orbit (in the three-body problem context) that makes a spacecraft to leave a given point A and goes to another given point B, arriving there after a specified time of flight". It means that this is a problem of finding trajectories linking two given points with a defined time.

However, the system of equations that describes the motion of the spacecraft, which is presented in Equation 2.8, has no analytical solutions and numerical integrations need to be applied to solve the problem. Thus, this problem is treated as a "Two Point Boundary Value Problem" (TPBVP), which is a problem where ordinary differential equations are required to satisfy boundary conditions at more than one value of the independent variable. As the terminology indicates, the most common case by far is where boundary conditions are supposed to be satisfied at two points, usually the starting and ending values of the integration.

As addressed by [Press et al. \(2007\)](#), there are two distinct classes of numerical methods to solve TPBVPs: shooting and relaxation methods. The former has been used in this work to compute a transfer trajectory. It provides an efficient approach to take a set of ranging shots that allows to improve the objective function systematically. At first, trial integrations are made to satisfy the boundary conditions at one endpoint. The error between the final condition achieved and the desired boundary condition, at the other endpoint, is used to adjust the starting values, until the conditions at both endpoints are ultimately satisfied. This method provides a systematic approach to taking a set of "ranging" shots that allow us to improve our "aim" systematically. The shooting method, is illustrated in [Figure 2.2](#).

Figure 2.2 - Schematic example of the shooting method.



Trial integrations that satisfy the boundary condition at one endpoint are "launched." The discrepancies from the desired boundary condition at the other endpoint are used to adjust the starting conditions, until boundary conditions at both endpoints are ultimately satisfied.

SOURCE: Press et al. (2007).

Therefore, the algorithm used in this work to solve the shooting method has the following steps:

- (i) The initial state is given by the initial velocity  $\vec{v}_i$  and the initial prescribed position  $\vec{r}_i$ , the initial state is completely known;
- (ii) The final state is given by the final desired velocity  $\vec{v}_d$  and the final desired position  $\vec{r}_d$ , the final state is completely known;
- (iii) Define the initial,  $\tau_0$ , and the final transfer time,  $\tau_f$ ;
- (iv) Integrate the equations of motion from the initial time  $\tau_0$  until the final time  $\tau_f$ ;
- (v) Compute the new state, composed by a velocity vector  $\vec{v}_f$ , and a position vector  $\vec{r}_f$ , both of them obtained from the numerical integration method.
- (vi) Check the final position. If  $|r_f - r_d|$  is smaller than a given tolerance,  $10^{-5}$ , the solution is found and this process stops. Otherwise, the process returns to step i and an increment in the initial velocity  $\vec{v}_i$  is made.

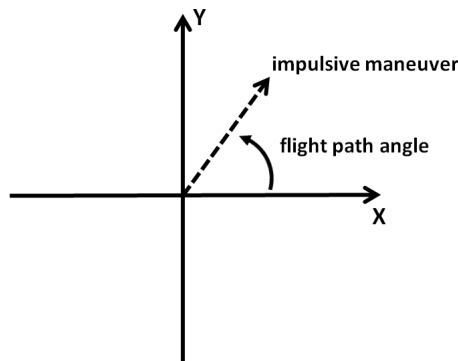
The variation of velocity  $\Delta V_1$  is the difference between the incremented initial velocity  $\vec{v}_i$ , obtained in the step vi, and the initial velocity  $\vec{v}_i$ , given in the first initial state in step i. The variation of velocity  $\Delta V_2$  is the difference between the velocity  $\vec{v}_f$ , found in step v, and the final desired velocity  $\vec{v}_d$ , given in step ii.

This algorithm was previously used in several works: Broucke (1979), Prado e Broucke (1995), Prado (1996), Prado e Broucke (1996), Prado (2006), Yang et al. (2015), Oliveira et al. (2016), Oliveira et al. (2016), Oliveira et al. (2017b), Oliveira et al. (2017a), Santos et al. (2017), Santos (2013), Oliveira et al. (2018).

The solution gives the trajectory of the spacecraft, as well as quantities of the fuel consumption, specified by the amount of  $\Delta V$  in the entire transfer time, *i.e.*,  $\Delta V_1$  in the launch of the spacecraft and  $\Delta V_2$  in the desired final point of the spacecraft. So, by changing the time of flight, it is possible to find a family of transfer orbits.

In the results are also shown, the plots with the variation of velocity  $\Delta v$  against time, and the variation of velocity  $\Delta v$  against the initial flight path angle (*fpa*), as done by Prado (1996). The definition of this angle is such that the zero is in the "X" axis pointing to the positive direction and it increases in the counterclockwise sense. This definition is shown in Figure 2.3.

Figure 2.3 - Flight path angle (*fpa*).

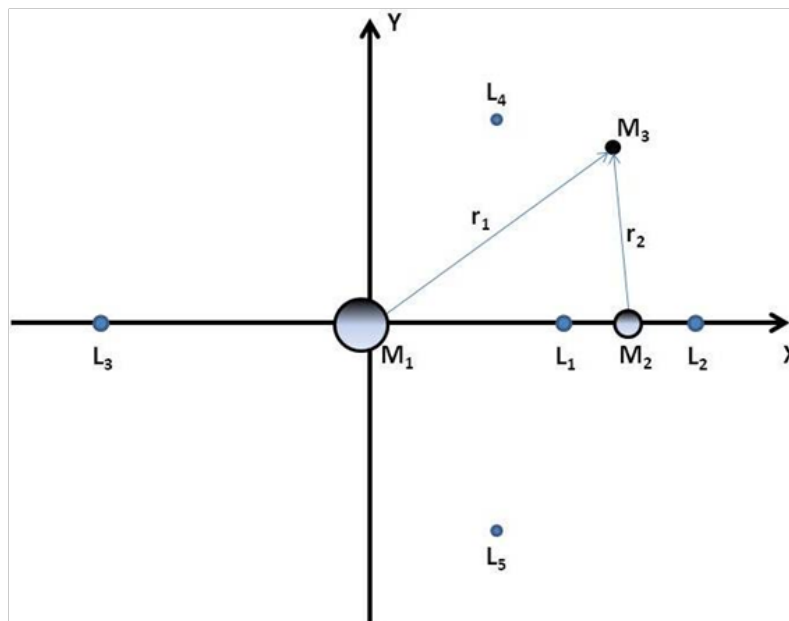


SOURCE: Oliveira et al. (2017b).

### 3 ORBITAL TRANSFERS BETWEEN THE LANGRANGE POINTS AND THE PRIMARIES

The equilibrium Lagrangian points that appear in the restricted three-body problem (SZEBEHELY, 1967) have several applications, like the location of space stations, relay satellites for communications, etc (BOND et al., 1991; FARQUHAR, 1969). They are five points of equilibrium of the system and a spacecraft placed there with zero velocity will remain there forever.  $L_1$ ,  $L_2$  and  $L_3$  are the collinear points, located in the line connecting the two primaries, and they are always unstable.  $L_4$  and  $L_5$  are the triangular points, because they make an equilateral triangle with the two primaries. They are stable for the more important cases of the Solar System (Earth-Moon, Sun-Earth, Sun-Jupiter). Figure 3.1 shows a sketch of the locations of those points.

Figure 3.1 - Location of the Lagrangian points and the primaries.



SOURCE: Oliveira et al. (2016).

This chapter considers the problem of bi-impulsive transfers between the Lagrangian points and from those Lagrangian points to the primaries, considering four different systems of primaries:

- (1) Earth-Moon;
- (2) Sun-Earth;
- (3) the triple asteroid 2001SN263 (ARAÚJO et al., 2012; ARAÚJO et al., 2015);
- (4) the double asteroid 1996FG3 (WOLTERS et al., 2011; SCHEIRICH et al., 2015).

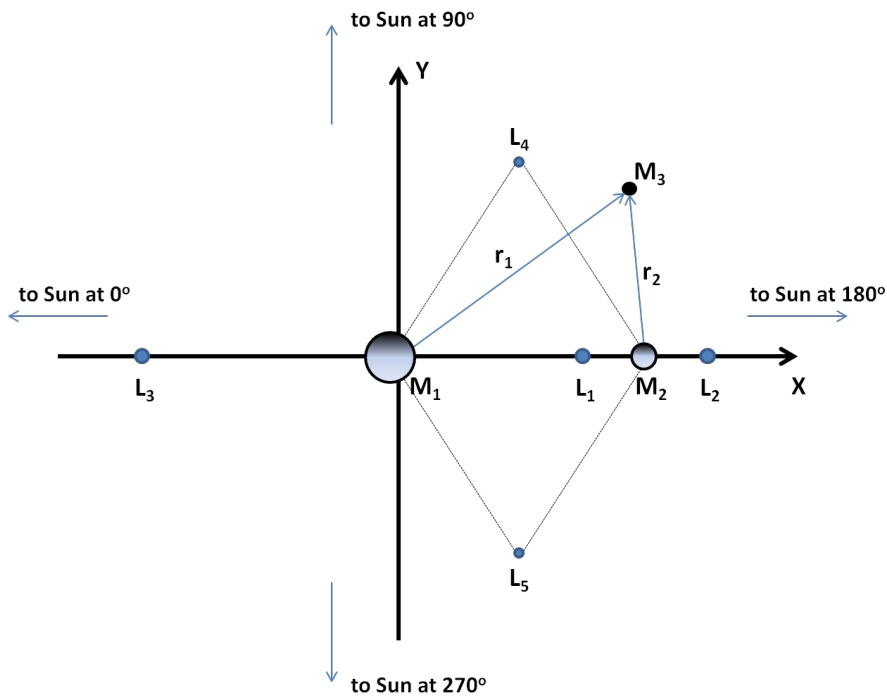
It is considered that the maneuver starts with the application of the first impulse at the initial position of the spacecraft and ends with the application of the second impulse in the final position of the spacecraft, as described in Section 2.3. The effects of the solar radiation pressure, as described in Section 2.1, are not used as a control, but it is assumed to be a perturbation present in the system. Previous researches have been done in similar problems. (BROUCKE, 1979; PRADO, 1996; PRADO, 2006; CABETTE; PRADO, 2008)

The main goal is to show the relative importance of the solar radiation pressure as a function of the masses of the primaries. It will be shown that this point is very important and the effects of the solar radiation pressure goes from almost negligible to very high, depending on the system of primaries.

The effects of the solar radiation pressure in the trajectory of the spacecraft can be modulated by changing the area/mass of the spacecraft, so it is possible to increase those effects by adding large panels to the spacecraft, if it is interesting for the mission. Those panels may be necessary to get solar energy to supply the spacecraft and the main point is that the spacecraft will not reach the target if this force is not considered.

Another key point that is considered in the simulations made here is the initial position of the Sun at the beginning of the maneuvers. In order to measure and verify the effects of the solar radiation pressure, it is simulated five different cases. In the first case the solar radiation pressure is not considered. The next cases consider the Sun in four different positions with respect to the asteroid system when the maneuvers are followed. It is assumed that the Sun is situated at 0 degree, 90 degrees, 180 degrees and 270 degrees with respect to the asteroid system. The geometry of problem is shown in Figure 3.2.

Figure 3.2 - Reference frame in the planar circular restricted three-body problem.



Location of the Sun with respect to the primaries.  $M_1$  represents the larger primary,  $M_2$  the smaller one and  $M_3$  the spacecraft. The five Lagrange points are also presented.

SOURCE: Oliveira et al. (2017b).

### 3.1 Earth-Moon system

Table 3.1 shows the parameters used to calculate the acceleration of the solar radiation pressure in the Earth-Moon system, as described in section 2.1, where  $r_e$  is the Sun-Earth distance.

Table 3.1 - Parameters of the Earth-Moon system.

$r_e$	$1.495978707 \times 10^{11} m$
$r_s$	$1 r_e$
$S_r/c$	$4.56 \times 10^{-6} N/m^2$
$\mu_{earth}$	$3.986 \times 10^{14} m^3/s^2$
$\mu_{moon}$	$4.900 \times 10^{12} m^3/s^2$
$A/m \text{ ratio}$	$10.0 m^2/kg$
$C_r$	1.5

SOURCE: Luzum et al. (2011)

Table 3.2 presents the canonical values used in the equation of motion of the Earth-Moon system, as described in section 2.2.

Table 3.2 - Canonical system of units for the Earth-Moon system.

Unit of distance	$3.844 \times 10^5 \text{ km}$
Unit of time	$2.357 \times 10^6 \text{ sec}$
Unit of velocity	$1.025 \text{ km/s}$

SOURCE: Luzum et al. (2011)

Table 3.3 presents the positions of the Lagrange points and the primaries of the Earth-Moon system which are considered for the orbital transfers.

Table 3.3 - Lagrange points and primaries of the Earth-Moon system.

Point	$x$ (nd)	$y$ (nd)
$L_1$	0.836915	0
$L_2$	1.155682	0
$L_3$	-1.005063	0
$L_4$	0.487849	0.866025
$L_5$	0.487849	-0.866025
Earth	-0.012144	0
Moon	0.987856	0

SOURCE: Author

Where the position of the Earth is given by:  $-\mu = -M_{Moon}/(M_{Earth} + M_{Moon})$ , and the position of Moon is given by:  $1 - \mu$ .

The first families of transfer orbits studied consider transfers between the collinear Lagrangian points in the Earth-Moon system in two directions: clockwise and counterclockwise. The results are organized in plots of the  $\Delta v$  against the initial flight path angle (in degrees) in the rotating frame. Different locations of the Sun are considered, and the geometry of the problem is shown in Figure 3.2, where  $M_1$  represents the Earth,  $M_2$  the Moon and  $M_3$  the spacecraft.

Figures 3.3 to 3.6 show the results for the maneuvers linking the three collinear Lagrangian points. They are plots showing the variation of velocities required by the transfers against the initial flight path angle, described in Section 2.4.

Figure 3.3 shows the results for transfers from the Lagrange point  $L_1$ , the initial point, to the Lagrange point  $L_2$ , the final point. The initial conditions, in the rotating frame of reference, for this transfer are given in Table 3.4. The results show that the solar radiation pressure has a small influence in the process, the minimum values of  $\Delta v$  found for the five cases are very close.

Table 3.4 - Parameters for  $L_1$  and  $L_2$ .

Point	$x$ (nd)	$y$ (nd)	$v$ (nd)
$L_1$ (initial)	0.836915	0	0
$L_2$ (final)	1.155682	0	0

SOURCE: Author

Figure 3.3 - Transfers from  $L_1$  and  $L_2$ .

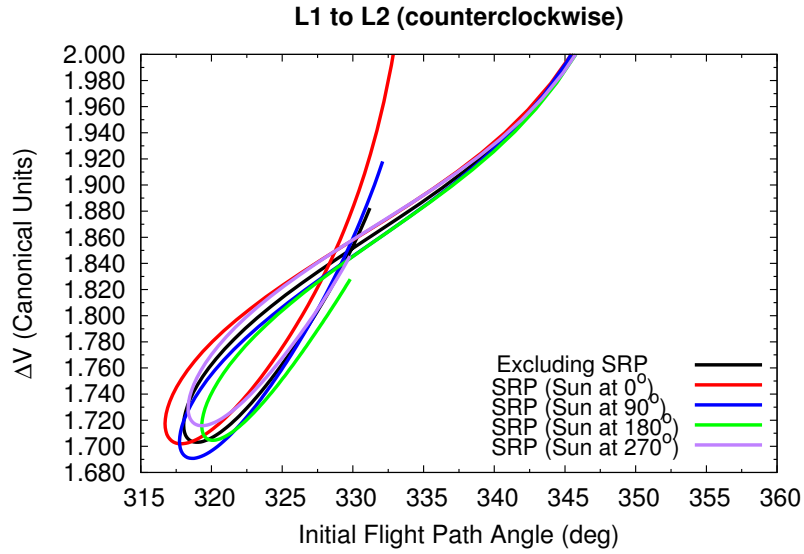


Figure 3.4 shows the results for transfers from  $L_1$ , the initial point, to  $L_3$ , the final point. The initial conditions, in the rotating frame of reference, for this transfer are given in Table 3.5. The results, in this case, show that the solar radiation pressure has an important influence in this transfer. When the transfer is taken with the Sun at 270 degrees with respect to the system, we found a minimum value for  $\Delta v$ , however, with the Sun at 90 degrees we found a higher value for  $\Delta v$  required to perform this maneuver. For all other cases the  $\Delta v$  has small changes.

Table 3.5 - Parameters for  $L_1$  and  $L_3$ .

Point	$x$ (nd)	$y$ (nd)	$v$ (nd)
$L_1$ (initial)	0.836915	0	0
$L_3$ (final)	-1.005063	0	0

SOURCE: Author

Figure 3.4 - Transfers from  $L_1$  to  $L_3$ .

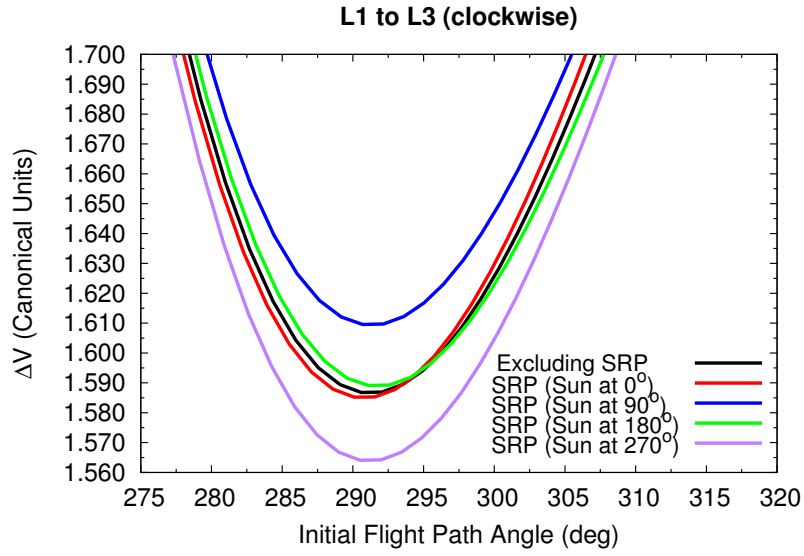


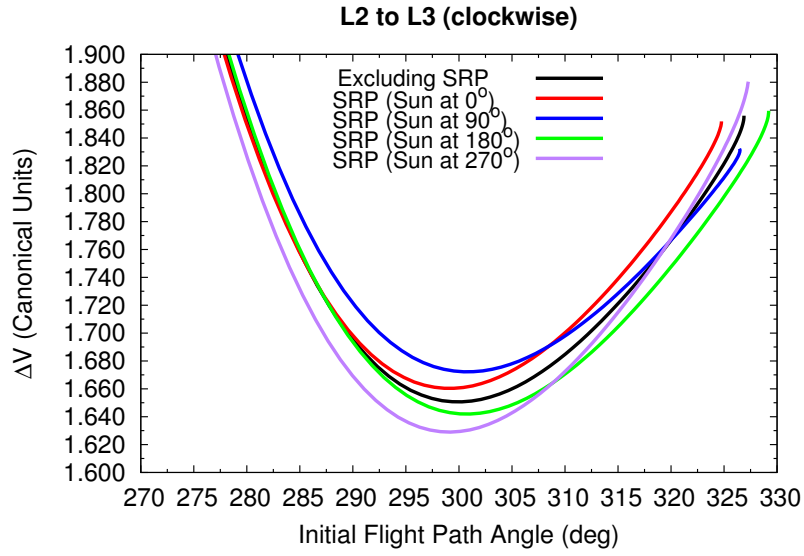
Figure 3.5 shows the results for transfers from  $L_2$ , the initial point, to  $L_3$ , the final point. The initial conditions, in the rotating frame of reference, for this transfer are given in Table 3.6. The results show that the solar radiation pressure has a small influence for each case.

Table 3.6 - Parameters for  $L_2$  and  $L_3$ .

Point	$x$ (nd)	$y$ (nd)	$v$ (nd)
$L_2$ (initial)	1.155682	0	0
$L_3$ (final)	-1.005063	0	0

SOURCE: Author

Figure 3.5 - Transfers from  $L_2$  to  $L_3$ .



SOURCE: Adapted from Oliveira et al. (2016).

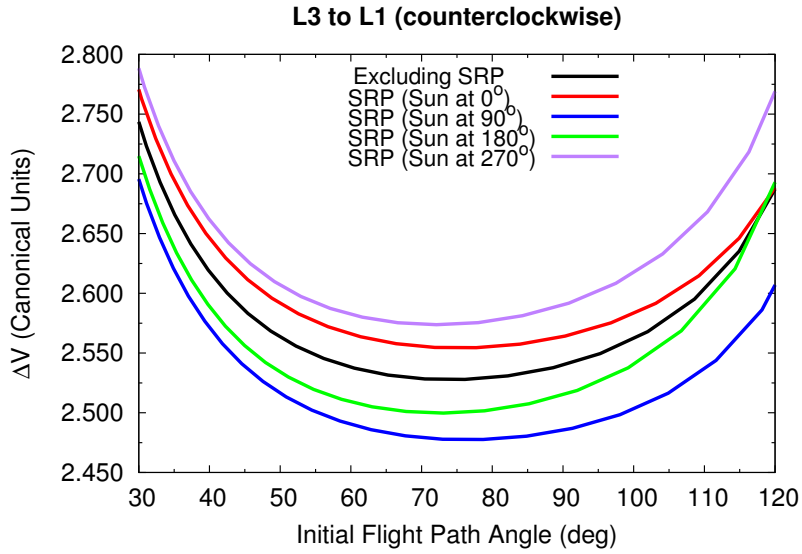
Figure 3.6 shows the results for transfers from  $L_3$ , the initial point, to  $L_1$ , the final point. The initial conditions, in the rotating frame of reference, for this transfer are given in Table 3.7. In this case, although not very large, it is possible to identify how the solar radiation pressure modifies the  $\Delta v$  required for each case.

Table 3.7 - Parameters for  $L_3$  and  $L_1$ .

Point	$x$ (nd)	$y$ (nd)	$v$ (nd)
$L_3$ (initial)	-1.005063	0	0
$L_1$ (final)	0.836915	0	0

SOURCE: Author

Figure 3.6 - Transfers from  $L_3$  to  $L_1$ .



SOURCE: Adapted from Oliveira et al. (2016).

The next study considers transfers between the Lagrangian points and the Earth, also using several values for the time of flight and two directions for the transfer: clockwise and counterclockwise. Figures 3.7 to 3.11 show the results, plotting the variation of velocity against the initial flight angle, as done before.

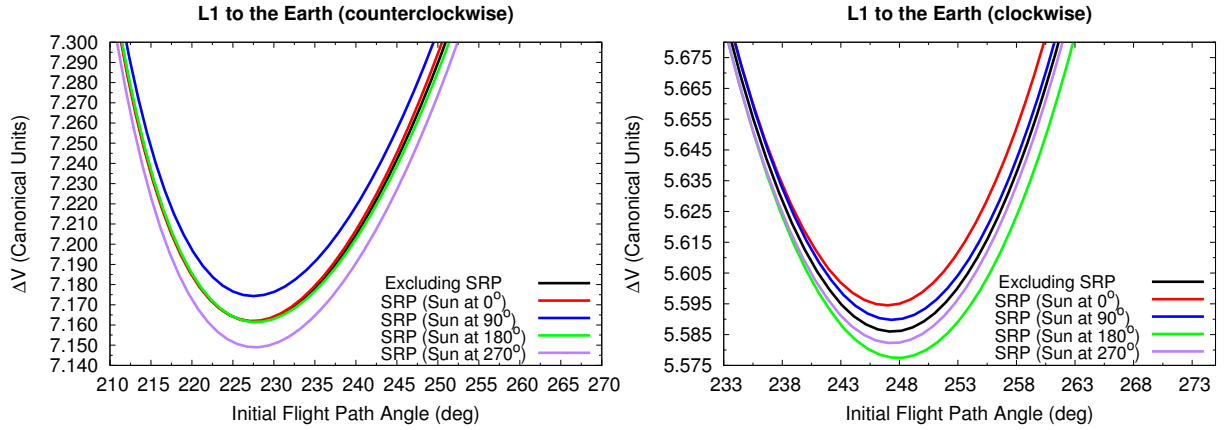
Figure 3.7 shows the results for transfers from  $L_1$ , the initial point, to the Earth, the final point. The initial conditions, in the rotating frame of reference, for this transfer are given in Table 3.8. The results show that for the clockwise transfer the  $\Delta v$  is smaller than the required for the counterclockwise transfer. It can be noted, although not very large, how the solar radiation pressure modifies the  $\Delta v$  required for each case of the clockwise transfer.

Table 3.8 - Parameters for  $L_1$  and the Earth.

Point	$x$ (nd)	$y$ (nd)	$v$ (nd)
$L_1$ (initial)	0.836915	0	0
Earth (final)	-0.030354	0	0

SOURCE: Author

Figure 3.7 - Transfers from  $L_1$  to the Earth.



SOURCE: Adapted from Oliveira et al. (2016).

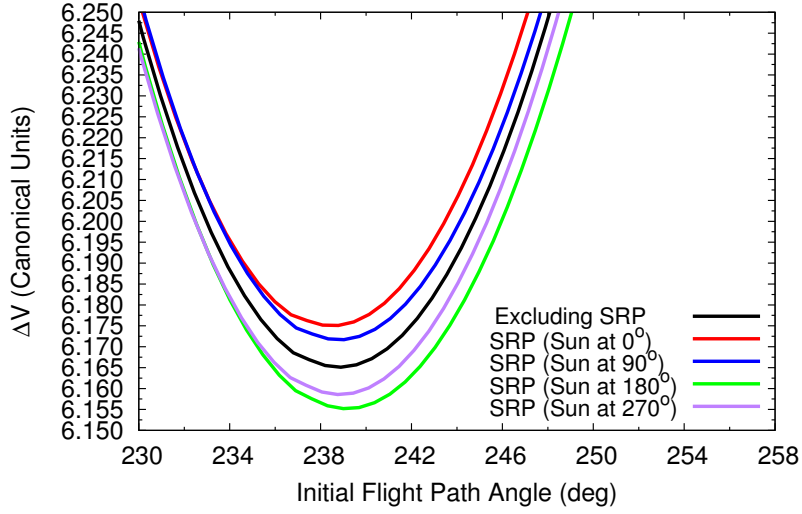
Figure 3.8 shows the results for transfers from  $L_2$ , the initial point, to the Earth, the final point. The initial conditions, in the rotating frame of reference, for this transfer are given in Table 3.9. This case is similar to the previous one, however the values for  $\Delta v$  are higher.

Table 3.9 - Parameters for  $L_2$  and the Earth.

Point	$x$ (nd)	$y$ (nd)	$v$ (nd)
$L_2$ (initial)	1.155682	0	0
Earth (final)	-0.030354	0	0

SOURCE: Author

Figure 3.8 - Transfers from  $L_2$  to the Earth.  
 **$L_2$  to the Earth (clockwise)**



SOURCE: Adapted from Oliveira et al. (2016).

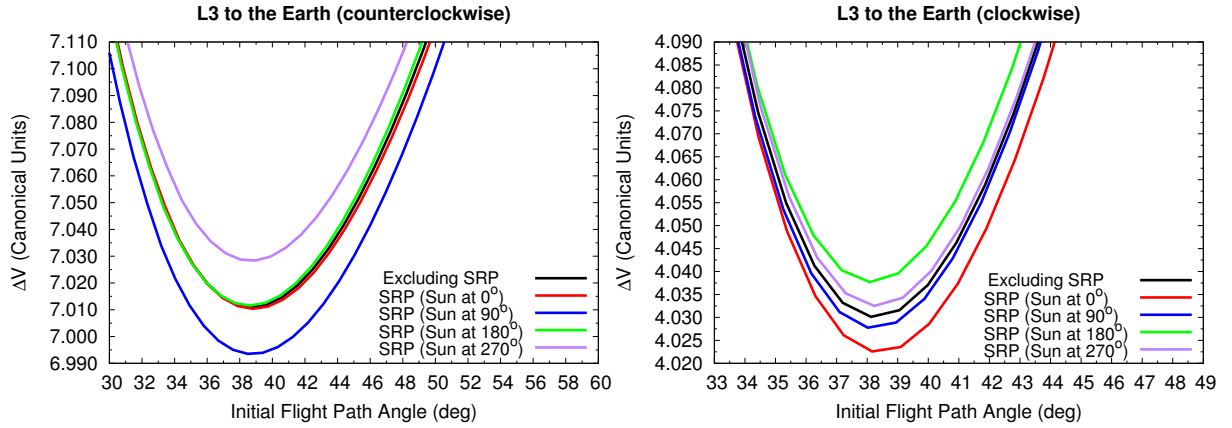
Figure 3.9 shows the results for transfers from  $L_3$ , the initial point, to the Earth, the final point. The initial conditions, in the rotating frame of reference, for this transfer are given in Table 3.10. The results show that for the clockwise transfer the  $\Delta v$  is smaller than the required for the counterclockwise transfer. It can be noted, although not very large, how the solar radiation pressure modifies the  $\Delta v$  required for each case of the clockwise transfer.

Table 3.10 - Parameters for  $L_3$  and the Earth.

Point	$x$ (nd)	$y$ (nd)	$v$ (nd)
$L_3$ (initial)	-1.005063	0	0
Earth (final)	0.006067	0	0

SOURCE: Author

Figure 3.9 - Transfers from  $L_3$  to the Earth.



SOURCE: Adapted from Oliveira et al. (2016).

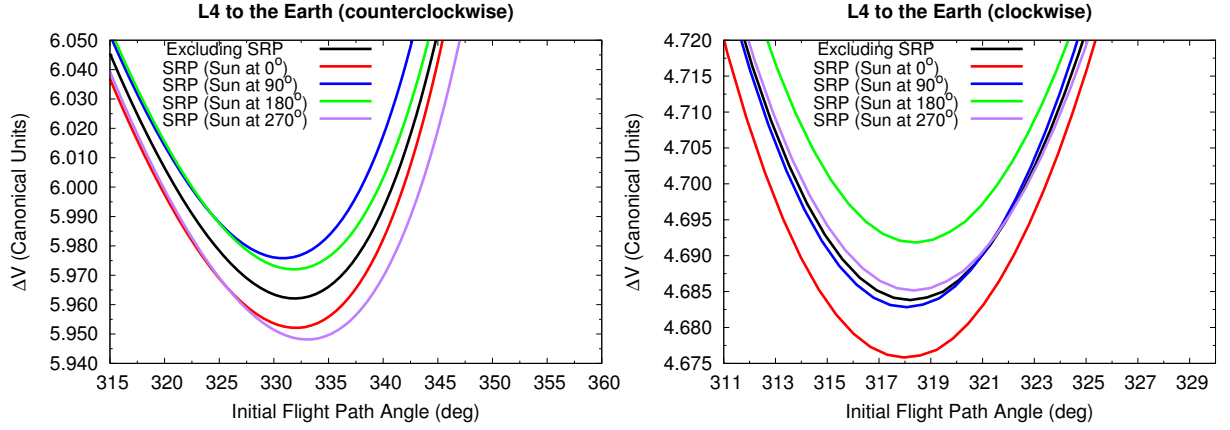
Figure 3.10 shows the results for transfers from  $L_4$ , the initial point, to the Earth, the final point. The initial conditions, in the rotating frame of reference, for this transfer are given in Table 3.11. The results show that for the clockwise transfer the  $\Delta v$  is smaller than the required for the counterclockwise transfer. It can be noted, although not very large, how the solar radiation pressure modifies the  $\Delta v$  required for each case of the counterclockwise transfer.

Table 3.11 - Parameters for  $L_4$  and the Earth.

Point	$x$ (nd)	$y$ (nd)	$v$ (nd)
$L_4$ (initial)	0.487849	0.866025	0
Earth (final)	-0.021248	-0.015770	0

SOURCE: Author

Figure 3.10 - Transfers from L<sub>4</sub> to the Earth.



SOURCE: Adapted from Oliveira et al. (2016).

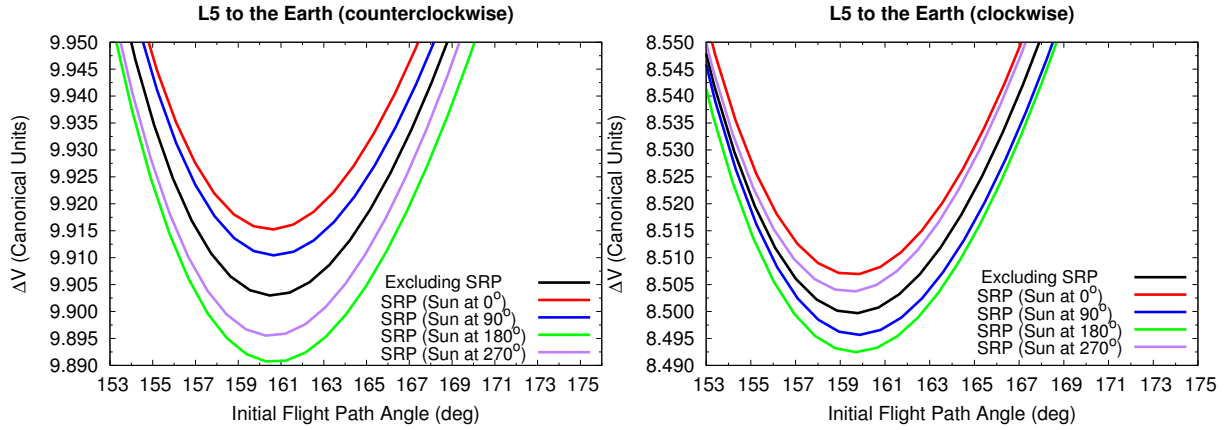
Figure 3.11 shows the results for transfers from L<sub>5</sub>, the initial point, to the Earth, the final point. The initial conditions, in the rotating frame of reference, for this transfer are given in Table 3.12. The results show that for the clockwise transfer the  $\Delta v$  is smaller than the required for the counterclockwise transfer. It can be noted, although not very large, how the solar radiation pressure modifies the  $\Delta v$  required for each case of the clockwise and counterclockwise transfer.

Table 3.12 - Parameters for L<sub>5</sub> and the Earth.

Point	$x$ (nd)	$y$ (nd)	$v$ (nd)
L <sub>5</sub> (initial)	0.487849	-0.866025	0
Earth (final)	-0.021248624678959	0.015770493825419	0

SOURCE: Author

Figure 3.11 - Transfers from L<sub>5</sub> to the Earth.



SOURCE: Adapted from Oliveira et al. (2016).

The results found here indicate that the solar radiation pressure modifies the trajectory of the spacecraft, changing the initial flight path angle, also modifying the energy required for the transfers. When different locations of the Sun are considered, the  $\Delta v$  required in each transfer changes. Therefore, it is possible to choose the right moment to perform the maneuver such that the magnitudes of the impulses to be applied are minimized. So, the moment to start the maneuver is a type of indirect control. For the Earth-Moon system the differences are small, due to the large gravity of the bodies involved.

### 3.2 Sun-Earth system

Table 3.13 shows the parameters used to calculate the acceleration of the solar radiation pressure in the Sun-Earth system, as described in section 2.1. The geometry of the problem is shown in Figure 3.1, where  $M_1$  represents the Sun,  $M_2$  the Earth and  $M_3$  the spacecraft.

Table 3.13 - Parameters of the Sun-Earth system.

$r_s$	<i>variable</i>
$S_r/c$	$4.56 \times 10^{-6} \text{ N/m}^2$
$\mu_{sun}$	$1.327 \times 10^{20} \text{ m}^3/\text{s}^2$
$\mu_{earth}$	$3.986 \times 10^{14} \text{ m}^3/\text{s}^2$
<i>A/m ratio</i>	$10.0 \text{ m}^2/\text{kg}$
$C_r$	1.5

SOURCE: Luzum et al. (2011)

Table 3.14 shows the canonical values used in the equation of motion of the Sun-Earth system, as described in section 2.2.

Table 3.14 - Canonical system of units for the Sun-Earth system.

Unit of distance	$1.496 \times 10^8 \text{ km}$
Unit of time	$3.156 \times 10^7 \text{ sec}$
Unit of velocity	$29.785 \text{ km/s}$

SOURCE: Luzum et al. (2011)

Table 3.15 presents the positions of the Lagrange points and the primaries of the Sun-Earth system which are considered for the orbital transfers.

Table 3.15 - Lagrange points and primaries of the Sun-Earth system.

Point	$x$ (nd)	$y$ (nd)
L <sub>1</sub>	0.9899909	0
L <sub>2</sub>	1.0100702	0
L <sub>3</sub>	-1.0000013	0
L <sub>4</sub>	0.4999969	0.8660254
L <sub>5</sub>	0.4999969	-0.8660254
Sun	$-3.0035615 \times 10^{-6}$	0
Earth	0.9999970	0

SOURCE: Author

Where the position of Sun is given by:  $-\mu = -M_{Earth}/(M_{Sun} + M_{Earth})$ , and the position of Earth is given by:  $1 - \mu$ .

The families of transfer orbits studied here consider transfers between the collinear Lagrangian points in the Sun-Earth system in two directions: clockwise and counterclockwise. The results are organized in plots of the  $\Delta v$  against the initial flight path angle (in degrees) in the rotating frame. Figures 3.12 to 3.15 show the results.

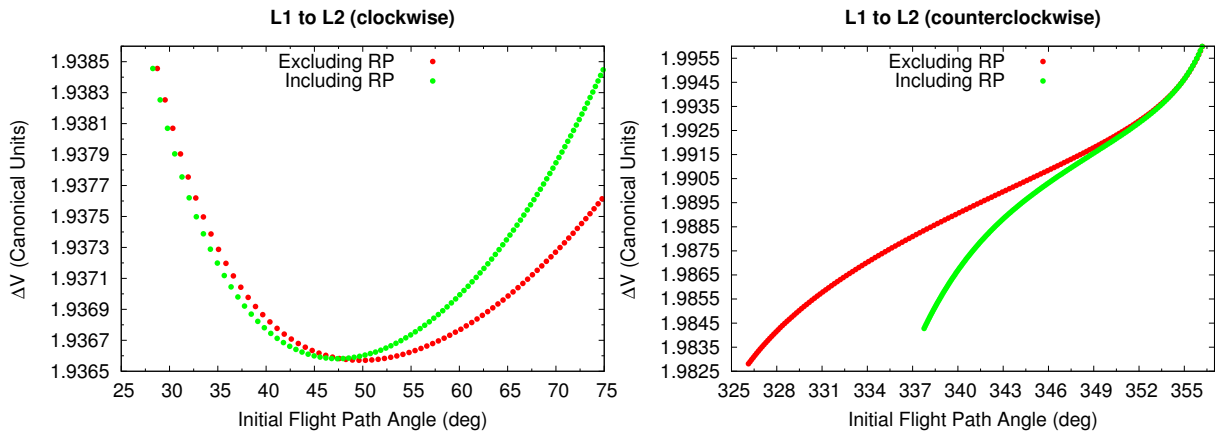
Figure 3.12 shows the results for tranfers from  $L_1$ , the initial point, to  $L_2$ , the final point. The initial conditions, in the rotating frame of reference, for this transfer are given in Table 3.16.

Table 3.16 - Parameters for  $L_1$  and  $L_2$ .

Point	$x$ (nd)	$y$ (nd)	$v$ (nd)
$L_1$ (initial)	0.9899909	0	0
$L_2$ (final)	1.0100702	0	0

SOURCE: Author

Figure 3.12 - Transfers from  $L_1$  to  $L_2$ .



SOURCE: Oliveira et al. (2016).

Figure 3.13 shows the results for tranfers from  $L_2$ , the initial point, to  $L_1$ , the final

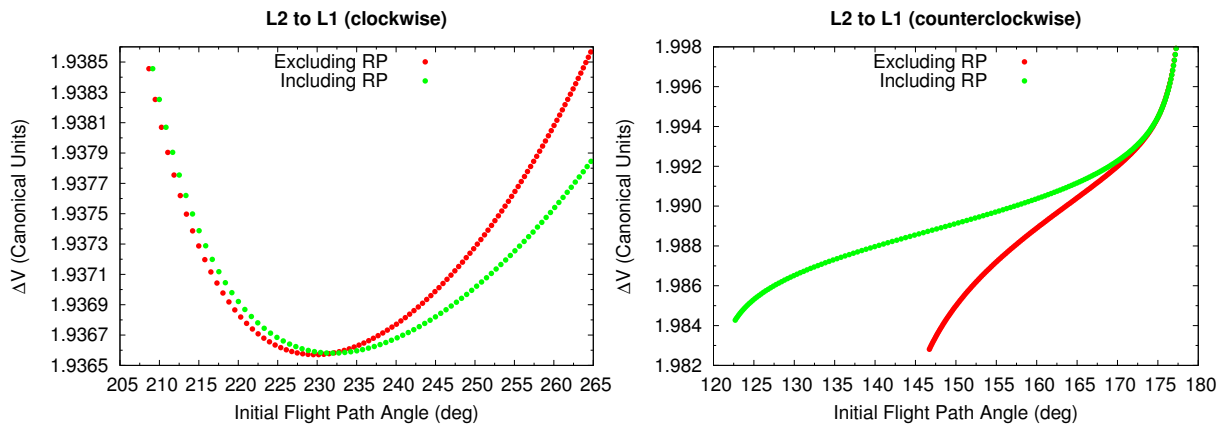
point. The initial conditions, in the rotating frame of reference, for this transfer are given in Table 3.17.

Table 3.17 - Parameters for  $L_2$  and  $L_1$ .

Point	$x$ (nd)	$y$ (nd)	$v$ (nd)
$L_2$ (initial)	1.0100702	0	0
$L_1$ (final)	0.9899909	0	0

SOURCE: Author

Figure 3.13 - Transfers from  $L_2$  to  $L_1$ .



SOURCE: Oliveira et al. (2016).

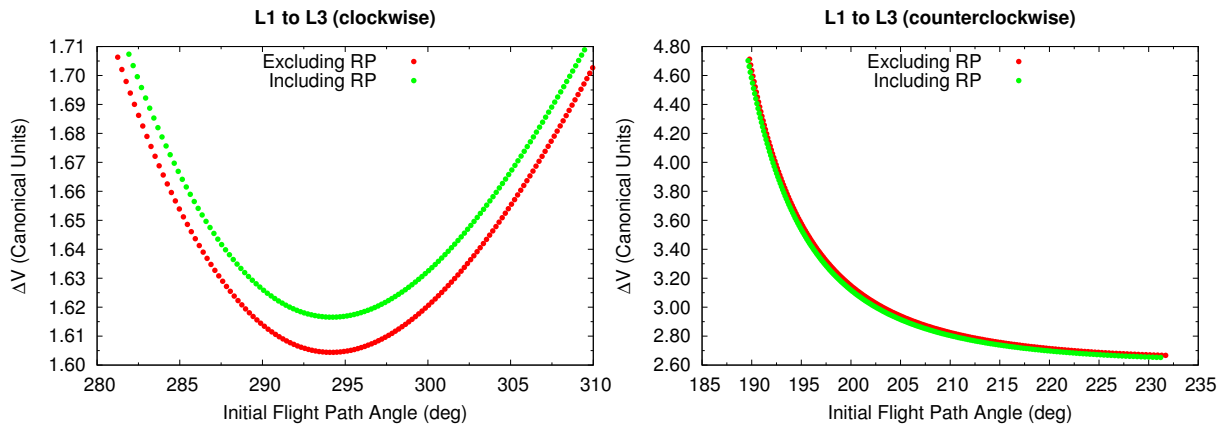
Figure 3.14 shows the results for transfers from  $L_1$ , the initial point, to  $L_3$ , the final point. The initial conditions, in the rotating frame of reference, for this transfer are given in Table 3.18.

Table 3.18 - Parameters for  $L_1$  and  $L_3$ .

Point	$x$ (nd)	$y$ (nd)	$v$ (nd)
$L_1$ (initial)	0.9899909	0	0
$L_3$ (final)	-1.0000013	0	0

SOURCE: Author

Figure 3.14 - Transfers from  $L_1$  to  $L_3$ .



SOURCE: Oliveira et al. (2016).

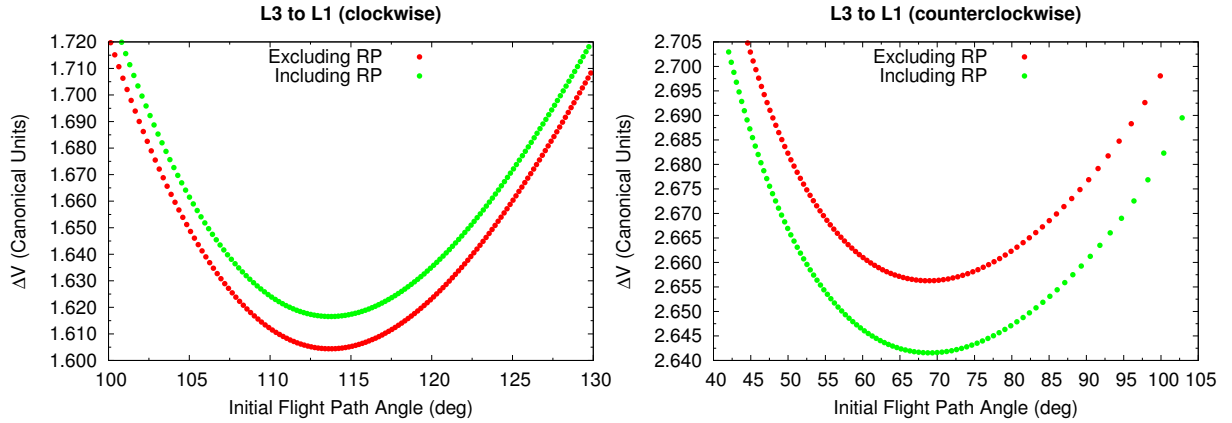
Figure 3.15 shows the results for transfers from  $L_3$ , the initial point, to  $L_1$ , the final point. The initial conditions, in the rotating frame of reference, for this transfer are given in Table 3.19.

Table 3.19 - Parameters for  $L_3$  and  $L_1$ .

Point	$x$ (nd)	$y$ (nd)	$v$ (nd)
$L_3$ (initial)	-1.0000013	0	0
$L_1$ (final)	0.9899909	0	0

SOURCE: Author

Figure 3.15 - Transfers from  $L_3$  to  $L_1$ .



SOURCE: Oliveira et al. (2016).

The results show the existence of two families of solutions. They also show that the effects of the solar radiation pressure, in terms of finding solutions with minimum fuel consumption, are small in those transfers. There are important effects in terms of changing the initial flight path angle. Looking in the  $x$  axis, it is clear that the initial flight path angle is different for a given variation of velocity. At the same time, looking in the  $y$  axis, it is clear that the solar radiation pressure increases the variation of velocity required for the same initial flight path angle. Looking for a more global result, the situations considering the solar radiation pressure have minimum variations of velocity that are larger when compared to the cases with no solar radiation pressure.

The next study considers transfers between the Lagrangian points and the Earth, also considering several values for the time of flight and two directions: clockwise and counterclockwise. Figures 3.16 to 3.20 show the results, plotting the variation of velocity against the initial flight angle, as done before.

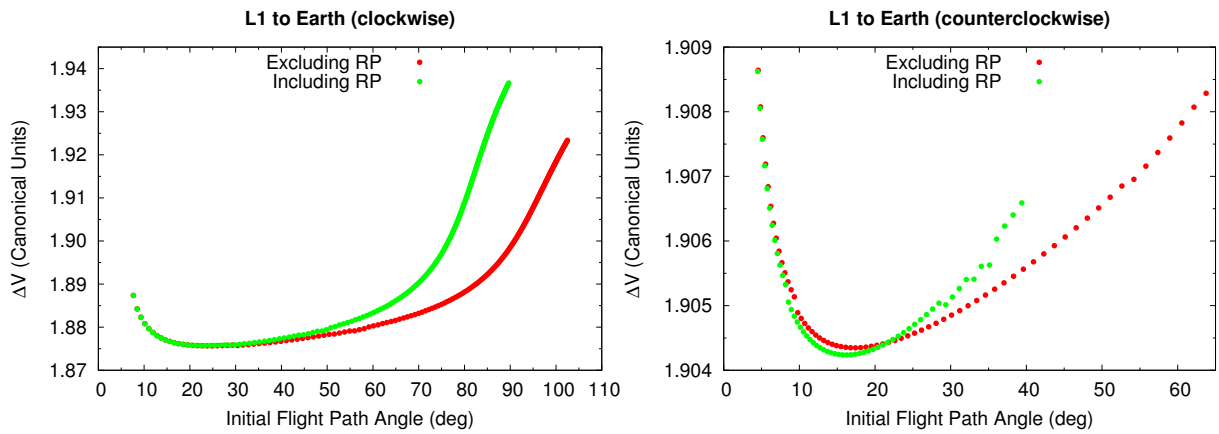
Figure 3.16 shows the results for transfers from  $L_1$ , the initial point, to the Earth, the final point. The initial conditions, in the rotating frame of reference, for this transfer are given in Table 3.20.

Table 3.20 - Parameters for  $L_1$  and the Earth.

Point	$x$ (nd)	$y$ (nd)	$v$ (nd)
$L_1$ (initial)	0.9899909	0	0
Earth (final)	1.0004649	0	0

SOURCE: Author

Figure 3.16 - Transfers from  $L_1$  to the Earth.



SOURCE: Oliveira et al. (2016).

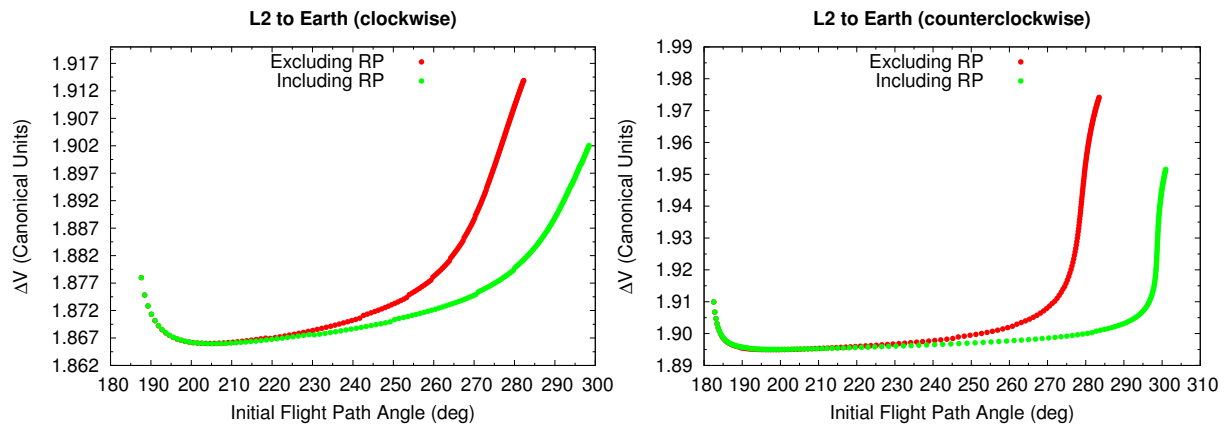
Figure 3.17 shows the results for transfers from  $L_2$ , the initial point, to the Earth, the final point. The initial conditions, in the rotating frame of reference, for this transfer are given in Table 3.21.

Table 3.21 - Parameters for  $L_2$  and the Earth.

Point	$x$ (nd)	$y$ (nd)	$v$ (nd)
$L_2$ (initial)	1.0100702	0	0
Earth (final)	0.9995291	0	0

SOURCE: Author

Figure 3.17 - Transfers from L<sub>2</sub> to the Earth.



SOURCE: Oliveira et al. (2016).

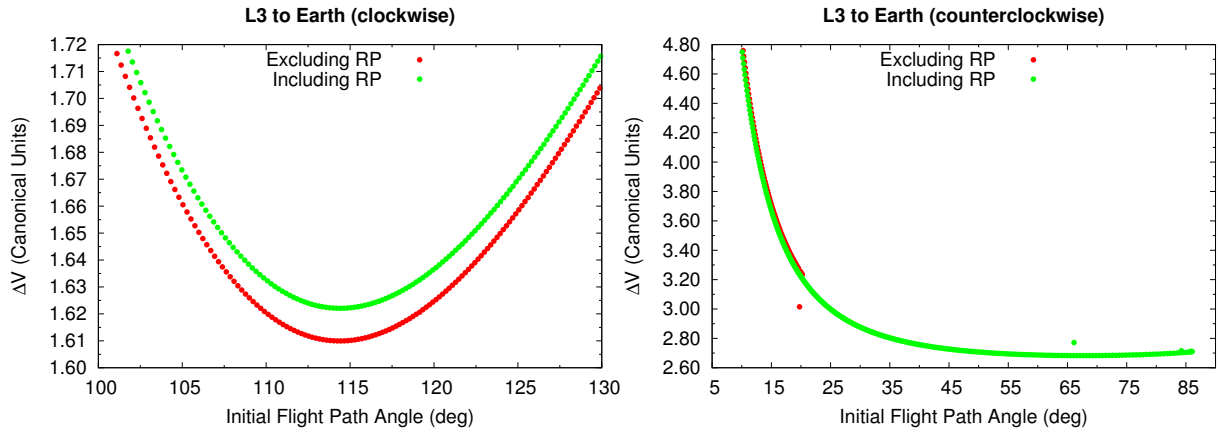
Figure 3.18 shows the results for transfers from L<sub>3</sub>, the initial point, to the Earth, the final point. The initial conditions, in the rotating frame of reference, for this transfer are given in Table 3.22.

Table 3.22 - Parameters for L<sub>3</sub> and the Earth.

Point	$x$ (nd)	$y$ (nd)	$v$ (nd)
L <sub>3</sub> (initial)	-1.0000013	0	0
Earth (final)	1.0004649	0	0

SOURCE: Author

Figure 3.18 - Transfers from  $L_3$  to the Earth.



SOURCE: Oliveira et al. (2016).

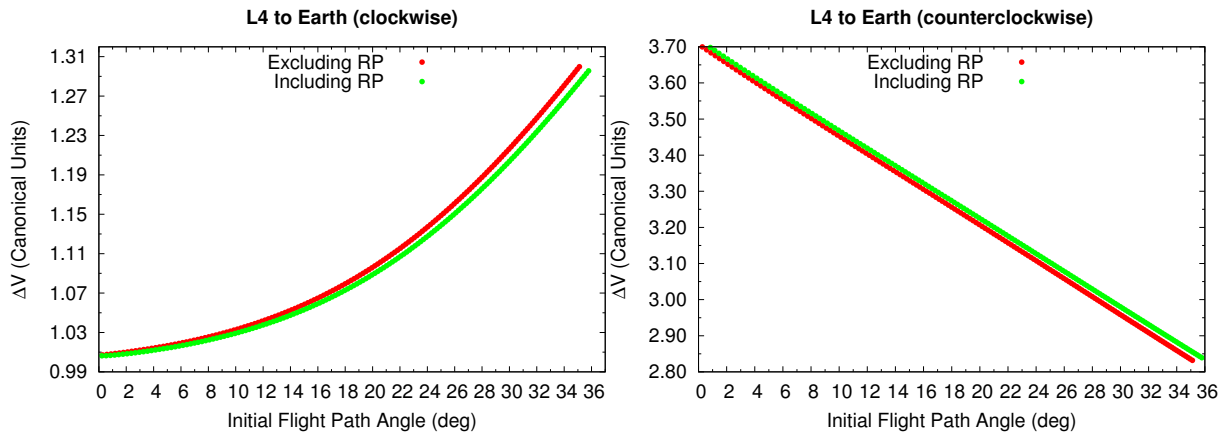
Figure 3.19 shows the results for transfers from  $L_4$ , the initial point, to the Earth, the final point. The initial conditions, in the rotating frame of reference, for this transfer are given in Table 3.23.

Table 3.23 - Parameters for  $L_4$  and the Earth.

Point	$x$ (nd)	$y$ (nd)	$v$ (nd)
$L_4$ (initial)	0.4999969	0.8660254	0
Earth (final)	1.0002309	-0.0004052	0

SOURCE: Author

Figure 3.19 - Transfers from L<sub>4</sub> to the Earth.



SOURCE: Oliveira et al. (2016).

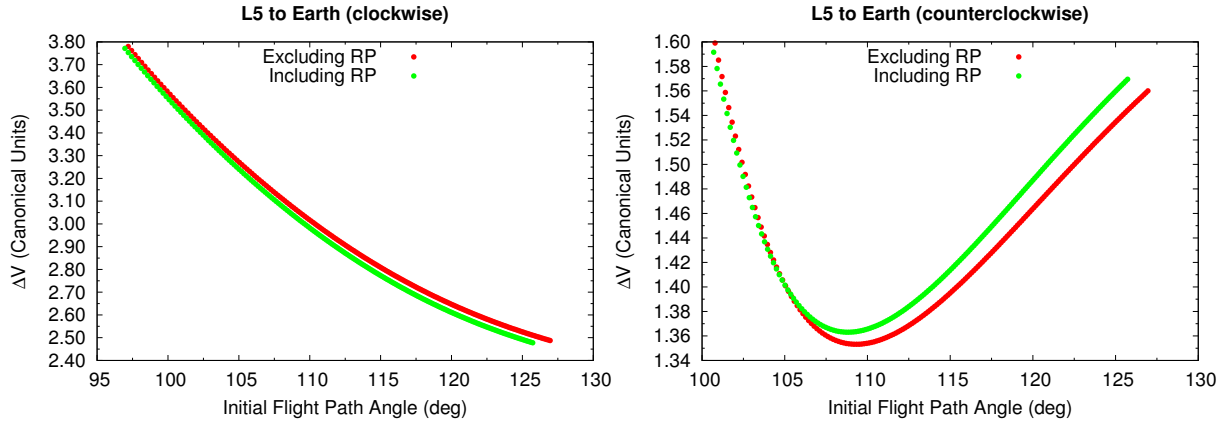
Figure 3.20 shows the results for transfers from L<sub>5</sub>, the initial point, to the Earth, the final point. The initial conditions, in the rotating frame of reference, for this transfer are given in Table 3.24.

Table 3.24 - Parameters for L<sub>5</sub> and the Earth.

Point	$x$ (nd)	$y$ (nd)	$v$ (nd)
L <sub>5</sub> (initial)	0.4999969	-0.8660254	0
Earth (final)	1.0002309	0.0004052	0

SOURCE: Author

Figure 3.20 - Transfers from L<sub>5</sub> to the Earth.



SOURCE: Oliveira et al. (2016).

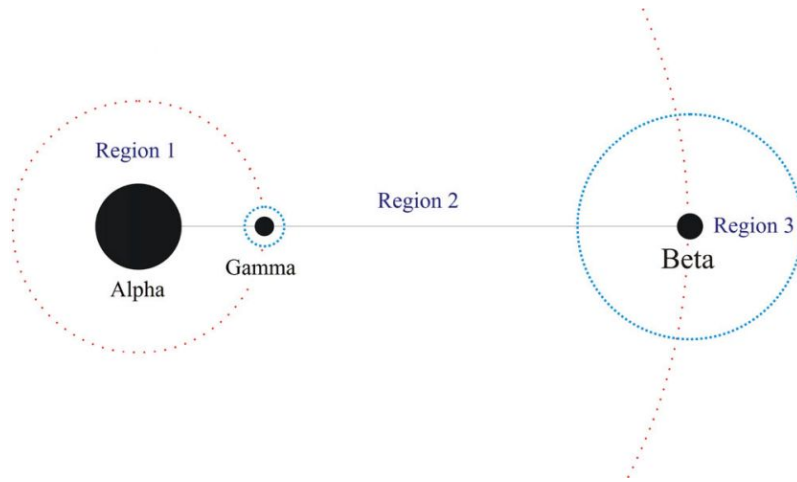
The results are similar to the ones obtained for the transfers between the Lagrangian points. The new aspect is the existence of some cases (like the one with transfers from L<sub>1</sub> to the Earth) where the global minimum occurs when the radiation pressure is considered, so this perturbing force is helping in the maneuver.

### 3.3 2001SN263 system

This section of results shows transfers in an asteroid system. The asteroid considered is the 2001SN263 (ARAÚJO et al., 2012; ARAÚJO et al., 2015), which is a triple system under study for the Aster mission (SUKHANOV et al., 2010), the First Brazilian Deep Space Mission. According to Araujo et al. (2012), this asteroid system was chosen taking into account the advantages of sending a spacecraft to a multiple system of asteroids, which increases the range of possible scientific investigations (for example into the internal structure, formation process and dynamical evolution) with respect to the economy of fuel, flight time and telecommunication system required in comparison to a similar mission aimed at an asteroid of the main belt.

Although it is a triple system, the full dynamics is not considered to calculate the Lagrangian points and the transfers itself. We follow the nomenclature adopted by Araujo et al. (2012) for this system. We refer to the central body (the most massive body) as Alpha, to the second most massive body as Beta (outer) and to the least massive body as Gamma (inner). Figure 3.21 is a representation of the system 2001SN263.

Figure 3.21 - Representation of the triple system 2001SN263.

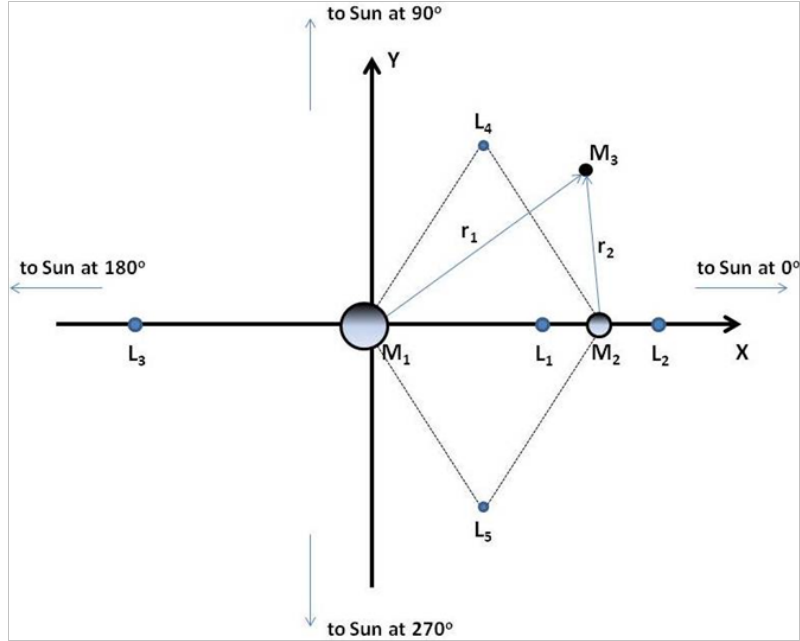


The blue circles represent Hill's radii of Beta and Gamma. The red dotted circles represent the collision-lines with Gamma and Beta, and by definition, the limits of the internal regions 1 and 2.

SOURCE: Araujo et al. (2012)

Instead, only one double system is considered in this work, which includes the asteroids Alpha and Beta. The geometry of the problem is shown in Figure 3.22, where  $M_1$  represents the asteroid Alpha,  $M_2$  the asteroid Beta and  $M_3$  the spacecraft.

Figure 3.22 - Reference frame in the planar circular restricted three-body problem.



SOURCE: Oliveira et al. (2016).

In order to measure and verify the effects of the solar radiation pressure, five different cases are presented. In the first case the solar radiation pressure is not considered. The next cases consider the Sun in four different positions with respect to the system when the maneuvers are followed. It is assumed that the Sun is situated at 0 degree, 90 degrees, 180 degrees and 270 degrees with respect to the system. These locations are shown in Figure 3.22.

This system has an eccentricity  $e = 0.48$  and a semi-major axis  $a = 1.99 \text{ au}$  (ARAUJO et al., 2012). So, at the periapsis, the distance from the Sun is  $1.03 \text{ au}$  and, at the apoapsis, the distance from the Sun is  $2.94 \text{ au}$ . Thereby, these two orbital positions were considered to perform the orbital maneuvers.

Table 3.25 shows the parameters used to calculate the acceleration value of the solar radiation pressure in the 2001SN263 system, as described in section 2.1, where  $r_e$  is the Sun-Earth distance. In this system, two values of area/mass ratio are used:  $0.1$  and  $0.01 \text{ m}^2/\text{kg}$ .

Table 3.25 - Parameters of the 2001SN263 system.

$r_e$	$1.495978707 \times 10^{11} m$
$r_s$ at periapsis	$1.03 r_e$
$r_s$ at apoapsis	$2.94 r_e$
$S_r/c$	$4.56 \times 10^{-6} N/m^2$
$\mu_{Alpha}$	$6.123 \times 10^2 m^3/s^2$
$\mu_{Beta}$	$1.605 \times 10^1 m^3/s^2$
$A/m$ ratio	0.01 and $0.1 m^2/kg$
$C_r$	1.5

SOURCE: Luzum et al. (2011), Araujo et al. (2012)

Table 3.26 shows the canonical values used in the equation of motion of the 2001SN263 system, as described in section 2.2.

Table 3.26 - Canonical system of units for the 2001SN263 system.

Unit of distance	16.63 km
Unit of time	$5.375 \times 10^5$ sec
Unit of velocity	$1.944 \times 10^{-4}$ km/s

SOURCE: Araujo et al. (2012), Araujo et al. (2015)

Table 3.27 presents the positions of the Lagrange points and the primaries of the 2001SN263 system which are considered for the orbital transfers.

Table 3.27 - Lagrange points and primaries of the 2001SN263 system.

Point	$x$ (nd)	$y$ (nd)
L <sub>1</sub>	0.7839	0
L <sub>2</sub>	1.1927	0
L <sub>3</sub>	-1.011	0
L <sub>4</sub>	0.4745	0.8660
L <sub>5</sub>	0.4745	-0.8660
Alpha	-0.0255	0
Beta	0.9745	0

SOURCE: Author

Where the position of Alpha is given by:  $-\mu = -M_{Beta}/(M_{Alpha} + M_{Beta})$ , and the position of Beta is given by:  $1 - \mu$ .

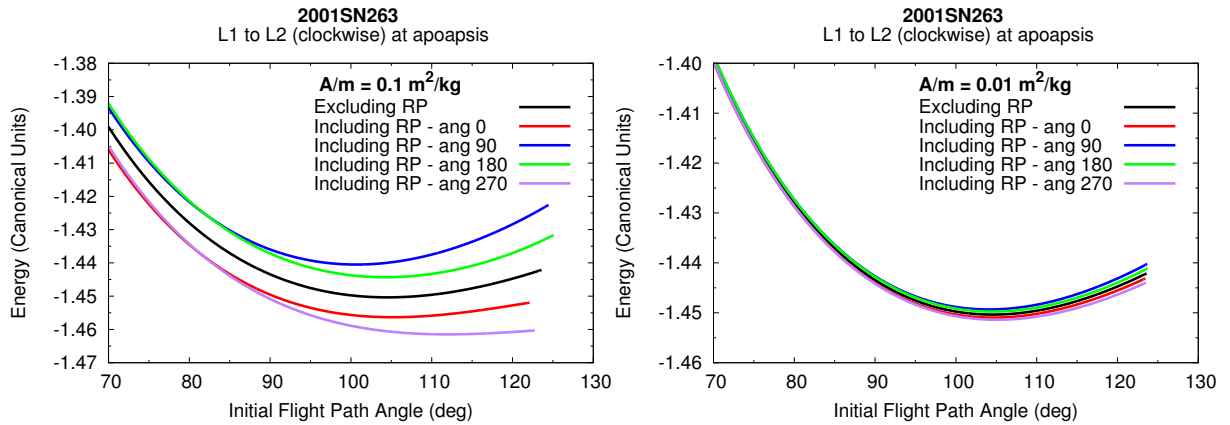
First, transfers between the collinear Lagrangian points are considered. Figures 3.23 to 3.27 show the results. Figures 3.23 and 3.24 show the results for transfers from  $L_1$ , the initial point, to  $L_2$ , the final point. The initial conditions, in the rotating frame of reference, for this transfer are given in Table 3.28.

Table 3.28 - Parameters for  $L_1$  and  $L_2$ .

Point	$x$ (nd)	$y$ (nd)	$v$ (nd)
$L_1$ (initial)	0.7839	0	0
$L_2$ (final)	1.1927	0	0

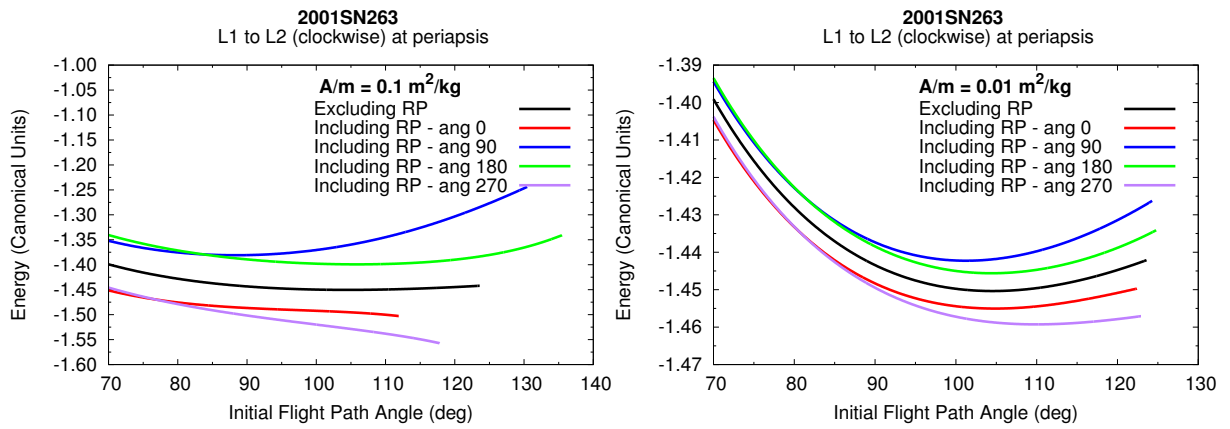
SOURCE: Author

Figure 3.23 - Transfers from  $L_1$  to  $L_2$ , asteroid at apoapsis.



SOURCE: Oliveira et al. (2016).

Figure 3.24 - Transfers from  $L_1$  to  $L_2$ , asteroid at periapsis.



SOURCE: Oliveira et al. (2016).

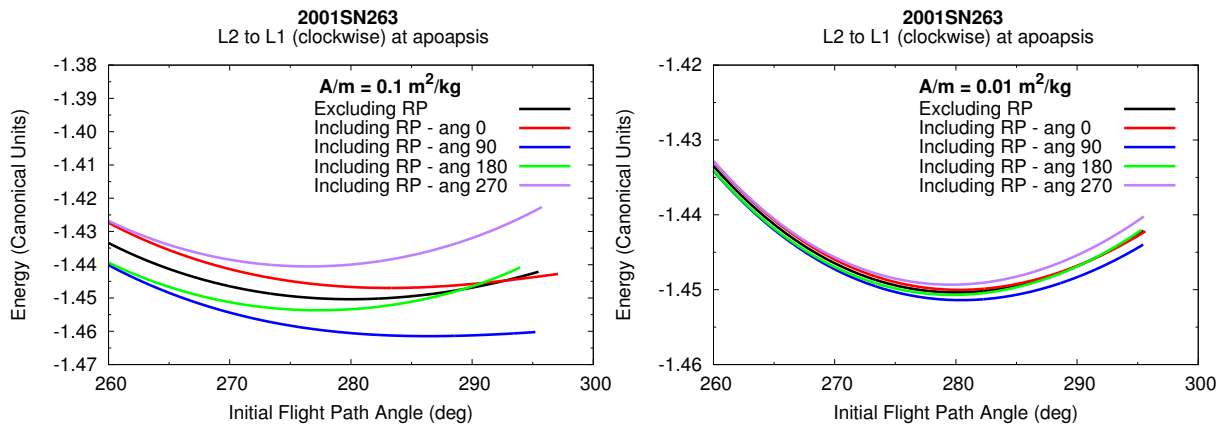
Figures 3.25 and 3.26 show the results for transfers from  $L_2$ , the initial point, to  $L_1$ , the final point. The initial conditions, in the rotating frame of reference, for this transfer are given in Table 3.29.

Table 3.29 - Parameters for  $L_2$  and  $L_1$ .

Point	$x$ (nd)	$y$ (nd)	$v$ (nd)
$L_2$ (initial)	1.1927	0	0
$L_1$ (final)	0.7839	0	0

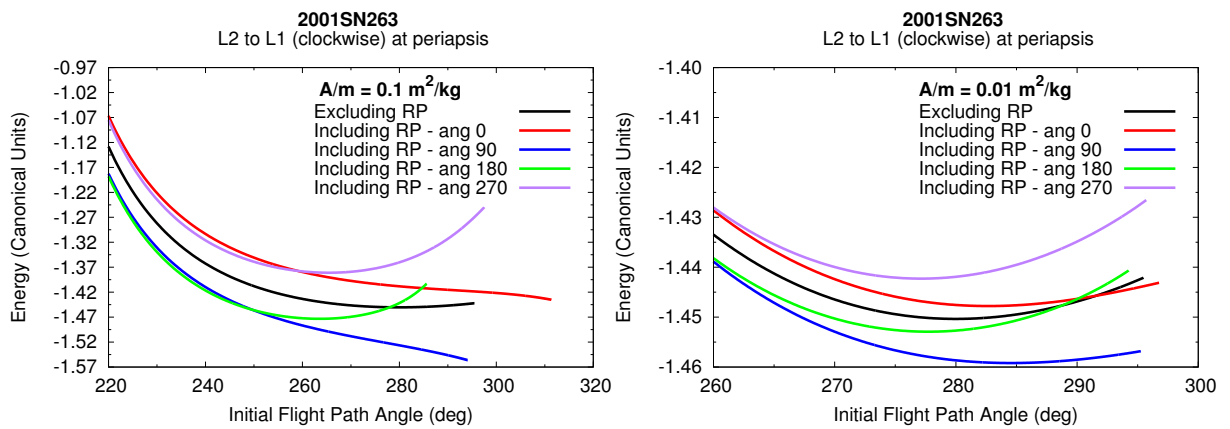
SOURCE: Author

Figure 3.25 - Transfers from  $L_2$  to  $L_1$ , asteroid at apoapsis.



SOURCE: Oliveira et al. (2016).

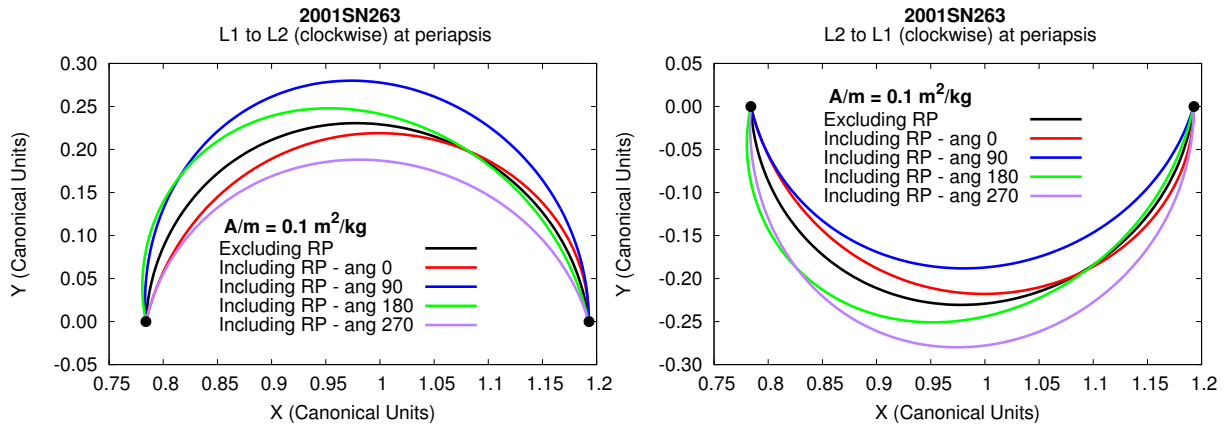
Figure 3.26 - Transfers from  $L_2$  to  $L_1$ , asteroid at periapsis.



SOURCE: Oliveira et al. (2016).

Figure 3.27 shows the trajectories for transfers from  $L_1$  to  $L_2$  and from  $L_2$  to  $L_1$ . The initial conditions, in the rotating frame of reference, for these transfers are given in Tables 3.28 and 3.29.

Figure 3.27 - Trajectories between the collinear Lagrangian points, asteroid at periapsis.



SOURCE: Oliveira et al. (2016).

The results show that the solar radiation pressure now has strong effects in the dynamics of the transfers. Even the ranges of initial flight path angle are different. The differences in the variations of velocity between both situations are larger and there are several cases where the solar radiation pressure decreases the variation of velocity required. The effects of the distance Sun-asteroid, periapsis and apoapsis position, and direction of the Sun are also considered. It is important to note the strong effect of the solar radiation pressure when the spacecraft is travelling against the Sun, in the curve with 180 degrees. And it is important to notice how the area/mass ratio modifies the results, decreasing and increasing the values of  $\Delta v$ .

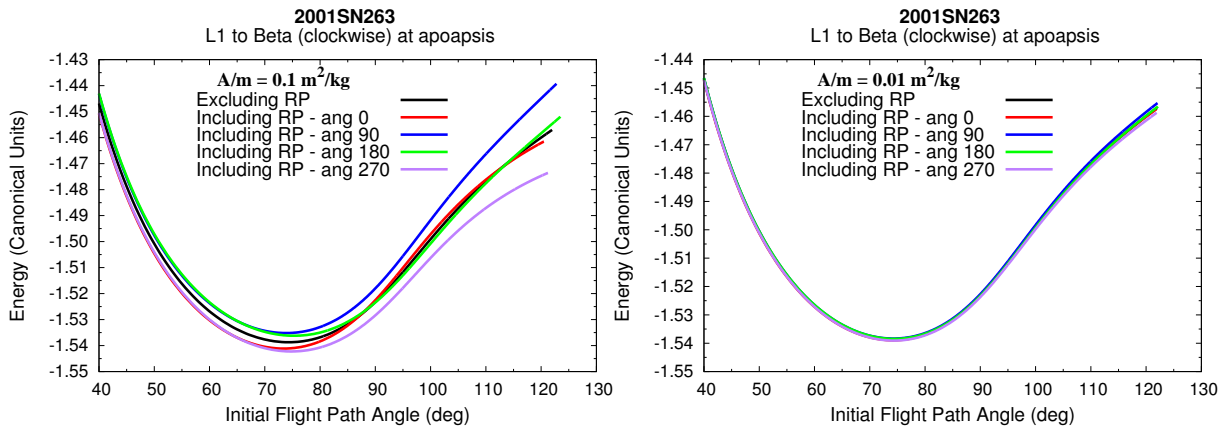
Now, transfers from the collinear Lagrangian points to the smaller asteroid (Beta) are studied. Figures 3.28 to 3.32 show the results. Figures 3.28 and 3.29 show the results for tranfers from  $L_1$ , the initial point, to the asteroid Beta, the final point. The initial conditions, in the rotating frame of reference, for this transfer are given in Table 3.30.

Table 3.30 - Parameters for  $L_1$  and Beta.

Point	$x$ (nd)	$y$ (nd)	$v$ (nd)
$L_1$ (initial)	0.7839	0	0
Beta (final)	1.0039	0	0

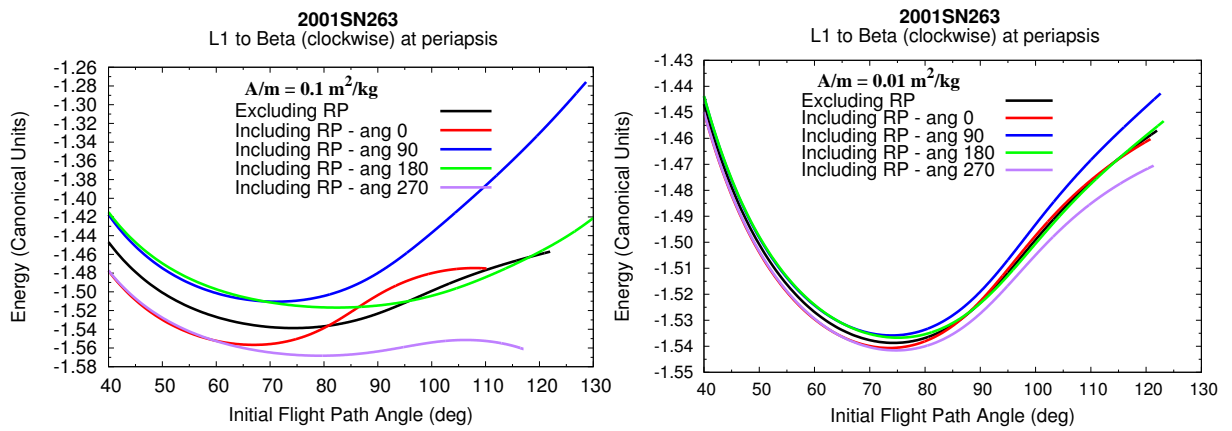
SOURCE: Author

Figure 3.28 - Transfers from  $L_1$  to Beta, asteroid at apoapsis.



SOURCE: Oliveira et al. (2016).

Figure 3.29 - Transfers from  $L_1$  to Beta, asteroid at periapsis.



SOURCE: Oliveira et al. (2016).

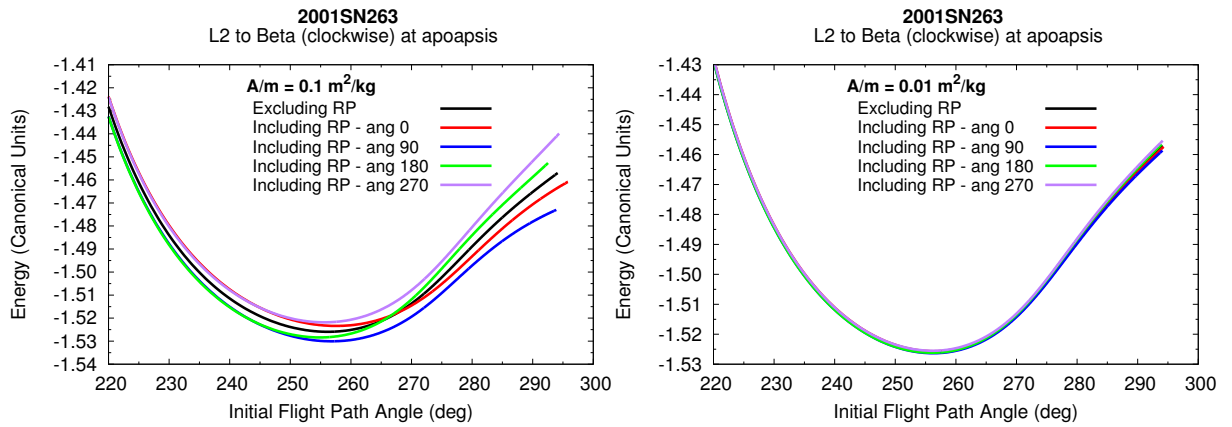
Figures 3.30 and 3.31 show the results for transfers from  $L_2$ , the initial point, to the asteroid Beta, the final point. The initial conditions, in the rotating frame of reference, for this transfer are given in Table 3.31.

Table 3.31 - Parameters for L<sub>2</sub> and Beta.

Point	$x$ (nd)	$y$ (nd)	$v$ (nd)
L <sub>2</sub> (initial)	1.1927	0	0
Beta (final)	0.9450	0	0

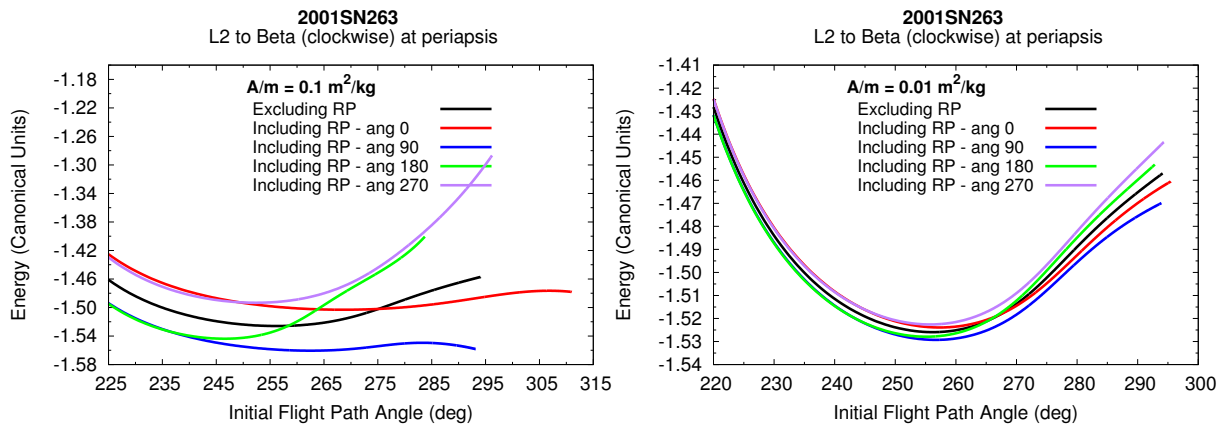
SOURCE: Author

Figure 3.30 - Transfers from L<sub>2</sub> to Beta, asteroid at apoapsis.



SOURCE: Oliveira et al. (2016).

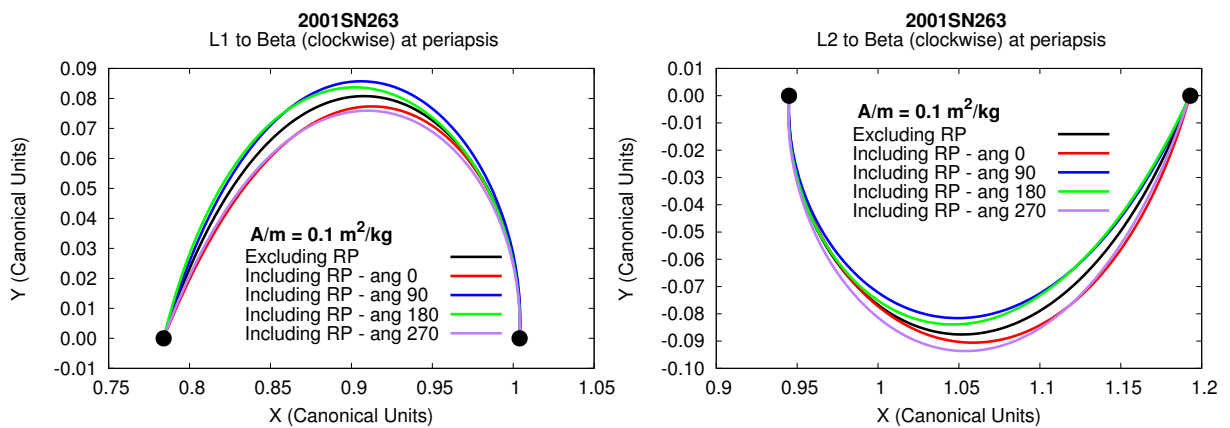
Figure 3.31 - Transfers from  $L_2$  to Beta, asteroid at periaapsis.



SOURCE: Oliveira et al. (2016).

Figure 3.32 shows the trajectories for tranfers from  $L_1$  to Beta and from  $L_2$  to Beta. The initial conditions, in the rotating frame of reference, for these transfers are given in Tables 3.30 and 3.31.

Figure 3.32 - Trajectories between the collinear Lagrangian points to Beta, asteroid at periaapsis.



SOURCE: Oliveira et al. (2016).

The results are similar to the ones obtained for the transfers between the Lagrangian

points. When considering smaller bodies, like the asteroid system, the importance of the solar radiation pressure increases, and the locations and values of the best transfers are different. It is also possible to choose the right moment to perform the maneuver, such that the magnitudes of the impulses to be applied are minimized. The difference is that, in those cases, the savings are very large.

### 3.4 1996FG<sub>3</sub> system

This session studies the effects of the solar radiation pressure in the trajectories of a spacecraft making bi-impulsive transfers between the collinear Lagrange points of a double asteroid system. The system considered in this study is formed by the double asteroid 1996FG<sub>3</sub> (WOLTERS et al., 2011; SCHEIRICH et al., 2015), which was already a target candidate for the MarcoPolo-R mission (MICHEL et al., 2014), but due to the budget constraints the mission was canceled. In a system formed by asteroids, the solar radiation pressure has a significant influence in the transfers paths, as showed in the previous section. This occurs because the gravitational forces in these systems are smaller, if compared with systems formed by larger bodies. Solutions with lower and higher fuel consumption can be found by adding the solar radiation pressure. The solar radiation pressure is not used as a control, but its effects over the transfers were measured. Thus, for a small system of primaries, such as an asteroid system, it is very important to take into account this force to make sure that the spacecraft will reach the desired point. Besides that, it is also possible to choose the best moment to start the maneuver such that fuel consumption is minimized.

One approach for a mission that would go closer to the Sun is that it could carry a solar sail and collect material from the Sun and, when it returns to the Earth, this material could be recovered and studied. The Genesis mission (LO et al., 1998) was launched in 2001 and returned to the Earth in 2004 with material collected from the solar wind. The Genesis spacecraft reached a Halo orbit around the Sun-Earth Lagrange point  $L_1$ , which is about  $0.989 au$  from the Sun. The asteroid system 1996FG<sub>3</sub> has an elliptical orbit, which has its periapsis at  $0.685 au$  from the Sun. In this way, a spacecraft that has this asteroid system as a target will reach a distance much closer to the Sun than the distance reached by the Genesis mission. Thus, such mission could study the asteroid system and also collect material from the solar wind more efficiently.

The asteroid 1996FG<sub>3</sub> has an elliptical orbit, so, in order to verify the influence of the solar radiation pressure on the spacecraft during the transfers between both asteroids, two points of the orbit of the asteroid are considered for the simulations,

the closest and the furthest to the Sun. The periapsis (0.685 *au*) and the apoapsis (1.423 *au*) were chosen to verify how influent the solar radiation pressure is in its maximum and minimum values.

Table 3.32 shows the parameters used to calculate the acceleration due to the solar radiation pressure in the 1996FG3 system, as described in section 2.1, where  $r_e$  is the Sun-Earth distance.

Table 3.32 - Parameters of the 1996FG3 system.

$r_e$	$1.495978707 \times 10^{11}m$
$r_s$ at periapsis	$0.685 r_e$
$r_s$ at apoapsis	$1.423 r_e$
$S_r/c$	$4.56 \times 10^{-6} N/m^2$
$\mu_{Alpha}$	$2.336 \times 10^2 m^3/s^2$
$\mu_{Beta}$	$0.667 \times 10^1 m^3/s^2$
$A/m$ ratio	0.02, 0.1 and 0.5 $m^2/kg$
$C_r$	1.5

SOURCE: Luzum et al. (2011), Wolters et al. (2011), Scheirich et al. (2015)

Three values of area/mass are used: 0.02  $m^2/kg$ , 0.1  $m^2/kg$  and 0.5  $m^2/kg$ . This wide range of values are considered to verify the effects of the solar radiation pressure over many types of missions. A mission with a simple spacecraft and no or small solar panels has a small area/mass ratio, but when it is considered a mission with a larger panel, for example to study and catch particles from the solar wind, the area/mass ratio increases.

We follow the same nomenclature adopted in the previous section for this system. We refer to the central body (the most massive body) as Alpha and to the second most massive body as Beta. Table 3.33 shows the values for the parameters of the system considered in this study, as described in section 2.2, where  $M_1$  is the main asteroid (Alpha) and  $M_2$  is the smaller one (Beta).

Table 3.33 - Canonical system of units for the binary asteroid 1996FG3.

Unit of distance	2.8 km
Unit of time	$6.005 \times 10^4$ sec
Unit of velocity	$2.929 \times 10^{-4}$ km/s

SOURCE: Wolters et al. (2011), Scheirich et al. (2015)

Table 3.34 presents the positions of the Lagrange points and the primaries of the 1996FG3 system which are considered for the orbital transfers.

Table 3.34 - Lagrange points and primaries of the 1996FG3 system.

Point	$x$ (nd)	$y$ (nd)
L <sub>1</sub>	0.776610957892686	0
L <sub>2</sub>	1.197128944950619	0
L <sub>3</sub>	-1.011572889921064	0
L <sub>4</sub>	0.472222222222222	0.866025403784439
L <sub>5</sub>	0.472222222222222	-0.866025403784439
Alpha	-0.027777777777778	0
Beta	0.972222222222222	0

SOURCE: Author

Where the position of Alpha is given by:  $-\mu = -M_{Beta}/(M_{Alpha} + M_{Beta})$ , and the position of Beta is given by:  $1 - \mu$ .

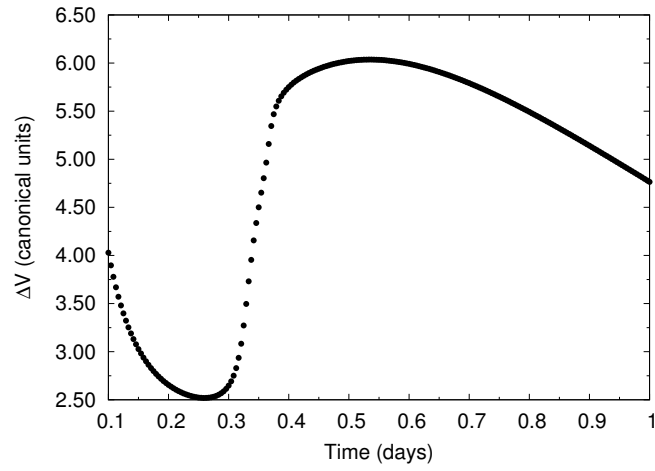
As mentioned above, the purpose of this section is to study orbital transfers around the binary asteroid 1996FG<sub>3</sub>. Thus, some simulations of orbital transfers between the collinear Lagrange points of this system have been done. The geometry of the problem is shown in Figure 3.2, where M<sub>1</sub> represents the asteroid Alpha, M<sub>2</sub> the asteroid Beta and M<sub>3</sub> the spacecraft.

As a result, it is shown the plots with the variation of velocity  $\Delta v$  against time and the variation of velocity  $\Delta v$  against the initial flight path angle ( $fpa$ ), as done in previous sections. It is also presented, in Tables 3.37 to 3.42, the values that indicate the minimums found for  $\Delta v$ , the  $fpa$  and the respective transfer times for the four different initial position of the Sun. It is also included one more case, which is when

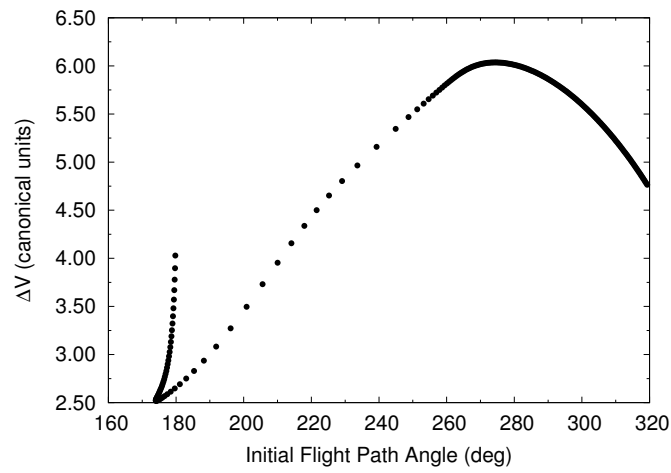
the solar radiation pressure is neglected. This is done to clearly show the effects of the solar radiation pressure.

Figure 3.33 shows the required  $\Delta v$  to move the probe from the Lagrange point  $L_1$  to  $L_3$ , when the asteroid is at its periapsis and the solar radiation pressure is not considered. Figure 3.33a plots the  $\Delta v$  as a function of time and Figure 3.33b plots the  $\Delta v$  as a function of the  $fpa$ . Figure 3.34 shows the trajectories for the minimum and maximum variation of velocity. Note that the trajectory for the minimum  $\Delta v$  is direct, passing very close to Alpha, what requires low values of  $\Delta v_1$  and  $\Delta v_2$ , resulting in a lower final  $\Delta v$ . However, the trajectory for the maximum  $\Delta v$  makes a complete revolution before reaching  $L_3$ , which requires high values of  $\Delta v_1$  and  $\Delta v_2$ , resulting in a higher final  $\Delta v$ .

Figure 3.33 - Transfers from  $L_1$  to  $L_3$  with the asteroid at periaapsis and excluding the solar radiation pressure.



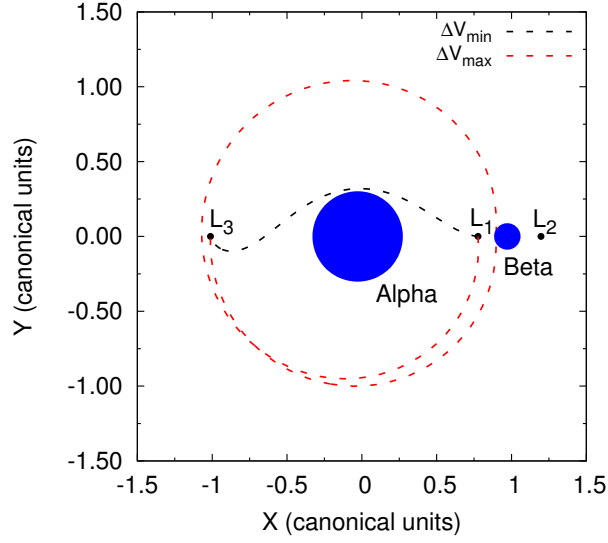
(a)  $\Delta v$  as function of time.



(b)  $\Delta v$  as function of the flight path angle.

SOURCE: Oliveira et al. (2017b).

Figure 3.34 - Trajectories from  $L_1$  to  $L_3$  for  $\Delta v_{min}$  and  $\Delta v_{max}$ .



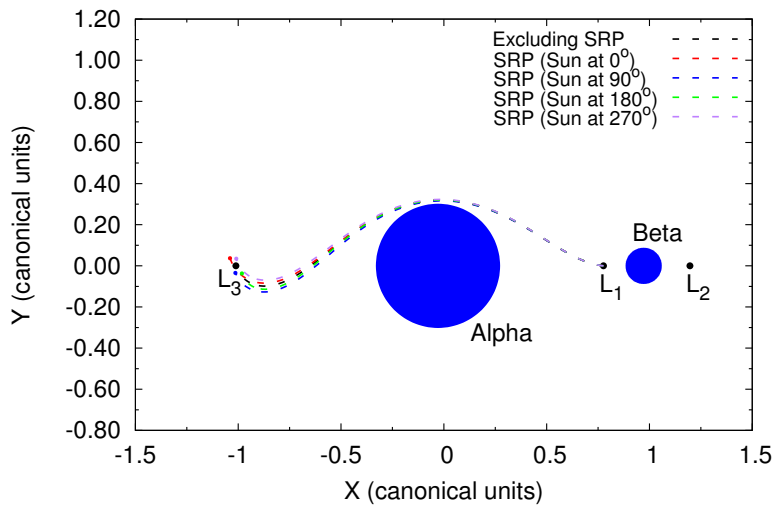
SOURCE: Oliveira et al. (2017b).

To verify the influence of the solar radiation pressure over the transfers, it is used the maneuver with the minimum  $\Delta v$ , the flight path angle of 174.113 degrees and the time transfer of 0.258 days. Four cases of the initial position of the Sun with respect to the asteroid are considered.

Figures 3.35, 3.36 and 3.37 show the trajectories from  $L_1$  to  $L_3$  for the three cases of area/mass: 0.02, 0.1 and 0.5  $\text{m}^2/\text{kg}$ . It is possible to verify that the spacecraft does not reach the final Lagrange point  $L_3$ , due to the solar radiation pressure. The final position reached by the probe depends of the initial position of the Sun. These figures clearly show the expected effects of the solar radiation pressure. When the maneuver is calculated based in a dynamics without solar radiation pressure, Lagrange point  $L_3$  is reached exactly, based in the numerical accuracy defined. In this case, the acceleration of the spacecraft is  $1.05 \times 10^{-12} \text{ m/s}^2$ . When including the solar radiation pressure with the Sun at 0 degrees, there is an extra force in the direction of the motion of the probe. The probe is accelerated and it passes by the Lagrange point  $L_3$ . For an area/mass of 0.02  $\text{m}^2/\text{kg}$  this acceleration is  $2.25 \times 10^{-5} \text{ m/s}^2$ ; for an area/mass of 0.1  $\text{m}^2/\text{kg}$  this acceleration is  $2.33 \times 10^{-5} \text{ m/s}^2$ ; and for an area/mass of 0.5  $\text{m}^2/\text{kg}$  this acceleration is  $2.75 \times 10^{-5} \text{ m/s}^2$ . These new values of accelerations are greater than the one without solar radiation pressure and the magnitude of deviation depends on the area/mass ratio. For larger values

the deviation is larger, as shown in the Figures 3.35, 3.36 and 3.37. When the Sun is at 90 degrees, there is an extra force pointing to the negative direction of the vertical axis. The probe is shifted to the bottom of the plot, also the negative direction of the vertical axis, proportional to the area/mass ratio. It is noted that this shift is large enough to cause a collision between the spacecraft and Alpha as shown in Figure 3.37. In the situation where the Sun is at 180 degrees, the solar radiation pressure points in the direction opposite to the motion of the probe, so it is decelerated and does not reach the Lagrange point  $L_3$ . These deviations are proportional to the area/mass ratio. When the Sun is at 270 degrees, there is an extra force pointing to the positive direction of the vertical axis and the probe is shifted to the top of the plot, also the positive direction of the vertical axis. The shifts are also proportional to the area/mass ratio. It is also noted the occurrence of a collision with Alpha. Therefore, Figures 3.35, 3.36 and 3.37 show very well the importance of considering the solar radiation pressure in the dynamical model.

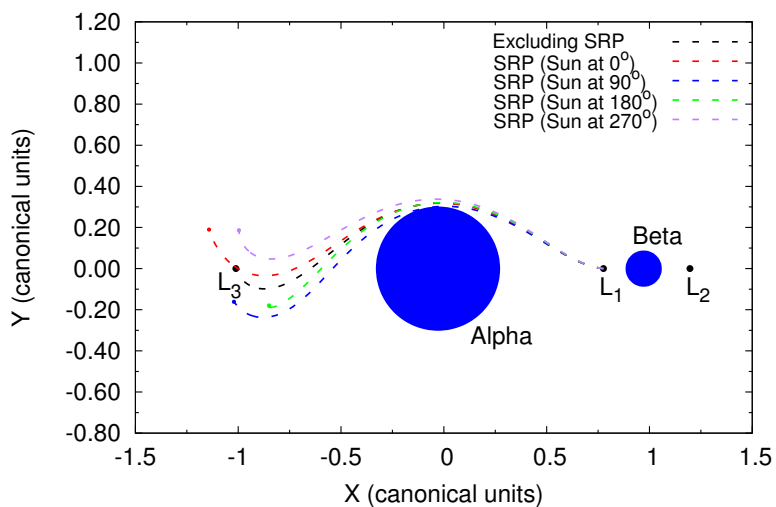
Figure 3.35 -  $L_1$  to  $L_3$ ,  $A/m = 0.02 \text{ m}^2/\text{kg}$



Trajectories from  $L_1$  to  $L_3$  with the asteroid at periaapsis of its orbit.

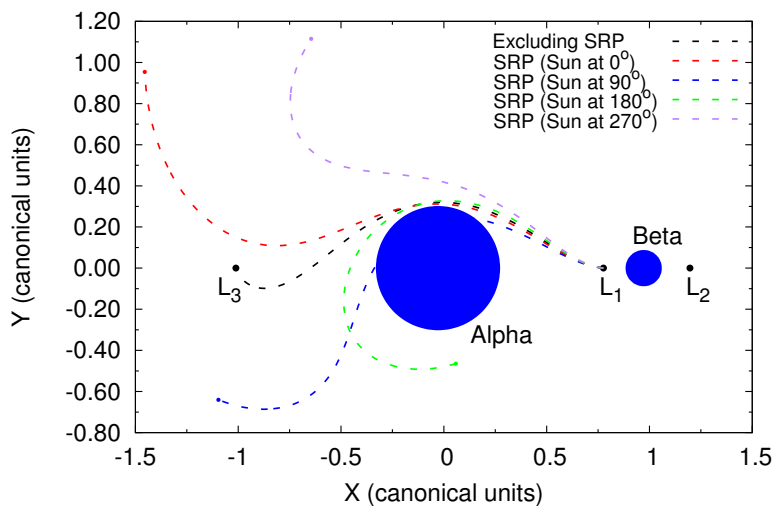
SOURCE: Oliveira et al. (2017b).

Figure 3.36 -  $L_1$  to  $L_3$ ,  $A/m = 0.1 \text{ m}^2/\text{kg}$



Trajectories from  $L_1$  to  $L_3$  with the asteroid at periapsis of its orbit.  
SOURCE: Oliveira et al. (2017b).

Figure 3.37 -  $L_1$  to  $L_3$ ,  $A/m = 0.5 \text{ m}^2/\text{kg}$



Trajectories from  $L_1$  to  $L_3$  with the asteroid at periapsis of its orbit.  
SOURCE: Oliveira et al. (2017b).

Table 3.35 shows the minimum distances from  $L_3$  reached by the probe according to the initial position of the Sun.

Table 3.35 - Minimum distances from  $L_3$

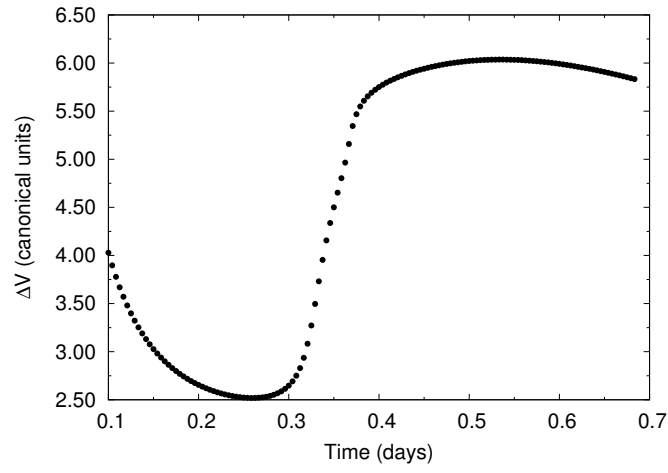
	A/m = 0.02 m <sup>2</sup> /kg		A/m = 0.1 m <sup>2</sup> /kg		A/m = 0.5 m <sup>2</sup> /kg	
	d(nd)	d(m)	d(nd)	d(m)	d(nd)	d(m)
Excluding SRP	0.000	0.01	0.000	0.01	0.000	0.01
Sun at 0°	0.010	26.79	0.006	16.72	0.141	394.79
Sun at 90°	0.034	95.75	0.161	451.56	0.623	1744.21
Sun at 180°	0.047	132.72	0.241	674.94	0.539	1509.44
Sun at 270°	0.015	41.22	0.105	294.54	0.677	1894.89

SOURCE: Oliveira et al. (2017b).

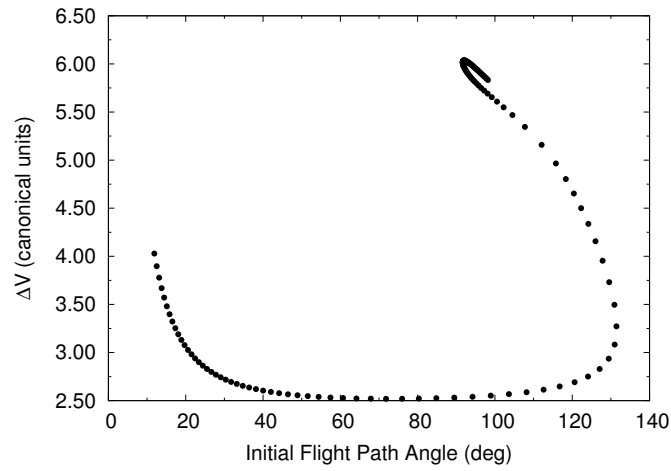
Table 3.35 shows in detail the effects of the solar radiation pressure in the error at the final point of the maneuver. If the probe has an area/mass = 0.02 m<sup>2</sup>/kg, the minimum distance between the probe and the Lagrange point goes from 26.79 meters to 132.72 meters, depending on the initial position of the Sun. As expected, the minimum error occurs when the Sun is initially at 0 degrees, with the probe being accelerated. The maximum error occurs when the Sun is initially at 180 degrees, with the probe being decelerated and the effect on the deviation of the trajectory is very large. Those values increases very much with the area/mass ratio, reaching levels of 674.94 meters for an area/mass = 0.1 m<sup>2</sup>/kg and 1894.89 meters for an area/mass = 0.5 m<sup>2</sup>/kg. It is also noted that, for this highest value of the area/mass ratio, the errors are stronger when the Sun is initially at the positions 90 and 270 degrees. The trajectories shown in Figures 3.35, 3.36, 3.37 identify the reason. With a such large solar radiation pressure, this force deviates too much the trajectories during the transfer, sending the probe away from  $L_3$ .

The next transfer considers the way back,  $L_3$  to  $L_1$ . Figure 3.38 shows the required  $\Delta v$  to move the probe from the Lagrange point  $L_3$  to  $L_1$  when the asteroid is at periapsis and the solar radiation pressure is not considered. The minimum  $\Delta v$  found is 2.519 canonical units, at the transfer time of 0.258 days. These are the same values found for the  $L_1$  to  $L_3$  transfer, but the flight path angle of 71.815 degrees is different, since the direction of motion is opposite.

Figure 3.38 - Transfer from  $L_3$  to  $L_1$  with the asteroid at periaapsis and excluding the solar radiation pressure



(a)  $\Delta v$  as function of time.

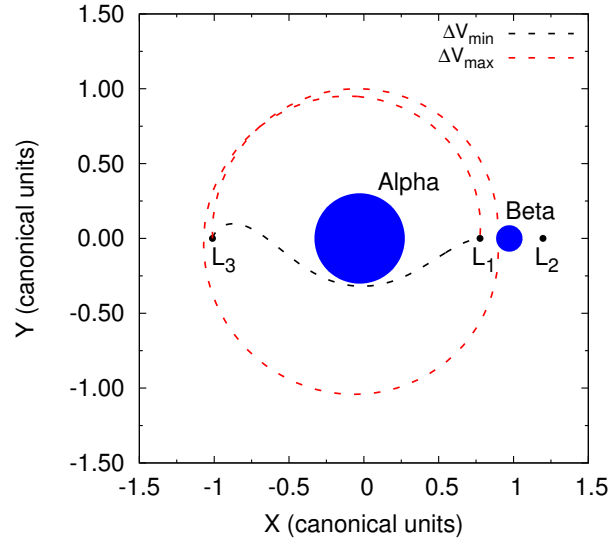


(b)  $\Delta v$  as function of the flight path angle.

SOURCE: Oliveira et al. (2017b).

Figure 3.39 shows the trajectories for the minimum and maximum variation of velocity.

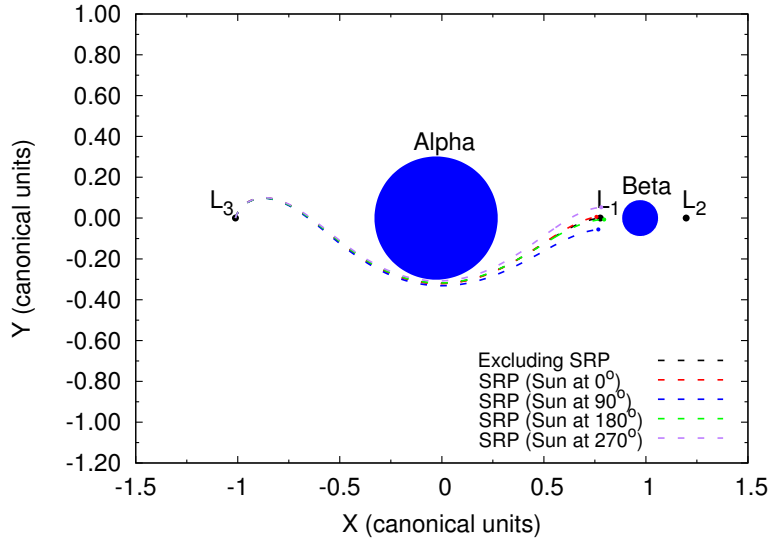
Figure 3.39 - Trajectories from  $L_3$  to  $L_1$  for  $\Delta v_{min}$  and  $\Delta v_{max}$ .



SOURCE: Oliveira et al. (2017b).

Figures 3.40, 3.41 and 3.42 show the plot of the trajectories from  $L_3$  to  $L_1$  for the three cases of area/mass: 0.02, 0.1 and 0.5  $\text{m}^2/\text{kg}$ . The  $\Delta v_1$  considered for these simulations are the minimum ones, and the total time used for the transfers is 0.258 days, the same for  $L_1$  to  $L_3$ . For all these five cases, the initial flight path angle is the same, 71.815 degrees. Figures 3.40, 3.41 and 3.42 have the same physical explanations made for Figures 3.35, 3.36 and 3.37, just the direction of motion is different. The probe now moves from the left to the right of the plots, so the acceleration of the probe occurs when the Sun is at 180 degrees and the deceleration occurs when the Sun is at 0 degree. The same types of shifts and occurrence of collisions with Alpha occur.

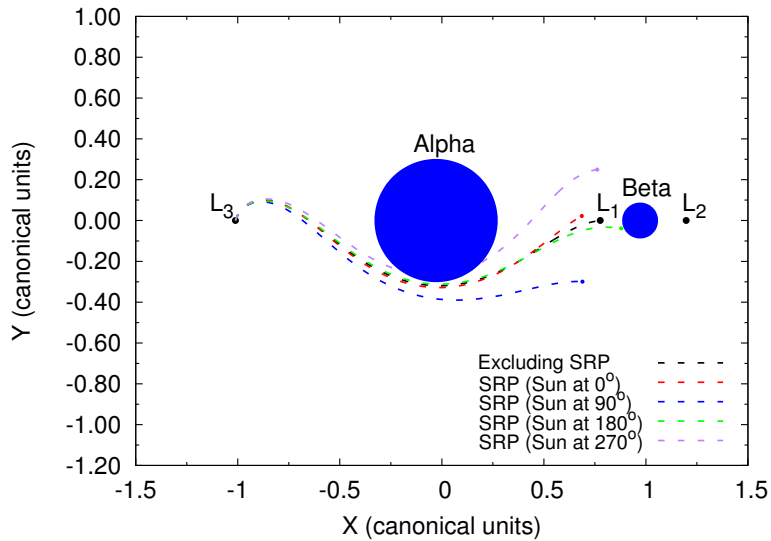
Figure 3.40 -  $L_3$  to  $L_1$ ,  $A/m = 0.02 \text{ m}^2/\text{kg}$



Trajectories from  $L_3$  to  $L_1$  with the asteroid at periaapsis and excluding the solar radiation pressure

SOURCE: Oliveira et al. (2017b).

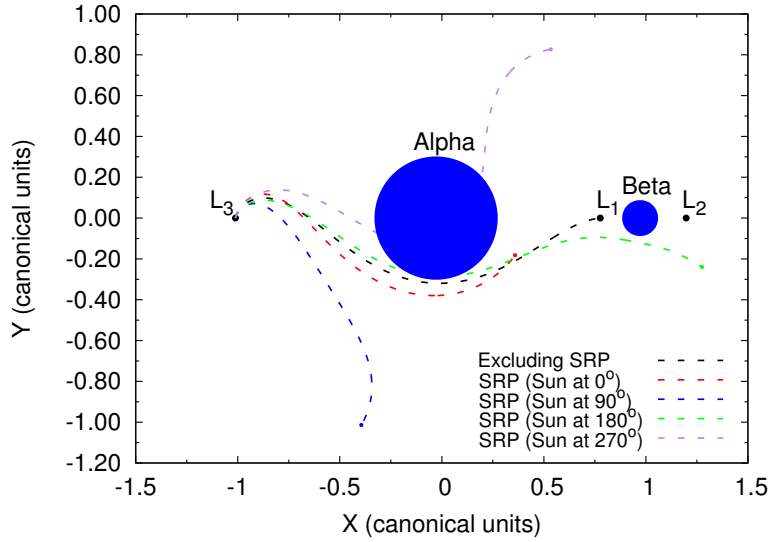
Figure 3.41 -  $L_3$  to  $L_1$ ,  $A/m = 0.1 \text{ m}^2/\text{kg}$



Trajectories from  $L_3$  to  $L_1$  with the asteroid at periaapsis and excluding the solar radiation pressure

SOURCE: Oliveira et al. (2017b).

Figure 3.42 -  $L_3$  to  $L_1$ ,  $A/m = 0.5 \text{ m}^2/\text{kg}$



Trajectories from  $L_3$  to  $L_1$  with the asteroid at periaapsis and excluding the solar radiation pressure

SOURCE: Oliveira et al. (2017b).

As found previously, it is possible to verify that the spacecraft does not reach the final Lagrange point  $L_1$ , due to the solar radiation pressure. The final position reached by the probe depends on the initial position of the Sun. Table 3.36 shows the minimum distances from  $L_1$  reached by the probe according to the initial position of the Sun. Table 3.36 has a very similar interpretation of Table 3.35. The only difference is the inversion of the minimum errors. The Sun, initially located in 180 degrees, now accelerated the probe and has the minimum errors for the lower values of the area/mass ratio. The maximum errors are located when the Sun is at the initial position of 0 degree, so decelerating the probe. For the highest value of the area/mass, the smallest errors occur when the Sun is at the positions 90 and 270 degrees, as occurred also in Table 3.35, but there is an inversion, and the case of 90 degrees now has larger errors.

Table 3.36 - Minimum distances from L<sub>1</sub>

	A/m = 0.02 m <sup>2</sup> /kg		A/m = 0.1 m <sup>2</sup> /kg		A/m = 0.5 m <sup>2</sup> /kg	
	d(nd)	d(m)	d(nd)	d(m)	d(nd)	d(m)
Excluding SRP	0.000	0.01	0.000	0.01	0.000	0.01
Sun at 0°	0.020	55.40	0.093	261.27	0.456	1275.53
Sun at 90°	0.056	158.11	0.313	872.89	1.320	3696.92
Sun at 180°	0.010	28.15	0.034	94.59	0.095	265.18
Sun at 270°	0.052	146.41	0.240	673.21	0.608	1701.10

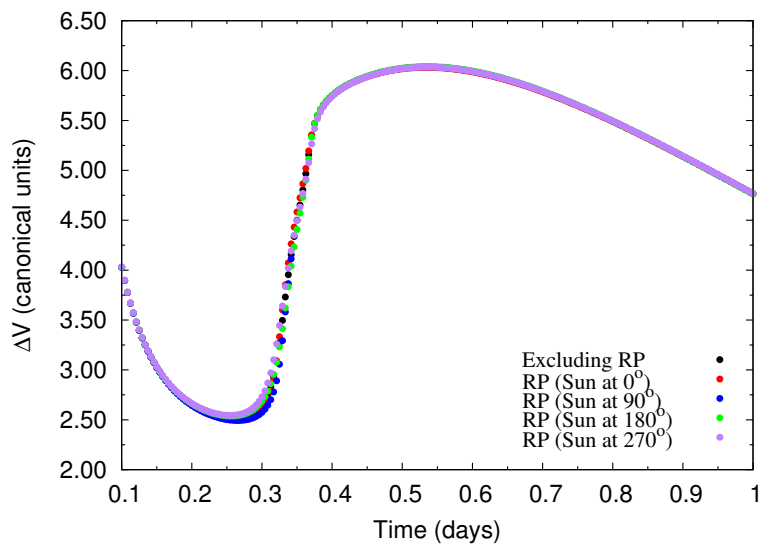
SOURCE: Oliveira et al. (2017b).

As a conclusion, the solar radiation pressure must be considered in the dynamics of the transfers, otherwise the spacecraft will not reach the desired Lagrange point in the end of the transfer. The next simulations show the real values of  $\Delta v$  required to achieve the desired final Lagrange point.

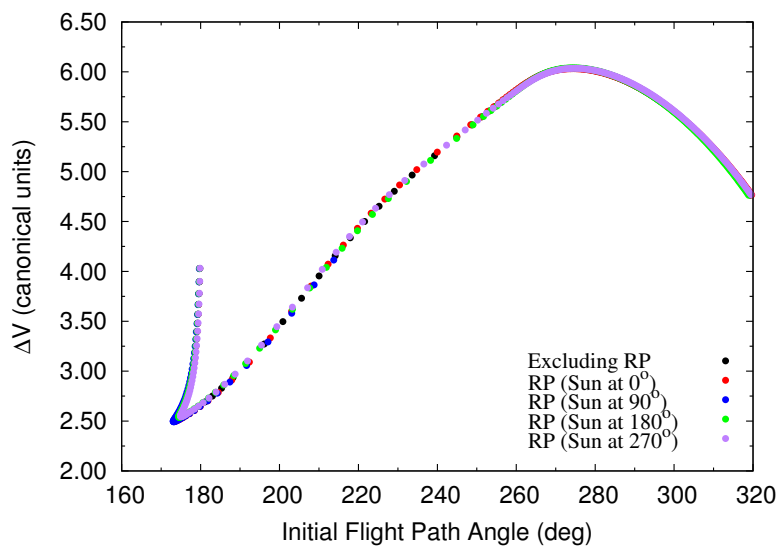
Figures 3.43 show in details the behavior of the velocity increment as a function of time and the flight path angle. It is possible to find the best transfers for every value of the area/mass ratio and initial position of the Sun. The discontinuities of the lines indicate points where there is a change of family of transfers. One family ended due to a collision with Alpha and the algorithm then needs to find a different family of transfers, with very different initial parameters.

Figures 3.43, 3.44 and 3.45 show the results for transfers when the asteroid is in the periapsis of its orbit around the Sun. It shows how  $\Delta v$  changes due to the area/mass ratio. As could be expected, the higher it turns, more changes in the plots of  $\Delta v$  are made.

Figure 3.43 - Transfers from  $L_1$  to  $L_3$  with the asteroid at periaapsis of its orbit.



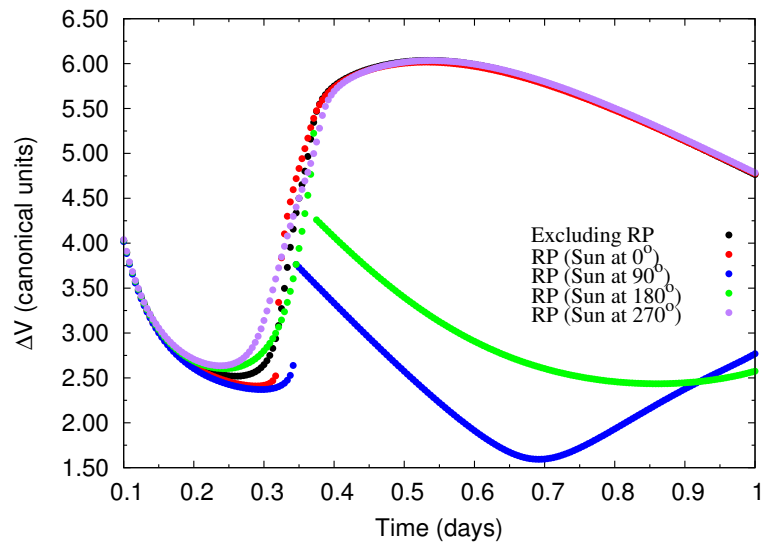
(a)  $\Delta v$  as function of time.  $A/m = 0.02 \text{ m}^2/\text{kg}$



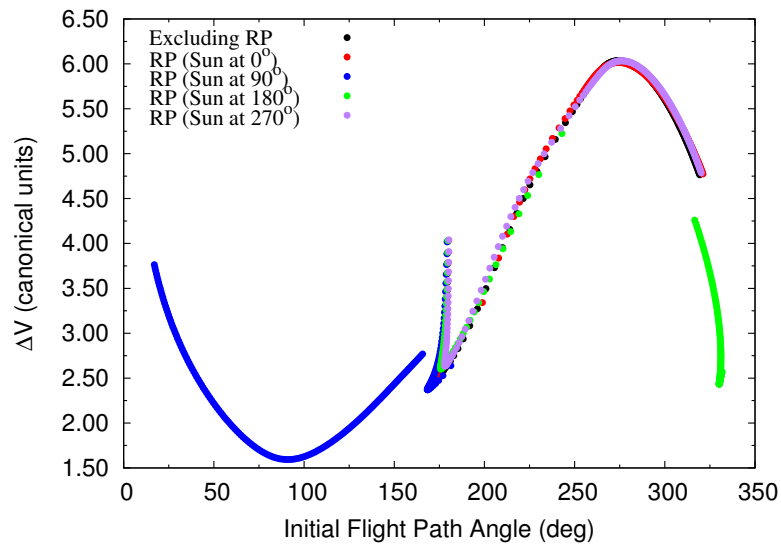
(b)  $\Delta v$  as function of fpa.  $A/m = 0.02 \text{ m}^2/\text{kg}$

SOURCE: Oliveira et al. (2017b).

Figure 3.44 - Transfers from  $L_1$  to  $L_3$  with the asteroid at periaapsis of its orbit.



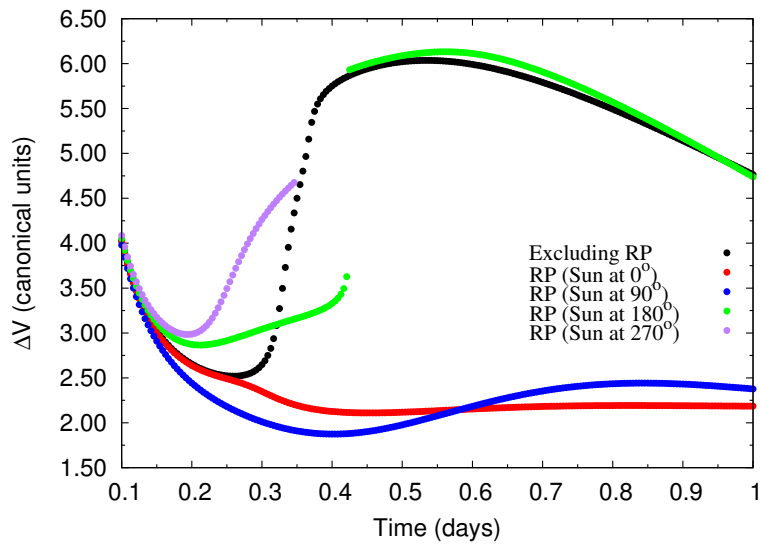
(a)  $\Delta v$  as function of time.  $A/m = 0.1 \text{ m}^2/\text{kg}$



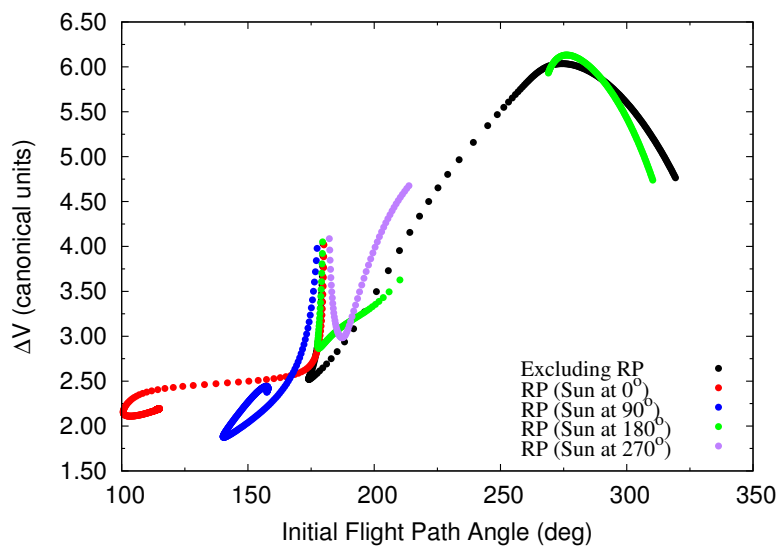
(b)  $\Delta v$  as function of fpa.  $A/m = 0.1 \text{ m}^2/\text{kg}$

SOURCE: Oliveira et al. (2017b).

Figure 3.45 - Transfers from  $L_1$  to  $L_3$  with the asteroid at periaapsis of its orbit.



(a)  $\Delta v$  as function of time.  $A/m = 0.5 \text{ m}^2/\text{kg}$



(b)  $\Delta v$  as function of fpa.  $A/m = 0.5 \text{ m}^2/\text{kg}$

SOURCE: Oliveira et al. (2017b).

Table 3.37 shows a comparison of  $\Delta v_{min}$ ,  $fpa$  and transfer time for all five cases for the initial position of the Sun. It identifies the best maneuver to be made under the solar radiation pressure effects. In other words, it shows how to use the solar radiation pressure in favor of minimizing the fuel consumed by the maneuver. The first line of this table shows the basic results, which are the ones valid for the situation

with no solar radiation pressure. It is shown that the minimum magnitude of the impulse to be applied depends on the initial position of the Sun. Those magnitudes can be smaller than the ones valid for the case without the solar radiation pressure, so helping to make the maneuver with less fuel; or higher, making the maneuver to be more expensive. It means that the choice of the time to perform the maneuver, so the initial position of the Sun, makes a difference in the fuel consumption of the maneuver. Those differences are of the order of plus 0.025 in the worst case and minus 0.023 in the best case, for an area/mass ratio of 0.02 m<sup>2</sup>. Those numbers are much higher for the other values of area/mass ratio, reaching savings of 0.926 (about 37%) for an area/mass ratio of 0.1 m<sup>2</sup> and 0.645 (about 26%) for an area/mass ratio of 0.5 m<sup>2</sup>.

Table 3.37 - 1996FG<sub>3</sub> at periapsis, L<sub>1</sub> to L<sub>3</sub>.

	A/m = 0.02 m <sup>2</sup> /kg			A/m = 0.1 m <sup>2</sup> /kg			A/m = 0.5 m <sup>2</sup> /kg		
	$\Delta v_{min}$	<i>fpa</i>	time	$\Delta v_{min}$	<i>fpa</i>	time	$\Delta v_{min}$	<i>fpa</i>	time
Excluding SRP	2.519	174.113	0.258	2.519	174.113	0.258	2.519	174.113	0.258
Sun at 0°	2.500	173.570	0.263	2.410	169.386	0.287	2.110	103.483	0.454
Sun at 90°	2.493	173.229	0.267	1.593	90.894	0.692	1.874	140.527	0.399
Sun at 180°	2.537	174.555	0.254	2.435	330.159	0.858	2.866	178.082	0.212
Sun at 270°	2.544	175.032	0.254	2.635	178.107	0.237	2.983	187.447	0.196

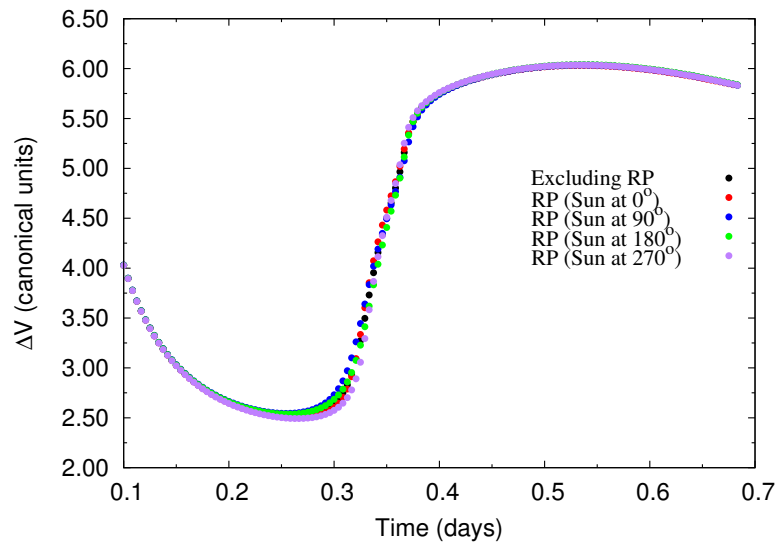
SOURCE: Oliveira et al. (2017b).

On the other side, if a wrong choice is made for the time to start the transfer, the extra variations of velocity required are of the order of 0.116 (about 5%) for an area/mass ratio of 0.1 m<sup>2</sup> and 0.464 (about 18%) for an area/mass ratio of 0.5 m<sup>2</sup>. It means differences between the best and the worst cases of 0.051 (about 2%) for an area/mass ratio of 0.02 m<sup>2</sup>; 1.042 (about 42%) for an area/mass ratio of 0.1 m<sup>2</sup> and 1.109 (about 44%) for an area/mass ratio of 0.5 m<sup>2</sup>. Another important point shown in this table is related to the flight path angle at departure. They are similar for the area/mass = 0.02 m<sup>2</sup>, but there are larger differences for the other higher values. For area/mass ratio = 0.1 m<sup>2</sup>, the values for the minimum increment of velocity are very different, going from 90.894 degrees to 330.159 degrees, compared to the value of 174.113 degrees for the maneuver without solar radiation pressure. It means that, even in situations where the velocity increment is not much different, as in the case with the Sun initially at 180 degrees, with only 0.084 difference, the flight path angle

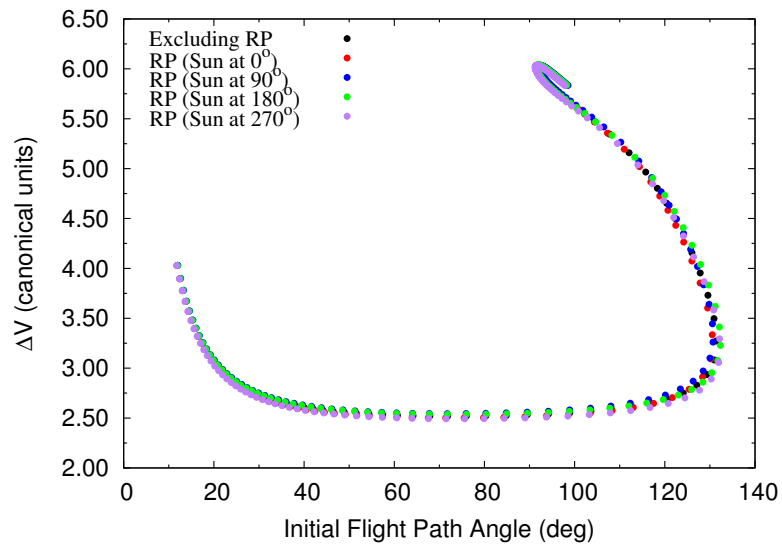
moves from 174.113 degrees to 330.159 degrees. So, it is very important to take into account this force in the model. The same is true for the time of flight, showing also larger variations for the minimum points. The reason for those large variations is the existence of several families of transfer orbits. They have similar values for all the three variables, velocity increment, flight path angle and transfer time. The border lines of those families have trajectories passing close to Alpha, and ending in collisions with the main asteroid. The presence of the solar radiation pressure makes shifts in those trajectories, changing the initial conditions of the border lines. It means that some new families of trajectories may appear due to those shifts, while some others may disappear due to collisions. This mechanism explains the appearance of new families of trajectories with lower values of velocity increment. Figures 3.35 to 3.37 and 3.40 to 3.40 show this point, with trajectories that does not collide with Alpha when the solar radiation pressure is not considered, but that collides with Alpha after the inclusion of this force.

Figures 3.46 to 3.48 show the results for transfers from  $L_3$  to  $L_1$  when the asteroid is in the periapsis of its orbit around the Sun. It is possible to observe, again, that the effects of the solar radiation pressure makes big changes over the transfers. As the area/mass ratio increases, more changes in  $\Delta v$  can be observed. Depending on the initial position of the Sun, the values of  $\Delta v$  decrease or increase.

Figure 3.46 - Transfers from  $L_3$  to  $L_1$  with the asteroid at periaapsis of its orbit.



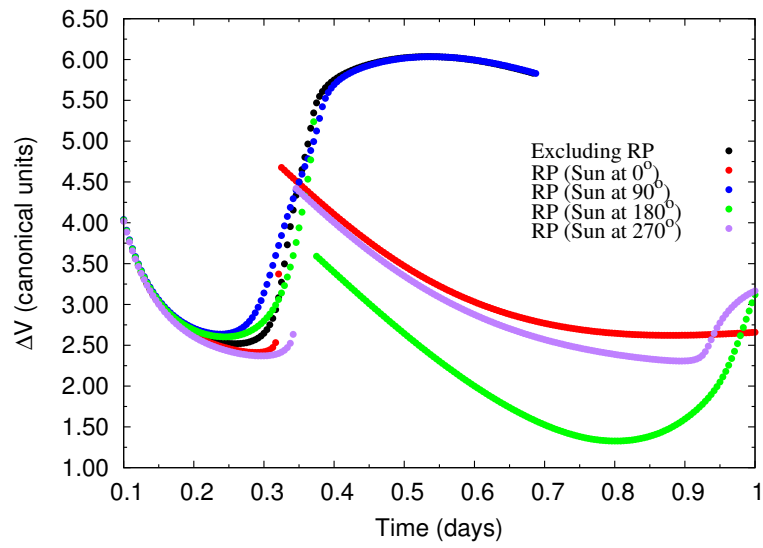
(a)  $\Delta v$  as function of time.  $A/m = 0.02 \text{ m}^2/\text{kg}$



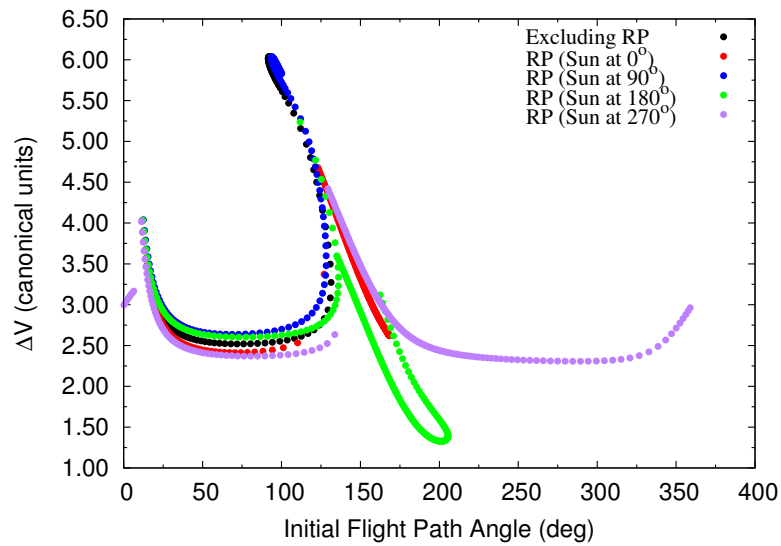
(b)  $\Delta v$  as function of fpa.  $A/m = 0.02 \text{ m}^2/\text{kg}$

SOURCE: Oliveira et al. (2017b).

Figure 3.47 - Transfers from  $L_3$  to  $L_1$  with the asteroid at periaapsis of its orbit.



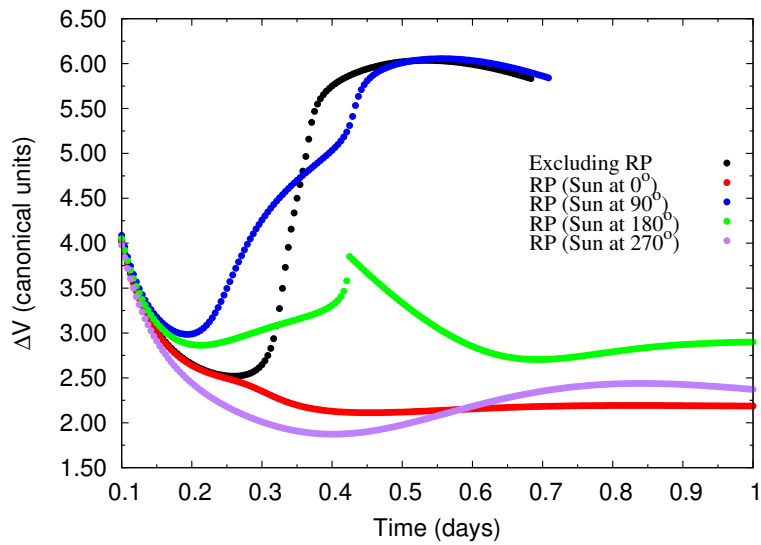
(a)  $\Delta v$  as function of time.  $A/m = 0.1 \text{ m}^2/\text{kg}$



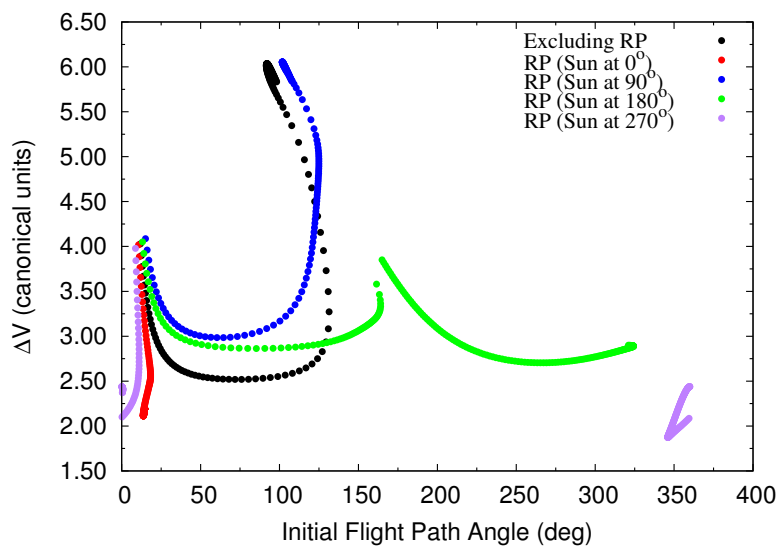
(b)  $\Delta v$  as function of fpa.  $A/m = 0.1 \text{ m}^2/\text{kg}$

SOURCE: Oliveira et al. (2017b).

Figure 3.48 - Transfers from  $L_3$  to  $L_1$  with the asteroid at periaapsis of its orbit.



(a)  $\Delta v$  as function of time.  $A/m = 0.5 \text{ m}^2/\text{kg}$



(b)  $\Delta v$  as function of fpa.  $A/m = 0.5 \text{ m}^2/\text{kg}$

SOURCE: Oliveira et al. (2017b).

Table 3.38 shows a comparison of  $\Delta v_{min}$ ,  $fpa$  and transfer time for all four cases of the initial position of the Sun and the situation with no solar radiation pressure. The results of Table 3.38 have exactly the same physical interpretations of the large variations of the parameters of the minimum increment of velocities.

Table 3.38 - 1996FG<sub>3</sub> at periapsis, L<sub>3</sub> to L<sub>1</sub>.

	A/m = 0.02 m <sup>2</sup> /kg			A/m = 0.1 m <sup>2</sup> /kg			A/m = 0.5 m <sup>2</sup> /kg		
	$\Delta v_{min}$	<i>fpa</i>	time	$\Delta v_{min}$	<i>fpa</i>	time	$\Delta v_{min}$	<i>fpa</i>	time
Excluding SRP	2.519	71.815	0.258	2.519	71.815	0.258	2.519	71.815	0.258
Sun at 0°	2.500	71.407	0.263	2.412	70.472	0.288	2.112	13.746	0.454
Sun at 90°	2.544	71.751	0.254	2.636	68.668	0.238	2.985	60.363	0.192
Sun at 180°	2.537	71.806	0.254	1.326	200.982	0.800	2.704	265.280	0.692
Sun at 270°	2.493	75.602	0.267	2.307	289.410	0.896	1.873	346.036	0.400

SOURCE: Oliveira et al. (2017b).

Tables 3.39 to 3.42 show a comparison of  $\Delta v_{min}$ , *fpa* and transfer time for transfers involving all the others collinear Lagrange points transfers. A detailed analysis is not made because the phenomenon involved is very similar to the case L<sub>1</sub>-L<sub>3</sub> shown in details before. This is the reason why only the tables are shown and the equivalent figures are omitted. Table 3.39 shows transfers from L<sub>1</sub> to L<sub>2</sub>. Those two points have the body Beta in the middle, which is smaller than Alpha. This is the reason why there are fewer collisions with Beta, and there are not many alternations of transfer families. The most noted point occurs for an area/mass ratio of 0.5 m<sup>2</sup>/kg with the Sun located initially at 0 and 270 degrees. The case of 0 degree is particularly interesting, with larger savings in increment of velocity. This is due to the appearance of a family that ended in collisions when the solar radiation pressure is not considered. Table 3.40 shows the opposite transfer, from L<sub>2</sub> to L<sub>1</sub>. The more interesting variation occurs when the Sun is located initially in 180 degrees, for the cases with area/mass of 0.02 and 0.1 m<sup>2</sup>/kg. A new family with much longer transfer times and smaller velocity increments appear. Tables 3.41 and 3.42 consider transfers from L<sub>2</sub> to L<sub>3</sub> and vice-versa. Alpha is again in the middle of the transfers, so the alternations of families are back and families with lower increment of velocities appear again. The magnitudes of the modifications are smaller, because L<sub>2</sub> is far away from Alpha, compared to L<sub>1</sub>, and it reduces the frequency of collisions.

Table 3.39 - 1996FG<sub>3</sub> at periapsis, L<sub>1</sub> to L<sub>2</sub>.

	A/m = 0.02 m <sup>2</sup> /kg			A/m = 0.1 m <sup>2</sup> /kg			A/m = 0.5 m <sup>2</sup> /kg		
	$\Delta v_{min}$	<i>fpa</i>	time	$\Delta v_{min}$	<i>fpa</i>	time	$\Delta v_{min}$	<i>fpa</i>	time
Excluding SRP	2.019	89.937	0.142	2.019	89.937	0.142	2.019	89.937	0.142
Sun at 0°	2.013	89.548	0.142	1.988	90.381	0.150	1.753	114.310	0.733
Sun at 90°	2.019	88.750	0.138	2.020	89.203	0.138	2.024	89.961	0.133
Sun at 180°	2.025	89.016	0.138	2.048	87.687	0.129	2.144	85.703	0.108
Sun at 270°	2.019	89.822	0.142	2.018	89.353	0.142	1.990	120.228	0.708

SOURCE: Oliveira et al. (2017b).

Table 3.40 - 1996FG<sub>3</sub> at periapsis, L<sub>2</sub> to L<sub>1</sub>.

	A/m = 0.02 m <sup>2</sup> /kg			A/m = 0.1 m <sup>2</sup> /kg			A/m = 0.5 m <sup>2</sup> /kg		
	$\Delta v_{min}$	<i>fpa</i>	time	$\Delta v_{min}$	<i>fpa</i>	time	$\Delta v_{min}$	<i>fpa</i>	time
Excluding SRP	2.204	155.651	0.167	2.204	155.651	0.167	2.204	155.651	0.167
Sun at 0°	2.204	155.238	0.167	2.204	155.238	0.167	2.217	123.026	0.288
Sun at 90°	2.205	155.693	0.163	2.205	155.693	0.163	2.245	148.599	0.142
Sun at 180°	2.110	326.143	1.000	2.110	326.143	1.000	2.215	165.261	0.142
Sun at 270°	2.202	156.375	0.167	2.202	156.375	0.167	2.089	278.733	0.183

SOURCE: Oliveira et al. (2017b).

Table 3.41 - 1996FG<sub>3</sub> at periapsis, L<sub>2</sub> to L<sub>3</sub>.

	A/m = 0.02 m <sup>2</sup> /kg			A/m = 0.1 m <sup>2</sup> /kg			A/m = 0.5 m <sup>2</sup> /kg		
	$\Delta v_{min}$	<i>fpa</i>	time	$\Delta v_{min}$	<i>fpa</i>	time	$\Delta v_{min}$	<i>fpa</i>	time
Excluding SRP	2.193	319.008	0.912	2.193	319.008	0.912	2.193	319.008	0.912
Sun at 0°	2.176	317.989	0.983	2.274	320.212	0.829	2.442	113.372	0.771
Sun at 90°	2.172	320.174	0.883	2.117	322.706	0.812	2.024	321.448	0.654
Sun at 180°	2.215	319.110	0.879	2.310	316.636	0.800	2.672	302.516	0.675
Sun at 270°	2.220	317.265	0.950	2.366	315.560	0.862	2.890	316.339	0.742

SOURCE: Oliveira et al. (2017b).

Table 3.42 - 1996FG<sub>3</sub> at periapsis, L<sub>3</sub> to L<sub>2</sub>.

	A/m = 0.02 m <sup>2</sup> /kg			A/m = 0.1 m <sup>2</sup> /kg			A/m = 0.5 m <sup>2</sup> /kg		
	$\Delta v_{min}$	<i>fpa</i>	time	$\Delta v_{min}$	<i>fpa</i>	time	$\Delta v_{min}$	<i>fpa</i>	time
Excluding SRP	2.193	277.601	0.912	2.193	277.601	0.912	2.193	277.601	0.912
Sun at 0°	2.177	295.062	0.983	2.043	37.173	0.517	2.269	14.461	0.496
Sun at 90°	2.220	263.116	0.946	2.365	181.091	0.862	2.720	65.400	0.250
Sun at 180°	2.215	273.443	0.875	2.308	271.443	0.800	2.668	265.838	0.671
Sun at 270°	2.172	283.621	0.887	2.083	85.605	0.421	1.968	350.776	0.433

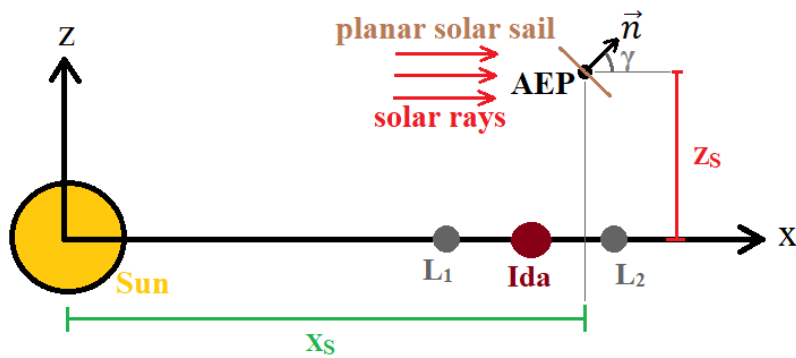
SOURCE: Oliveira et al. (2017b).



## 4 LOCATING AND PERFORMING TRANSFERS FOR ARTIFICIAL EQUILIBRIUM POINTS IN A SUN-ASTEROID SYSTEM

In the absence of a solar sail or any other forces, the traditional Lagrange points  $L_1$  and  $L_2$  are the only equilibrium points near the asteroid 243 Ida, which is a celestial body located in the asteroid belt. The use of a solar sail in the spacecraft gives new configurations for the equilibrium points, which depend on the position and the inclination of the vector normal to the solar sail with respect to the  $x$  axis. These new configurations of equilibrium points are the so called artificial equilibrium points (AEP). The geometry of the problem is shown in Figure 4.1.

Figure 4.1 - Reference frame in the circular restricted three-body problem.



The Sun and the asteroid Ida are the primaries in the circular restricted three-body problem. In the absence of a solar sail, the traditional Lagrange points  $L_1$  and  $L_2$  are the only equilibrium points near the smaller primary. Using a general thrust, new configurations of equilibrium may arise, which are the so called artificial equilibrium points.

SOURCE: Oliveira et al. (2018).

The use of a solar sail is interesting because it allows a spacecraft to park close to the body that is the object of study. The main idea of this chapter is to obtain the new locations of those points and to calculate the costs to transfer a spacecraft between those points, in particular showing some options to minimize the costs involved in these transfers.

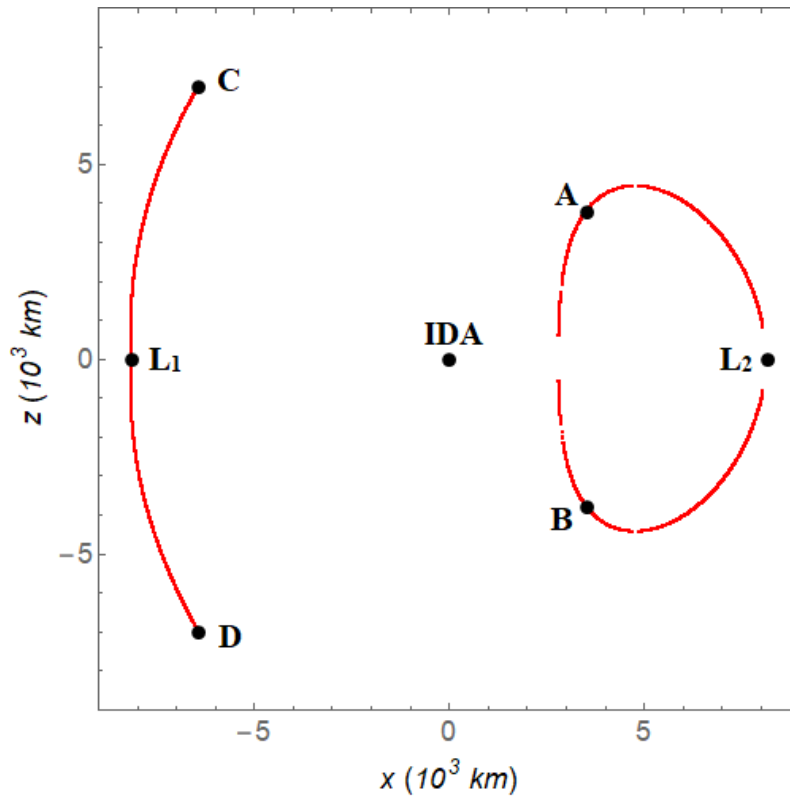
In this section, the Sun and the asteroid Ida (BELTON et al., 1995; BELTON et al., 1996; SIMONELLI et al., 1996) are considered the main bodies of the circular restricted three-body problem. In the absence of a solar sail, the traditional Lagrange points  $L_1$  and  $L_2$  are the only equilibrium points near the smaller primary (SZEBEHELY,

1967). Using a general thrust, new configurations of equilibrium may arise, which are the so called AEP (MORIMOTO et al., 2007; ALIASI et al., 2011; ALIASI et al., 2012; ALMEIDA et al., 2018). The recent technological development of new lightweight and highly reflexive materials makes possible the use of solar sails to generate the thrust required to achieve many general AEP in space (DANDOURAS et al., 2004; FARRÉS; JORBA, 2008). Important missions used these materials (O'SHAUGHNESSY et al., 2009; TSUDA et al., 2013b; O'SHAUGHNESSY et al., 2014).

Thus, the use of a solar sail gives new configurations for the equilibrium points, based in the position and in the inclination of the normal vector to the solar sail. A solar sail allows a spacecraft to park at a closer distance to the secondary main body than the traditional  $L_1$  or  $L_2$ . Besides that, new perspectives for viewing from above or below the ecliptic plane can be reached through the use of a solar sail to observe the body from a stationary condition (FORWARD, 1991; MCINNES, 2010; SALAZAR et al., 2016; JÚNIOR et al., 2017).

The objective of this chapter is to offer new perspectives for the observation of Ida using new AEP to place a spacecraft equipped with a solar sail and to calculate the costs to transfer the spacecraft between these different equilibrium points, with the goal of giving some options to minimize the fuel consumption of these transfers. These AEP found around the Lagrange points  $L_1$  and  $L_2$  in the Sun-Ida system are shown in Figure 4.2, identified as A, B, C and D. In this figure, the red curve represents a family of possible AEP in the  $(x,z)$  plane for a spacecraft with an area to mass ratio of  $0.3 \text{ m}^2/\text{kg}$ . The forces involved, the respective equations and the associated values for the parameters are described in the sections 2.1 and 2.2.

Figure 4.2 - Possible AEPs to place a stationary spacecraft around Ida in the Sun-Ida system above and below the ecliptic.



SOURCE: Oliveira et al. (2018).

## 4.1 Methodology

The mathematical tools used in this chapter are shown in this section. The mathematical description of the AEPs is shown in subsection 4.1.1. The dynamics of the system for the transfers between different AEPs are explained in subsection 4.1.2. The possible configurations of the solar sail during the transfers are shown in subsection 4.1.3.

### 4.1.1 Artificial equilibrium points

The Sun is assumed to be located in the center of a frame of reference that rotates with the same angular velocity of the secondary body, which is the asteroid Ida. A spacecraft equipped with a solar planar sail is subjected to the gravitational forces due to the Sun and Ida, and to the solar radiation pressure coming from the solar rays. The equation of motion of the spacecraft in this frame of reference is given

by (SYMON, 1971)

$$\frac{d^2\vec{r}_s}{dt^2} + 2\vec{\omega} \times \frac{d\vec{r}_s}{dt} + \vec{\omega} \times (\vec{\omega} \times \vec{r}_s) + \frac{d\vec{\omega}}{dt} \times \vec{r}_s = -\frac{\mu_s}{r_s^3}\vec{r}_s - \frac{\mu_i}{r_{ida}^3}\vec{r}_{ida} + \frac{1}{m}\vec{f}_s, \quad (4.1)$$

where  $\vec{\omega}$  is the angular velocity of the frame,  $\vec{r}_s = (x_s, y_s, z_s)$  is the position of the spacecraft,  $r_s = \|\vec{r}_s\|$ ,  $\vec{r}_{ida} = (x_s - R, y_s, z_s)$  is the position of the spacecraft with respect to Ida, where  $R$  is the distance Sun-Ida,  $r_{ida} = \|\vec{r}_{ida}\|$ ,  $\mu_s$  is the gravitational parameter of the Sun,  $\mu_i$  is the gravitational parameter of Ida, and  $\vec{f}_s$  is the force over a planar solar sail due to the solar radiation pressure.

Although the eccentricity of the orbit of Ida around the Sun is 0.041 (CHAMBERLIN; YEOMANS, 2017), we assume that this orbit is circular. Hence, the angular velocity vector of the frame of reference is given by  $\vec{\omega} = (0, 0, \omega)$ , where  $\omega = \sqrt{\mu_s/R^3}$  is a constant. In the case of a perfect reflection, the force  $\vec{f}_s$  is given by (MCINNES, 2004)

$$\vec{f}_s = \frac{2p_e A R_e^2 \cos^2(\gamma)}{r_s^2} \hat{n}, \quad (4.2)$$

where  $A$  is the area of the solar sail that reflects the rays of the Sun,  $R_e$  is the distance Sun-Earth,  $p_e$  is the value of the solar radiation pressure at a distance  $R_e$  from the Sun,  $\vec{n} = (n_x, n_y, n_z)$  is a unitary vector normal to the planar solar sail pointing upwards from the reflecting surface, and  $\gamma$  is the angle between  $\vec{n}$  and the  $x$  axis, which is the direction of the solar rays coming from the Sun. The AEP is defined by the condition given by (ALMEIDA et al., 2018)

$$\vec{\omega} \times (\vec{\omega} \times \vec{r}_s) = -\frac{\mu_s}{r_s^3}\vec{r}_s - \frac{\mu_i}{r_{ida}^3}\vec{r}_{ida} + \frac{1}{m}\vec{f}_s, \quad (4.3)$$

Using the above considerations, the Equation (4.3) is written in vector matrix form, to become

$$\frac{A}{m} \frac{2R_e^2 p_e \cos^2(\gamma)}{r_s^2} \begin{pmatrix} n_x \\ n_y \\ n_z \end{pmatrix} = \frac{\mu_s}{r_s^3} \begin{pmatrix} x_s \\ y_s \\ z_s \end{pmatrix} + \frac{\mu_i}{r_{ida}^3} \begin{pmatrix} x_s - R \\ y_s \\ z_s \end{pmatrix} - \frac{\mu_s}{R^3} \begin{pmatrix} x_s \\ y_s \\ 0 \end{pmatrix}. \quad (4.4)$$

The AEPs used in this work are located in the  $x - z$  plane ( $y_s = 0$ ), because AEPs in this plane can reach high values of  $z_s$ , which makes possible to observe the poles of Ida (JÚNIOR et al., 2017). Therefore, according to Equation (4.4),  $n_y$  must be zero. The  $n_x$  and  $n_z$  components of the normal vector to the solar sail becomes

$n_x = \cos(\gamma)$  and  $n_z = \sin(\gamma)$ . Therefore, the two nontrivial components left from Equation (4.4) can be written as

$$\left(\frac{A}{m}\right) \frac{2R_e^2 \cos^2(\gamma) p_e}{r_s^2} \cos(\gamma) = \frac{\mu_s}{r_s^3} x_s + \frac{\mu_i(x_s - R)}{r_{ida}^3} - \frac{x_s \mu_s}{R^3} \quad (4.5)$$

$$\left(\frac{A}{m}\right) \frac{2R_e^2 \cos^2(\gamma) p_e}{r_s^2} \sin(\gamma) = \left(\frac{\mu_s}{r_s^3} + \frac{\mu_i}{r_{ida}^3}\right) z_s. \quad (4.6)$$

A second frame of reference centered in Ida is defined as  $(x, y, z) = (x_s - R, y_s, z_s)$ , for clarity purposes in the analysis of the results. The values of the parameters used in this work are given in Table 4.1.

Table 4.1 - Parameters of the Sun-Ida system.

$R_e$	$1.495978707 \times 10^{11} m$
$R$	$2.862 R_e$
$p_e$	$4.56 \times 10^{-6} N/m^2$
$\mu_s$	$1.32712440041 \times 10^{20} m^3/s^2$
$\mu_i$	$2.750 \times 10^6 m^3/s^2$
$A/m \text{ ratio}$	$0.3 m^2/kg$

SOURCE: Luzum et al. (2011), Chamberlin e Yeomans (2017)

Table 4.2 shows the values for the parameters of the system considered in this study, as described in section 2.2, where  $M_1$  is the Sun,  $M_2$  is the asteroid Ida and  $M_3$  the spacecraft.

Table 4.2 - Canonical system of units for the Sun-Ida system.

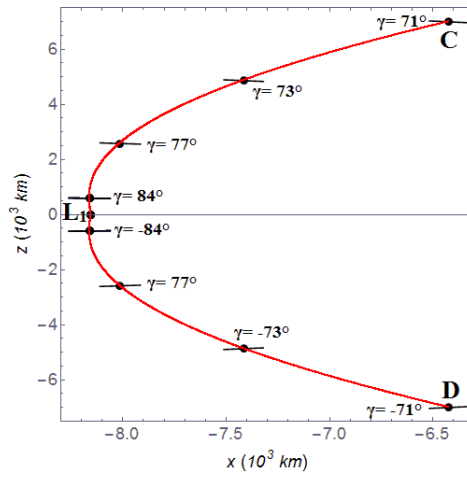
Unit of distance	$4.281 \times 10^8 km$
Unit of time	$1.528 \times 10^8 sec$
Unit of velocity	$17.606 km/s$

SOURCE: Luzum et al. (2011), Chamberlin e Yeomans (2017)

Using these values, the solution of both Equations (4.5) and (4.6) are found for both  $x$  and  $z$  as functions of the angle  $\gamma$ . They are shown in Figures 4.3 and 4.4.

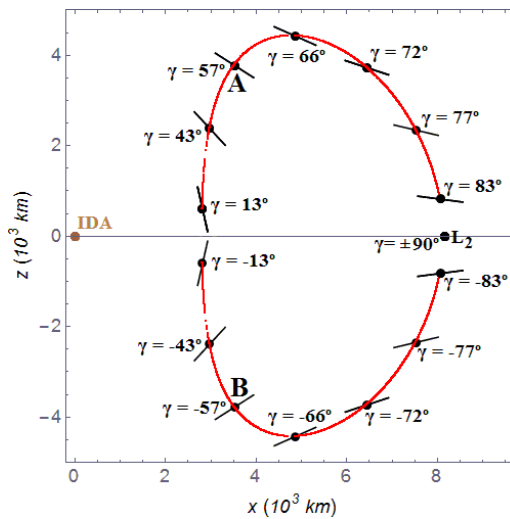
These solutions represent artificial equilibrium points, which are a combined set of parameters and position such that the motion of the spacecraft is stationary in the rotating frame of reference.

Figure 4.3 - The AEPs around the Lagrange point  $L_1$ .



SOURCE: Oliveira et al. (2018).

Figure 4.4 - The AEPs around the Lagrange point  $L_2$ .



SOURCE: Oliveira et al. (2018).

### 4.1.2 Transfers between the AEPs

In the case of a spacecraft equipped with a solar sail, different AEPs were found for the Sun-Ida system, as shown in Figure 4.1. Supposing that different perspectives are also good to observe regions of Ida, the transfer will be made between the  $A$ ,  $B$ ,  $C$ ,  $D$ ,  $L_1$ , and  $L_2$  points shown in this figure. The goal now is to simulate these transfers taken into account the solar radiation pressure over the spacecraft with the objective of finding the ones that consume as little fuel as possible. The fuel consumption of the transfers between the spots is greatly affected by the solar radiation pressure, as shown in the results.

The red lines in Figures 4.3 and 4.4 show the AEP close to the Lagrange points  $L_1$  and  $L_2$  in the Sun-Ida system. These points can be used to park a spacecraft to observe the asteroid 243 Ida from a stationary position. Some equilibrium points are highlighted in black next to their respective straight lines that represent the inclination of the planar solar sail with respect to the solar rays coming from the left side. The angle  $\gamma$  is the angle formed between the vector normal to the solar sail and the solar rays, as shown in Figure 4.1. Note that there are several different locations to observe Ida, including positions out-of-plane that can be used to study the poles of Ida. It is just a question of using the correct value of  $\gamma$ .

The orbital maneuvers are made using the three-dimensional restricted three-body problem (SZEBEHELY, 1967) and are assumed to be bi-impulsive, with the impulses applied at the initial and final points of the maneuver. This method was already used in several other problems Broucke (1979), Prado (1996), Prado (2006), Cabette e Prado (2008), Oliveira et al. (2016), Oliveira et al. (2016), Oliveira et al. (2017b), Santos et al. (2017), Santos (2013). Thus, the fuel consumed is specified by the total variation of the velocity  $\Delta V$  applied to the spacecraft in both impulses. The necessary conditions used to simulate the transfers between these points are:

- 1) the initial and final coordinates:  $(x_i, 0, z_i)$  and  $(x_f, 0, z_f)$ , where  $(x_i, 0, z_i)$  is the initial position of the spacecraft at the initial AEP and  $(x_f, 0, z_f)$  is the final position of the spacecraft at the final AEP;
- 2) the  $\gamma$  angle, that represents the attitude of the solar sail:  $(\gamma_i)$  in the initial point and  $(\gamma_f)$  in the final point;
- 3) the time  $t$  to transfer the spacecraft between these equilibrium points. In this work, the time  $t$  used to make the transfers ranges from 0 to 300 days, with intervals of 1 day;
- 4) the area/mass ratio of the spacecraft is fixed in  $0.3 \text{ m}^2/\text{kg}$ .

Table 4.3 shows the equilibrium positions in the  $(x, z)$  plane and their respective  $\gamma$ , for six points that are showed in Figures 4.3 and 4.4. These points are considered for the transfers in this work.

Table 4.3 - Parameters for the equilibrium points

Point	$x$ ( $10^6m$ )	$z$ ( $10^6m$ )	$\gamma$ ( $deg$ )
A	3.519864243875569	3.778571428571429	57.354409590796010
B	3.519864243875569	-3.778571428571429	-57.354409590796010
C	-6.422123430010099	7.000000000000000	70.743433587229617
D	-6.422123430010099	-7.000000000000000	-70.743433587229617
$L_1$	-8.153778060926010	0	90
$L_2$	8.153881583930910	0	90

SOURCE: Author

### 4.1.3 Solar sail configuration

The vector  $\vec{n}$  depends on the angle  $\gamma$ . According to Equation (4.7), the force due to the solar radiation pressure depends on the vector  $\vec{n}$  and directly on the angle between the vector normal to the solar sail and the  $x$  axis, which is the direction of the solar rays. In this work, it is assumed that the angle  $\gamma$  varies in time along the transfer according to the rule

$$\gamma(t) = \gamma_i + \alpha t, \quad (4.7)$$

where  $t$  is the transfer time in days;  $\gamma_i$  is  $\gamma$  in the initial position ( $\gamma_i = \gamma(0)$ );  $\alpha$  is a constant to be evaluated from  $\alpha = (\gamma_f - \gamma_i)/t$ , where  $\gamma_f = \gamma(t)$  ( $\gamma$  in the final position).

This assumption is made to give more control to the transfer, but keeping a law that is not too complex to be implemented in the solar sail. Note that, in the case where  $\gamma_i = \gamma_f$ , the angle  $\gamma(t)$  is assumed to be constant. For each transfer, four different configurations are considered for the solar sail, according to Equation (4.7):

- (i) case 1:  $\gamma$  has a linear variation in time with constraints in  $\gamma_i$  and  $\gamma_f$

In this configuration, the values for  $\gamma_i$  and  $\gamma_f$  are given by:

$\gamma_i$  :  $\gamma$  of the initial equilibrium point for  $t = 0$ , as shown in Table 4.3;

$\gamma_f$  :  $\gamma$  of the final equilibrium point, in the final time, as shown in Table 4.3.

- (ii) case 2:  $\gamma$  has a linear variation in time with no constraints in  $\gamma_i$  and  $\gamma_f$

In this configuration, the force due to the solar radiation pressure varies in time similarly to the previous configuration. However, the initial and final angles,  $\gamma_i$  and  $\gamma_f$ , have no restrictions. They are not fixed with the same values for the equilibrium points, as presented in Table 4.3.

(iii) case 3:  $\gamma_i = \gamma_f = 0^\circ$

In this configuration, according to Equation (4.7), the force due to the solar radiation pressure is considered constant and is maximum due to the term  $\cos^2(\gamma) = 1$ , which means that, during the transfer, the vector normal to the solar sail and the solar rays make an angle of  $0^\circ$ .

(iv) case 4:  $\gamma_i = \gamma_f = 90^\circ$

In this configuration, according to Equation (4.7), the force due to the solar radiation pressure is considered constant and will be null due to the term  $\cos^2(\gamma) = 0$ , which means that, during the transfer, the vector normal to the solar sail and the solar rays make an angle of  $90^\circ$ .

## 4.2 Results

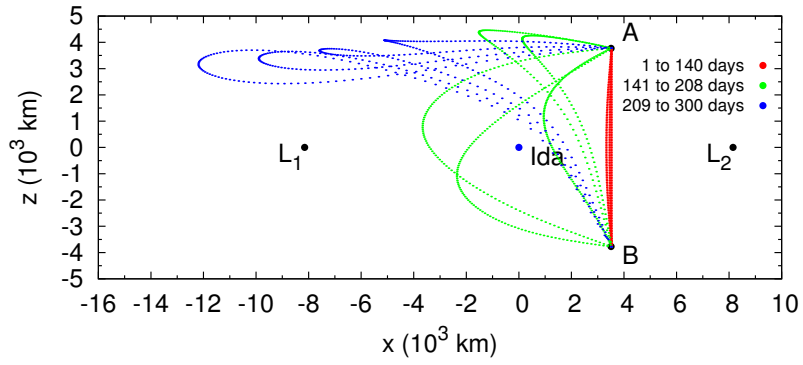
As a result of the different configurations shown in subsection 4.1.3, several families of transfer orbits between the equilibrium points are found, for several values of  $\gamma_i$ ,  $\gamma_f$  and the total time of flight. In this work, the transfers were considered between the points, whose coordinates are given in Table 4.3: A to B, C to D, L<sub>1</sub> to C, and L<sub>2</sub> to A. The results for each transfer are presented in the following subsections.

### 4.2.1 Transfer from *AEP A* to *B*

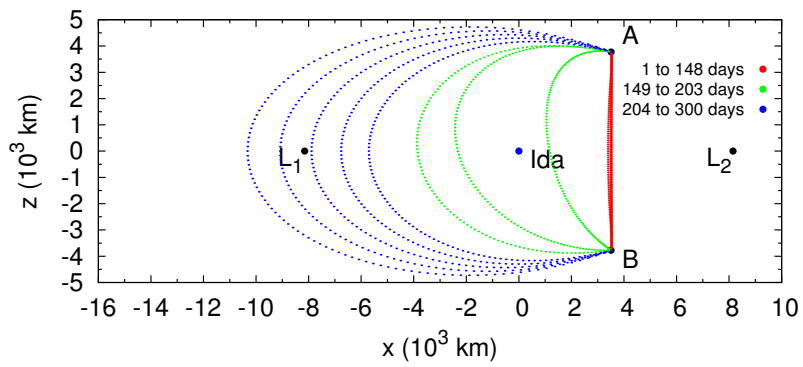
This transfer is between the two artificial equilibrium points A and B, the geometry of this transfer is shown in Figures 4.1 and 4.4. These AEP have two main advantages: they are closer to the asteroid than the Lagrange point L<sub>2</sub> and they are above/below the ecliptic ( $x$ - $y$ ) plane. Thus, these points have special perspectives to observe both poles of Ida. During the transfer, the spacecraft is able to observe different latitudes of the asteroid, moving from a positive  $z$  region to a negative one and vice-versa, as shown in Figure 4.5, which shows the trajectories projected in the ( $x$ - $z$ ) plane for different intervals of time of the transfer ranging from 1 to 300 days. The cases 1, 2, 3, and 4, given in subsection 4.1.3, are represented in Figures 4.5a, 4.5b, 4.5c, and 4.5d, respectively.

The results found for this transfer are shown in Figure 4.6. Figures 4.6a and 4.6b relates  $\Delta V$  and the transfer time. These results can be used to verify the  $\Delta V$  and the corresponding transfer time for a given solar sail configuration with an initial  $\gamma_i$  and a final  $\gamma_f$ . The minimum  $\Delta V$  found during the transfer, as a function of different initial and final values of the angles ( $\gamma_i$  and  $\gamma_f$ ), are shown in Figure 4.6a. The respective times of transfer for the minimum  $\Delta V$  found in Figure 4.6 are shown in Figure 4.6b. Note that the values of  $\gamma$  varies linearly according to Equation (4.7) in the range from  $-90^\circ$  to  $90^\circ$ .

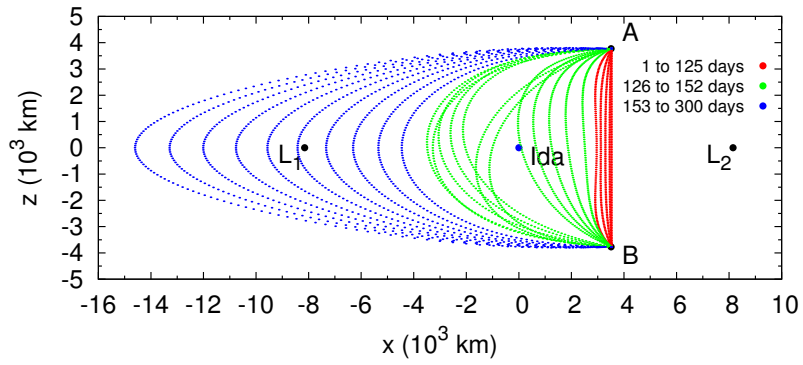
Figure 4.5 - Trajectories from A to B.



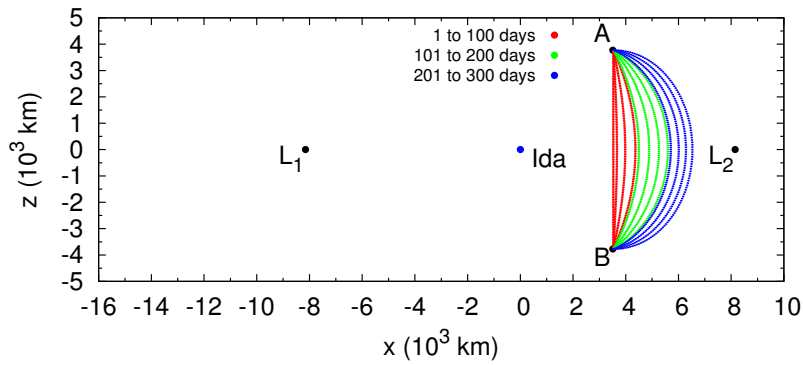
(a) Case 1: trajectories from  $\gamma = 57.35^\circ$  to  $-57.35^\circ$



(b) Case 2: trajectories from  $\gamma = -76.71^\circ$  to  $76.71^\circ$



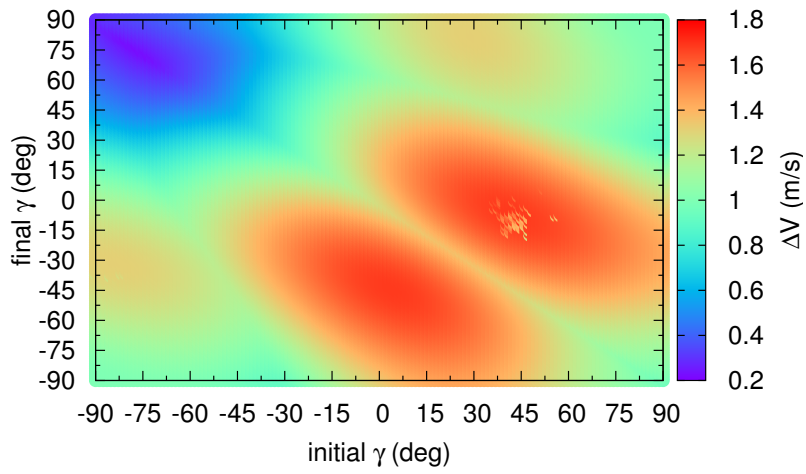
(c) Case 3: trajectories for  $\gamma = 0^\circ$



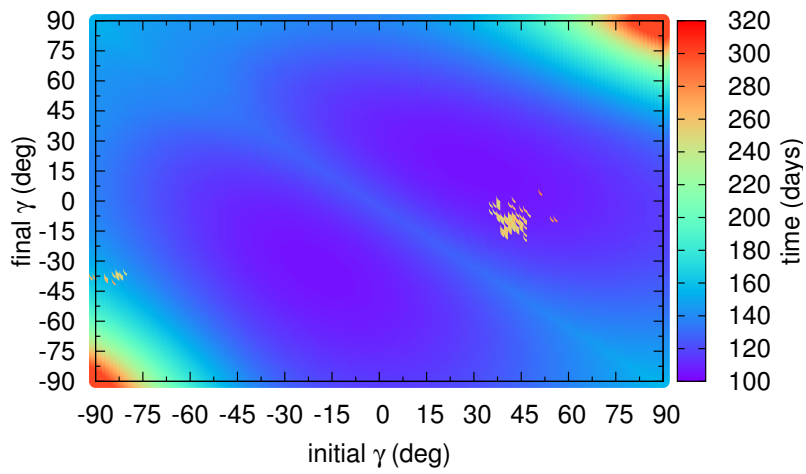
(d) Case 4: trajectories for  $\gamma = 90^\circ$

SOURCE: Author

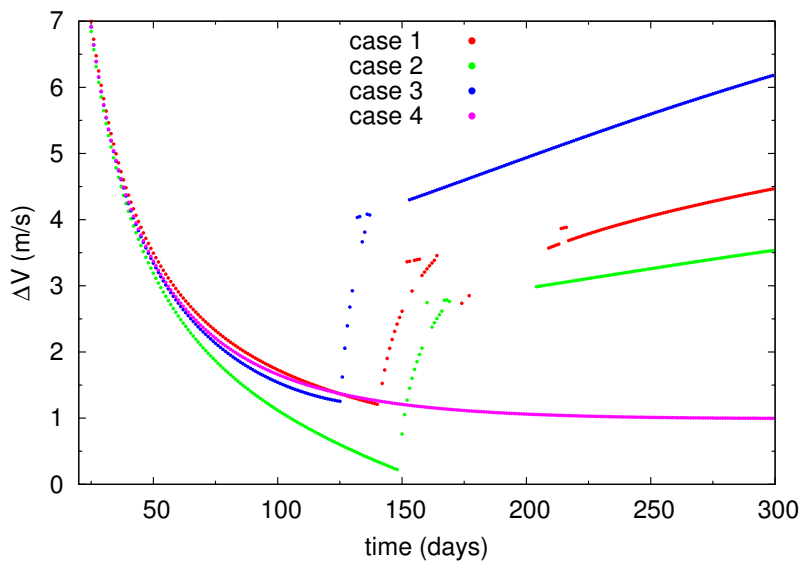
Figure 4.6 - Transfers from A to B.



(a)  $\Delta V$  for linear variation of  $\gamma$ .



(b) Transfer time for linear variation of  $\gamma$ .



(c)  $\Delta V$  as function of time.

SOURCE: Oliveira et al. (2018).

The best results with respect to the  $\Delta V$  costs for this transfer are found in the top left of the plot of Figure 4.6a, where the lowest values are found. It represents the region of minimum  $\Delta V$ , in the order of 0.2 m/s, represented in the dark blue region. On the opposite side, the red regions around  $\gamma_i$  from  $-45^\circ$  to  $90^\circ$  and  $\gamma_f$  from  $-90^\circ$  to  $45^\circ$  represent the regions of larger fuel consumptions. These regions in red also represent minimum times of flight, around 100 days, as can be seen if compared with Figure 4.6b, which shows that the longer transfer times are near  $\gamma_i = 90^\circ$ , in the order of 320 days, which in turn may also be useful for missions that requires long observation times.

The results for the four solar sail configurations given in subsection 4.1.3 are shown in Figure 4.6c. Note that the minimum  $\Delta v$  are reached for a transfer time between 125 to 150 days, for most of the cases, as can be checked in Table 4.4. Case 1 is

Table 4.4 - Transfers from A to B

solar sail configuration	$\gamma_i$ (deg)	$\gamma_f$ (deg)	lowest $\Delta v$ (m/s)	time (days)
case 1	57.35	-57.35	1.210	140
case 2	-76.71	76.71	0.223	148
case 3	0	0	1.254	125
case 4	90	90	0.997	300

SOURCE: Author

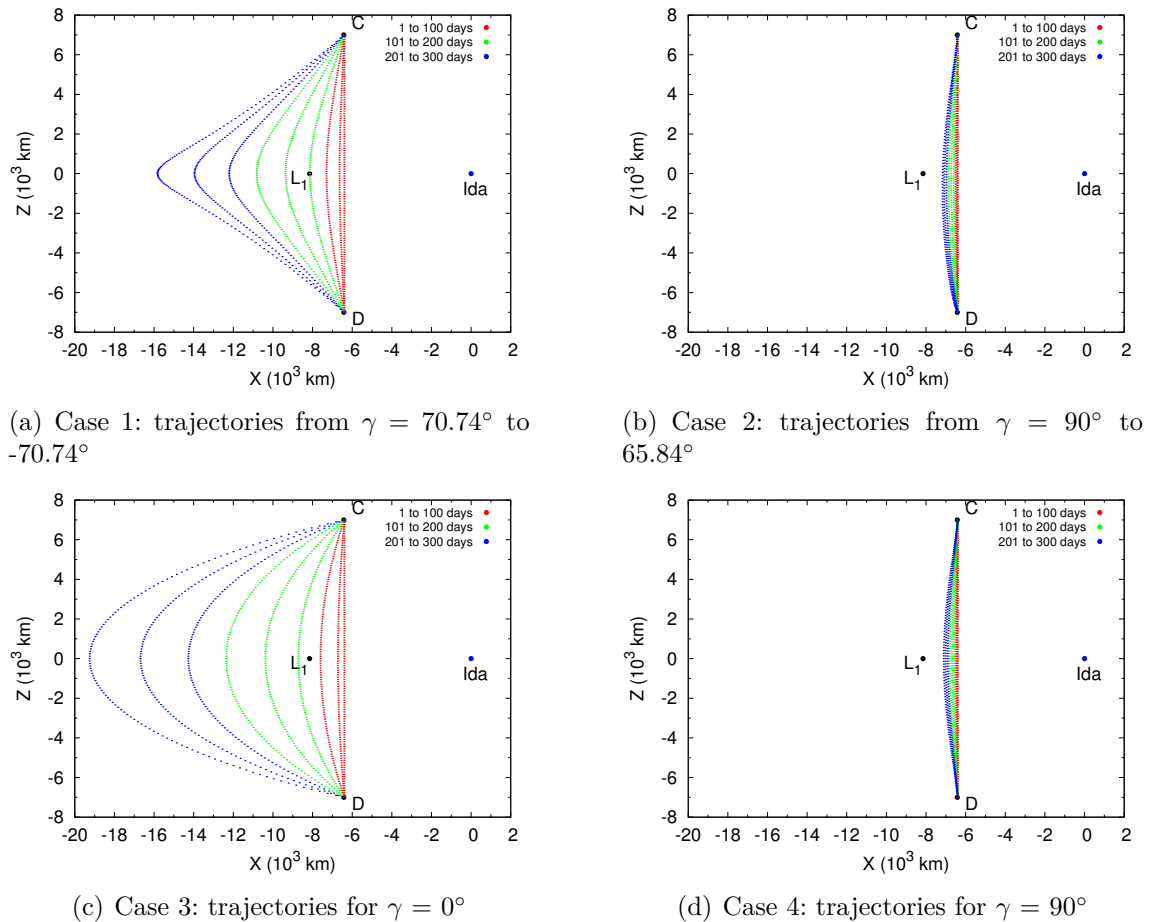
shown by the red line, where  $\gamma_i = 57.35^\circ$  and  $\gamma_f = -57.35^\circ$ , which are the values of  $\gamma$  that allows the spacecraft to remain in equilibrium at the points A and B. Case 2 is represented by the green line, where  $\gamma_i = -76.71^\circ$  and  $\gamma_f = 76.71^\circ$ , showing the values of  $\gamma$  that resulted in the lowest fuel consumption. These values do not let the spacecraft to remain in equilibrium neither before nor after the transfer. It means that attitude maneuvers are required before and after the transfer to place the spacecraft in equilibrium. Case 3 is shown by the blue line, where  $\gamma_i = 0^\circ$  and  $\gamma_f = 0^\circ$ , which means that, during the transfer, the normal vector to the solar sail and the solar rays will always make an angle of  $0^\circ$ , so maximizing the force applied over the spacecraft during the transfer. Case 4 is indicated by the purple line, where  $\gamma_i = 90^\circ$  and  $\gamma_f = 90^\circ$ , which means that during the transfer the vector normal to the solar sail and the solar rays will always make an angle of  $90^\circ$ , so minimizing the force applied over the spacecraft. Table 4.4 shows the lowest values of  $\Delta V$  found for each solar sail configuration and the corresponding time required by the transfer. The discontinuities shown in Figure 4.6c for the cases 1 to 3 around the minimum

$\Delta v$ , are due to a close approach to Ida during the transfer, as can be observed in the projection of the trajectories shown in Figure 4.5. These discontinuities exist around the minimum  $\Delta V$ .

#### 4.2.2 Transfer from AEP C to D

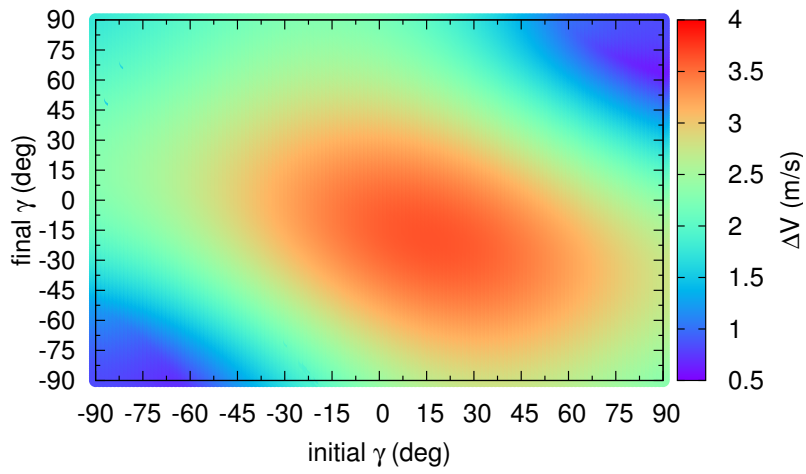
It is now studied transfers between the two artificial equilibrium points C and D, the geometry of this transfer is shown in Figures 4.1 and 4.3. They are close to the Lagrange point  $L_1$ . As occurred in the previous case, in this transfer it is also possible for the spacecraft to observe both poles of the asteroid, moving from a positive  $z$  region to a negative  $z$  region. The results found for these points are presented in Figures 4.7 and 4.8.

Figure 4.7 - Trajectories from C to D.

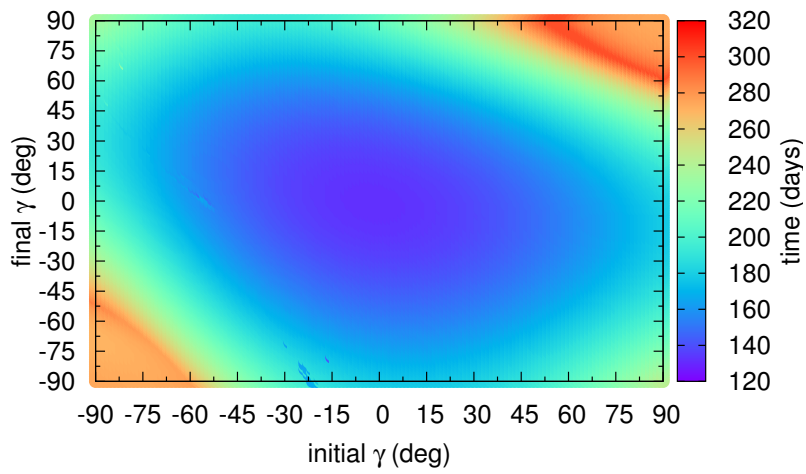


SOURCE: Author

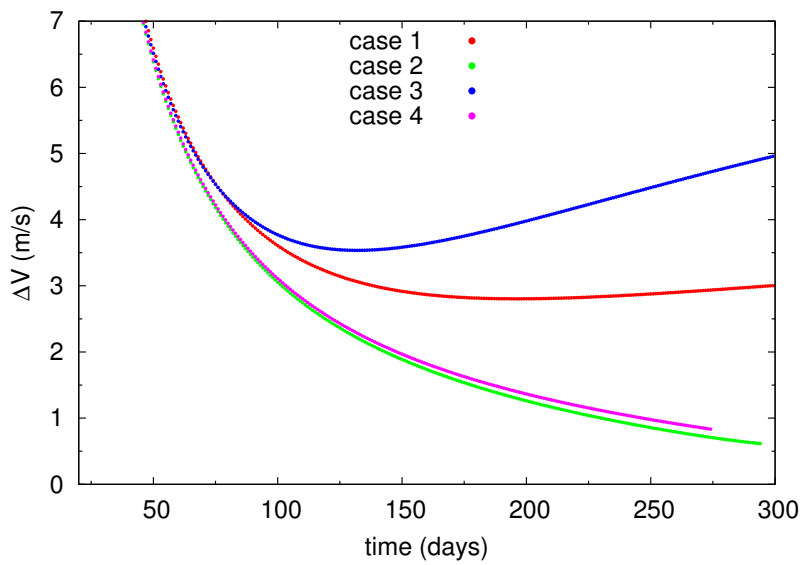
Figure 4.8 - Transfers from C to D.



(a)  $\Delta V$  for linear variation of  $\gamma$ .



(b) Transfer time for linear variation of  $\gamma$ .



(c)  $\Delta V$  as function of time.

SOURCE: Oliveira et al. (2018).

Figure 4.8a shows the  $\Delta V$  as a function of  $\gamma_i$  and  $\gamma_f$ . The values of  $\gamma$  varies according to Equation (4.7), in the range from  $-90^\circ$  to  $90^\circ$ .

The best results with respect to the  $\Delta V$  costs for this transfer are found in the bottom left and in the top right of the plot of Figure 4.8a, where the lowest values are found. It represents the region of minimum  $\Delta V$ , in the order of 1 m/s, represented in the dark blue regions. On the opposite side, the red region around  $\gamma_i$ , from  $-30^\circ$  to  $75^\circ$  and,  $\gamma_f$  from  $-75^\circ$  to  $30^\circ$ , represent the regions of larger fuel consumptions. This region in red also represent minimum times of flight, between 140 to 180 days, as can be seen if compared with Figure 4.8b, which shows that the longer transfer times are near  $\gamma_i -90^\circ$  and  $90^\circ$ , in the order of 280 days, which may also be useful for missions that requires long observation times. The results for the four solar sail configurations given in subsection 4.1.3 are shown in Figure 4.8c. Note that the minimum  $\Delta v$  are reached for a transfer time between 270 to 300 days, for cases 2 and 4, as can be checked in Table 4.5.

Case 1 is shown by the red line, where  $\gamma_i = 70.74^\circ$  and  $\gamma_f = -70.74^\circ$ , the values of  $\gamma$  that allows the spacecraft to remain in equilibrium at points C and D. Case 2 is represented by the green line, where  $\gamma_i = 90^\circ$  and  $\gamma_f = 65.84^\circ$ , the values of  $\gamma$  that results in the lowest fuel consumption, although these values do not let the spacecraft to remain in equilibrium neither before nor after the transfer. Attitude maneuvers are required here. Case 3 is the blue line, where  $\gamma_i = 0^\circ$  and  $\gamma_f = 0^\circ$ , which means that during the transfer the normal vector to the solar sail and the solar rays will always make an angle of  $0^\circ$ , so maximizing the force applied over the spacecraft during the transfer. Case 4 is the purple line, where  $\gamma_i = 90^\circ$  and  $\gamma_f = 90^\circ$ , which means that, during the transfer, the vector normal to the solar sail and the solar rays will always make an angle of  $90^\circ$ , so minimizing the force applied over the spacecraft.

Table 4.5 shows the lowest values of  $\Delta V$  found for each solar sail configuration and the corresponding time required by the transfer.

### 4.2.3 Transfer from $L_1$ to AEP A

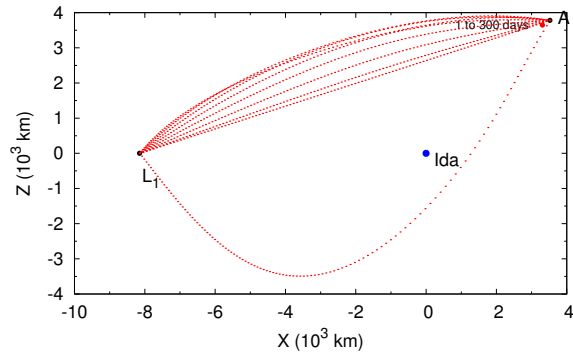
This transfer is now between the Langrange point  $L_1$  and the artificial equilibrium point A, the geometry of this transfer is shown in Figures 4.1 and 4.2. In this transfer the spacecraft goes closer to the asteroid than the previous transfers. However, in this case, it can observe only one pole of the asteroid, moving from  $z = 0$  to a positive  $z$  region.

solar sail configuration	$\gamma_i$ (deg)	$\gamma_f$ (deg)	lowest $\Delta v$ (m/s)	time (days)
case 1	70.74	-70.74	2.803	196
case 2	90	65.84	0.616	294
case 3	0	0	3.536	132
case 4	90	90	0.834	274

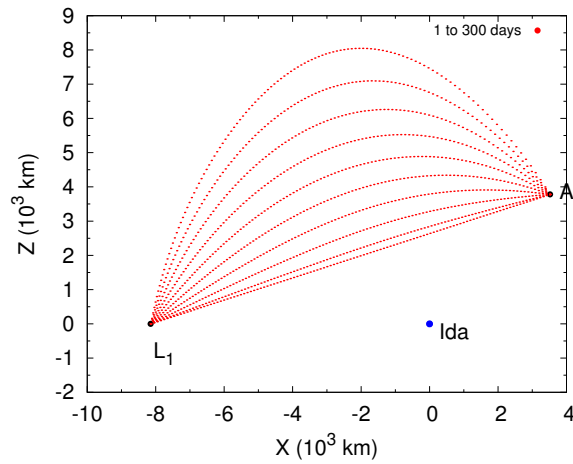
SOURCE: Author

The results found for these points are presented in Figures 4.9 and 4.10. Figure 4.10a shows the  $\Delta V$  as a function of  $\gamma_i$  and  $\gamma_f$ . The values of  $\gamma$  varies according to Equation (4.7) in the range from  $-90^\circ$  to  $90^\circ$ . The best results for this transfer are found in the bottom left of the plot, where the lowest values are found. Figure 4.10b shows the time for the minimum  $\Delta v$  found for the respective  $\gamma_i$  and  $\gamma_f$ . For most of the transfers the minimum  $\Delta v$  are found for the time between 100 to 200 days. Figure 4.10c shows the results for the four solar sail configuration. Case 1 is the red line, where  $\gamma_i = 90^\circ$  and  $\gamma_f = 57.35^\circ$ , the values of  $\gamma$  that allows the spacecraft to remain in the Lagrange point  $L_1$  and at the equilibrium point C. Case 2 is the green line, where  $\gamma_i = -85.16^\circ$  and  $\gamma_f = -44.09^\circ$ , the values of  $\gamma$  that results in the lowest fuel consumption, although these values do not let the spacecraft to remain in equilibrium neither before nor after the transfer. Case 3 is the blue line, where  $\gamma_i = 0^\circ$  and  $\gamma_f = 0^\circ$ , which means that during the transfer the vector normal to the solar sail and the solar rays will always make an angle of  $0^\circ$ , so maximizing the force applied over the spacecraft during the transfer. Case 4 is the purple line, where  $\gamma_i = 90^\circ$  and  $\gamma_f = 90^\circ$ , which means that during the transfer the vector normal to the solar sail and the solar rays will always make an angle of  $90^\circ$ , so minimizing the force applied over the spacecraft.

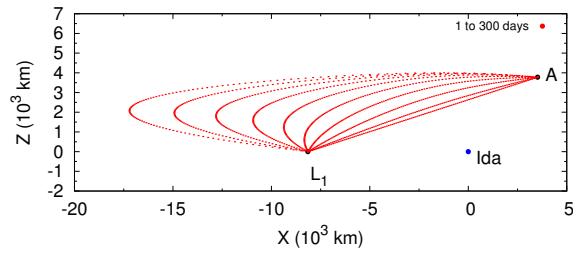
Figure 4.9 - Trajectories from  $L_1$  to A.



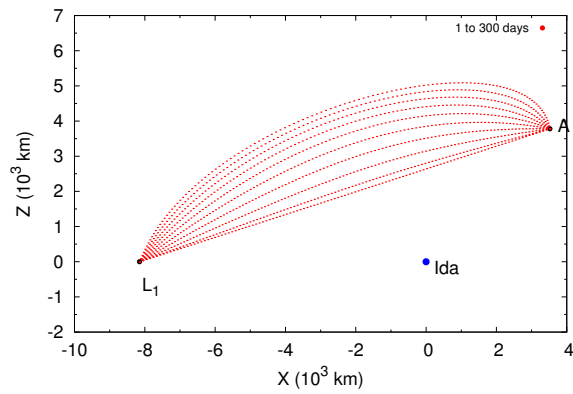
(a) Case 1: trajectories from  $\gamma = 90^\circ$  to  $57.35^\circ$



(b) Case 2: trajectories from  $\gamma = -85.16^\circ$  to  $-44.09^\circ$

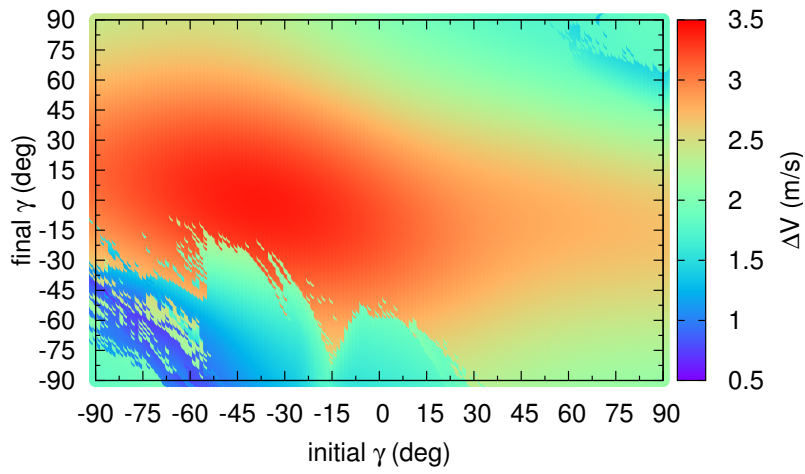


(c) Case 3: trajectories for  $\gamma = 0^\circ$

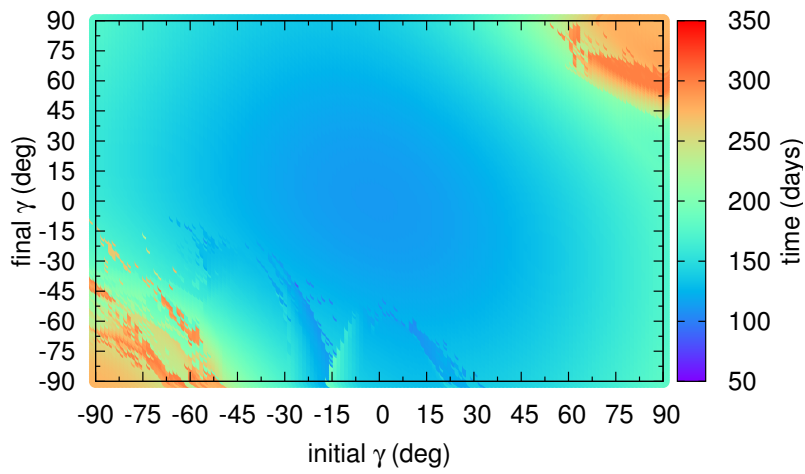


(d) Case 4: trajectories for  $\gamma = 90^\circ$

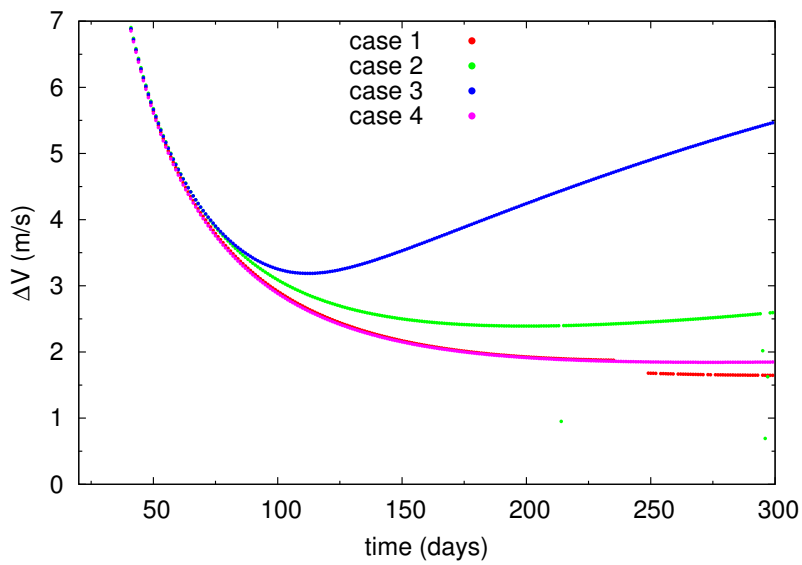
Figure 4.10 - Transfers from  $L_1$  to A.



(a)  $\Delta V$  for linear variation of  $\gamma$ .



(b) Transfer time for linear variation of  $\gamma$ .



(c)  $\Delta V$  as function of time.

SOURCE: Oliveira et al. (2018).

Table 4.6 shows the lowest values of  $\Delta V$  found for each solar sail configuration and the corresponding time required by the transfer.

Table 4.6 - Transfers from  $L_1$  to A

solar sail configuration	$\gamma_i$ (deg)	$\gamma_f$ (deg)	lowest $\Delta v$ (m/s)	time (days)
case 1	90	57.35	1.647	300
case 2	-85.16	-44.09	0.692	296
case 3	0	0	3.187	112
case 4	90	90	1.844	274

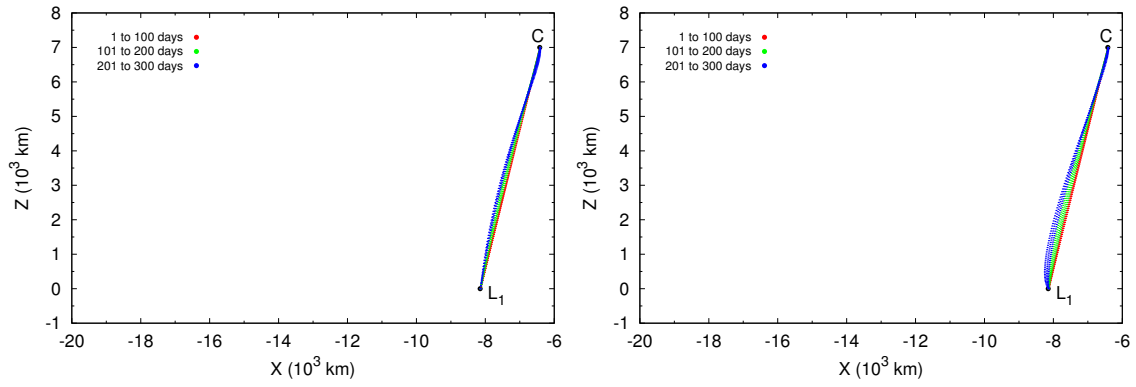
SOURCE: Author

#### 4.2.4 Transfer from $L_1$ to $AEP C$

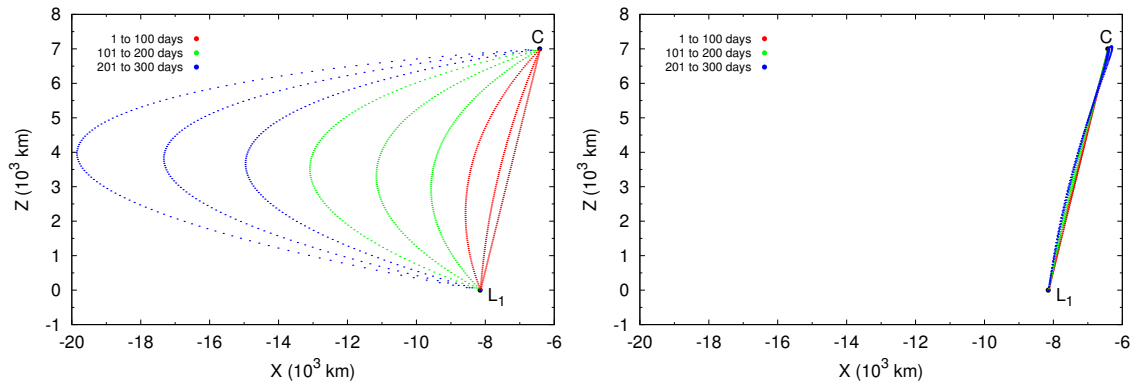
The transfers are now between the Langrange point  $L_1$  and the artificial equilibrium point C, shown in Figures 4.1 and 4.3. In this transfer it is possible to make the spacecraft to observe only one pole of the asteroid. It will be moved from  $z = 0$  to a positive  $z$  region. However, in this transfer, the  $\Delta V$  is smaller than the one necessary to move the spacecraft from C to D. The results found for these points are presented in Figures 4.11 and 4.12.

Figure 4.12a shows the  $\Delta V$  as a function of  $\gamma_i$  and  $\gamma_f$ . The values of  $\gamma$  varies according to Equation (4.7) in the range from  $-90^\circ$  to  $90^\circ$ . The best results with respect to the  $\Delta v$  costs for this transfer are found in the bottom left and top right of the plot of Figure 4.12a, where the lowest values are found. It represents the region of minimum  $\Delta V$ , in the order of 0.5 m/s, represented by the blue regions. On the opposite side, the orange region around  $\gamma_i$  from  $-90^\circ$  to  $30^\circ$  and  $\gamma_f$  from  $-30^\circ$  to  $90^\circ$  represent the region of larger fuel consumptions. This region in orange also represents the minimum times of flight, around 100 days, as can be seen if compared with Figure 4.12b, which shows that the longer transfer times are near  $\gamma_i = 75^\circ$ , in the order of 300 days, which in turn may also be useful for missions that requires long observation times. The results for the four solar sail configurations given in subsection 4.1.3 are shown in Figure 4.12c. Note that the minimum  $\Delta V$  are reached for a transfer time between 240 to 300 days, for most cases, as can be checked in Table 4.7.

Figure 4.11 - Trajectories from  $L_1$  to C.



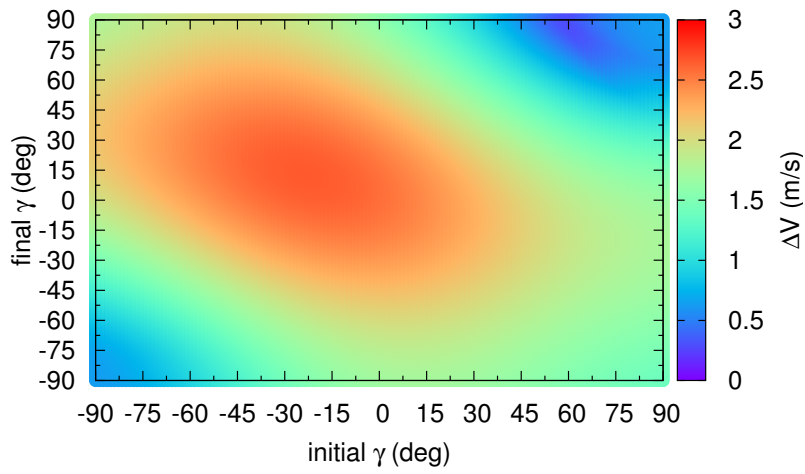
(a) Case 1: trajectories from  $\gamma = 90^\circ$  to  $70.74^\circ$  (b) Case 2: trajectories from  $\gamma = 59.79^\circ$  to  $90^\circ$



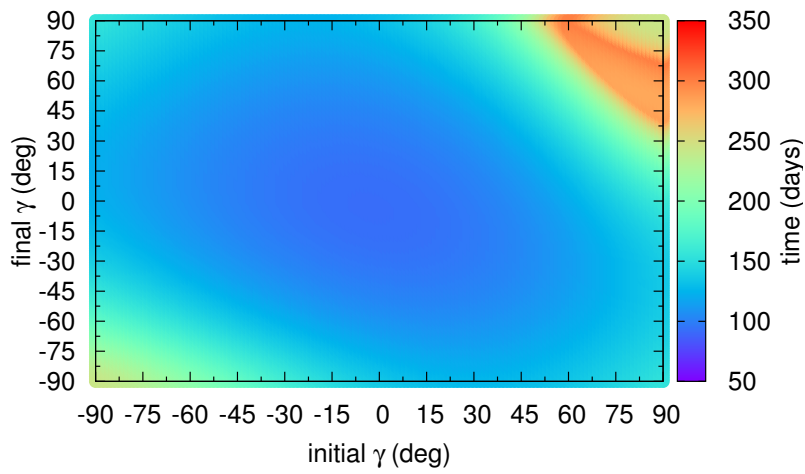
(c) Case 3: trajectories for  $\gamma = 0^\circ$  (d) Case 4: trajectories for  $\gamma = 90^\circ$

SOURCE: Author

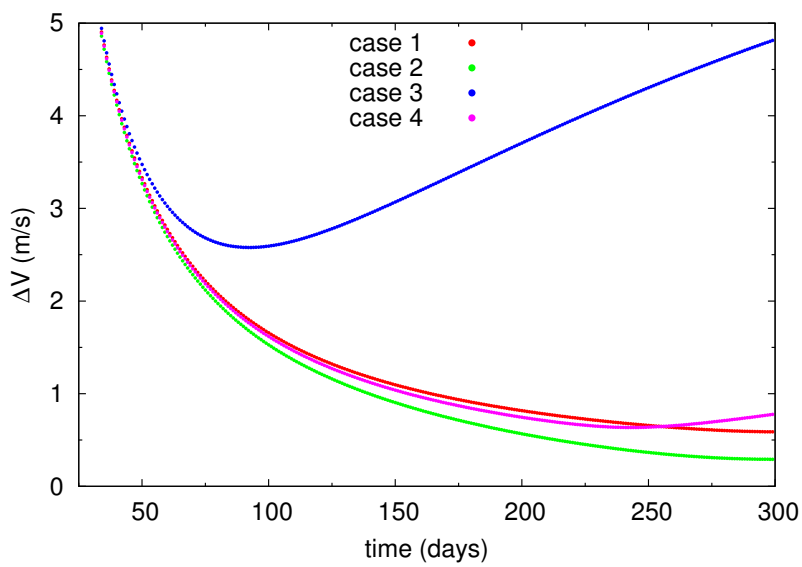
Figure 4.12 - Transfers from  $L_1$  to C.



(a)  $\Delta V$  for linear variation of  $\gamma$ .



(b) Transfer time for linear variation of  $\gamma$ .



(c)  $\Delta V$  as function of time.

SOURCE: Oliveira et al. (2018).

Case 1 is shown by the red line, where  $\gamma_i = 90^\circ$  and  $\gamma_f = 70.74^\circ$ , the values of  $\gamma$  that allows the spacecraft to remain in the Lagrange point  $L_1$  and at the equilibrium point C. Case 2 is indicated by the green line, where  $\gamma_i = 59.79^\circ$  and  $\gamma_f = 90^\circ$ , the values of  $\gamma$  that result in the lowest fuel consumption. These values do not let the spacecraft to remain in equilibrium positions, neither before nor after the transfer. It means that attitude maneuvers are required here. Case 3 is represented by the blue line, where  $\gamma_i = 0^\circ$  and  $\gamma_f = 0^\circ$ , which means that during the transfer the vector normal to the solar sail and the solar rays will always make an angle of  $0^\circ$ , so maximizing the force applied over the spacecraft during the transfer. Case 4 is shown by the purple line, where  $\gamma_i = 90^\circ$  and  $\gamma_f = 90^\circ$ , which means that during the transfer the vector normal to the solar sail and the solar rays will always make an angle of  $90^\circ$ , so minimizing the force applied over the spacecraft. Table 4.7 shows the lowest values of  $\Delta v$  found for each solar sail configuration and the corresponding time required by the transfer.

Table 4.7 - Transfers from  $L_1$  to C

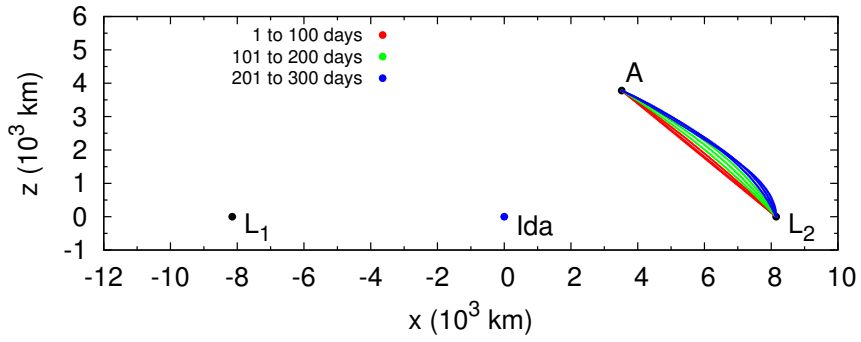
solar sail configuration	$\gamma_i$ (deg)	$\gamma_f$ (deg)	lowest $\Delta v$ (m/s)	time (days)
case 1	90	70.74	0.588	300
case 2	59.79	90	0.292	299
case 3	0	0	2.578	92
case 4	90	90	0.635	243

SOURCE: Author

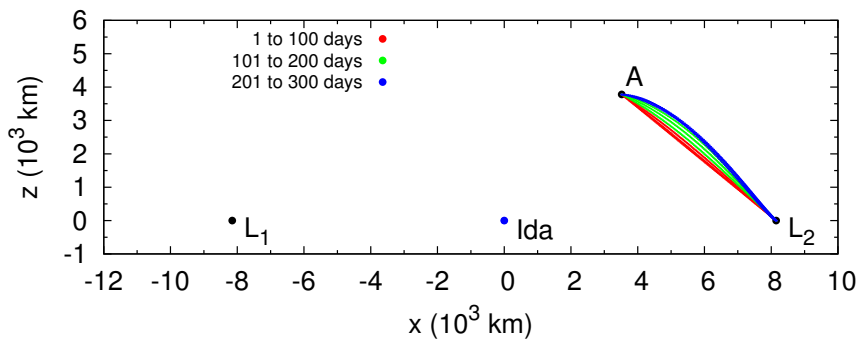
#### 4.2.5 Transfer from $L_2$ to $AEP A$

This transfer is now between the Langrange point  $L_2$  and the artificial equilibrium point A, shown in Figures 4.1 and 4.4. Similarly to the transfers from  $L_1$  to A, in this case the spacecraft goes close to the asteroid. In the same way it can observe only one pole of the asteroid, moving from  $z = 0$  to a positive  $z$  region. The results found for these points are presented in Figures 4.13 and 4.14.

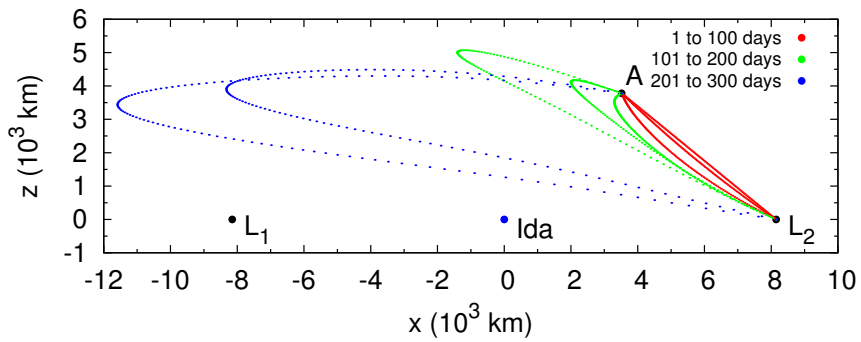
Figure 4.13 - Trajectories from  $L_2$  to A.



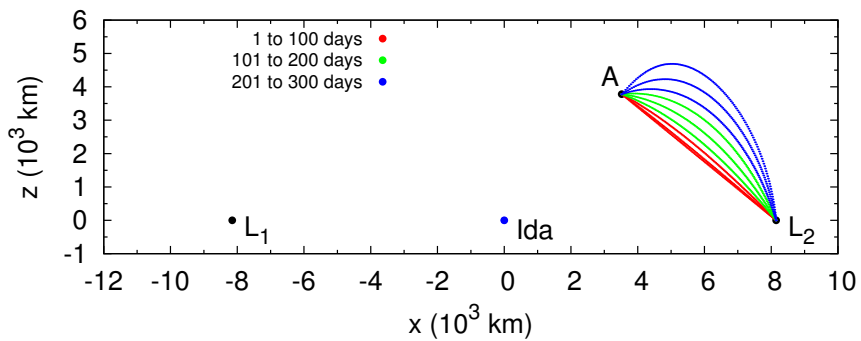
(a) Case 1: trajectories from  $\gamma = 90^\circ$  to  $57.35^\circ$



(b) Case 2: trajectories for  $\gamma = 71.88^\circ$



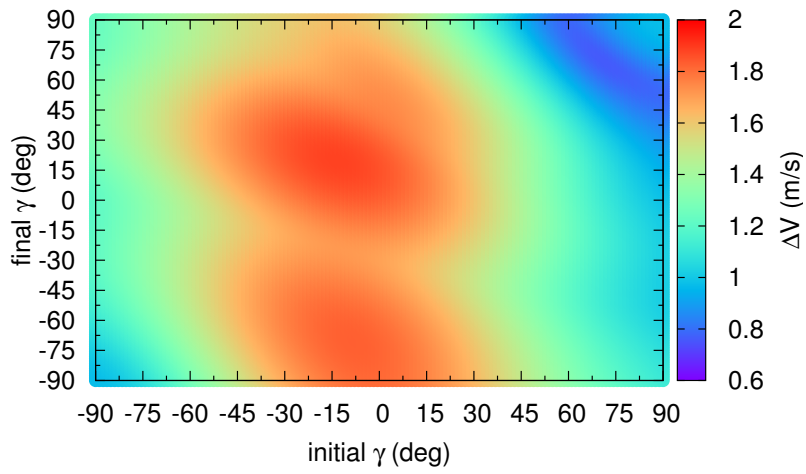
(c) Case 3: trajectories for  $\gamma = 0^\circ$



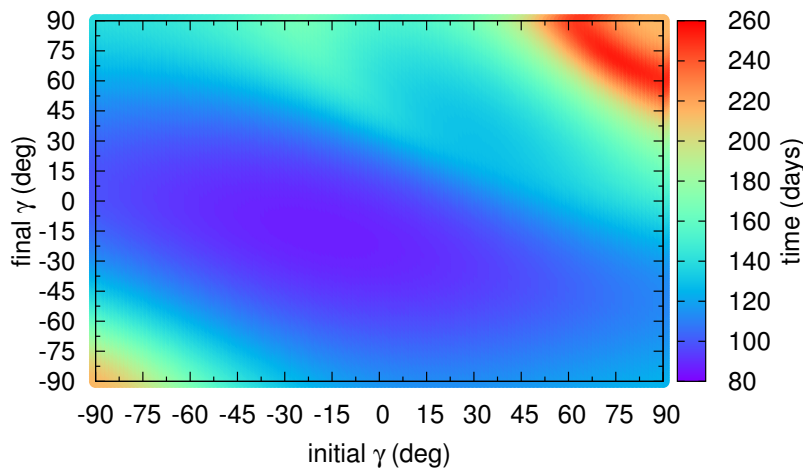
(d) Case 4: trajectories for  $\gamma = 90^\circ$

SOURCE: Author

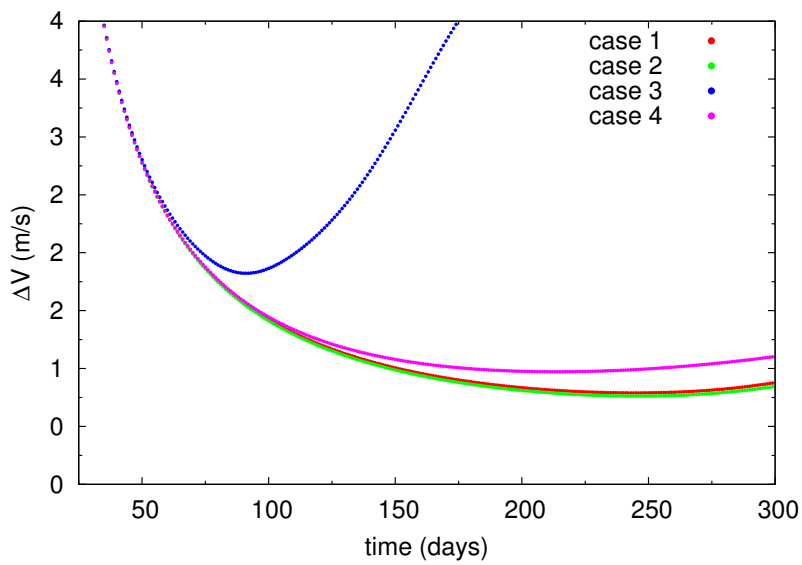
Figure 4.14 - Transfers from L<sub>2</sub> to A.



(a)  $\Delta V$  for linear variation of  $\gamma$ .



(b) Transfer time for linear variation of  $\gamma$ .



(c)  $\Delta V$  as function of time.

SOURCE: Oliveira et al. (2018).

Figure 4.14a shows the  $\Delta V$  as a function of  $\gamma_i$  and  $\gamma_f$ . The values of  $\gamma$  varies according to Equation (4.7) in the range from  $-90^\circ$  to  $90^\circ$ .

The best results with respect to the  $\Delta V$  costs for this transfer are found in the top right of the plot of Figure 4.14a, where the lowest values are found. It represents the region of minimum  $\Delta V$ , in the order of 0.8 m/s, represented by the dark blue region. On the opposite side, the red regions around  $\gamma_i$  from  $-45^\circ$  to  $30^\circ$  and  $\gamma_f$  from  $-90^\circ$  to  $90^\circ$  represent the regions of larger fuel consumptions. These regions in red also represent the minimum times of flight, around 100 days, as can be seen if compared with Figure 4.14b, which shows that the longer transfer times are near  $\gamma_i = 90^\circ$ , in the order of 220 days, which in turn may also be useful for missions that requires long observation times. The results for the four solar sail configurations given in subsection 4.1.3 are shown in Figure 4.14c. Note that the minimum  $\Delta V$  are reached for a transfer time between 200 to 250 days, for most cases, as can be checked in Table 4.8.

Case 1 is represented by the red line, where  $\gamma_i = 90^\circ$  and  $\gamma_f = 57.35^\circ$ , which are the values of  $\gamma$  that allows the spacecraft to remain in the Lagrange point  $L_2$  and at the equilibrium point A. Case 2 is shown by the green line, where  $\gamma_i = 71.88^\circ$  and  $\gamma_f = 71.88^\circ$ , the values of  $\gamma$  that results in the lowest fuel consumption, although these values do not let the spacecraft to remain in equilibrium neither before nor after the transfer. Once again attitude maneuvers are required here. Case 3 can be seen in the blue line, where  $\gamma_i = 0^\circ$  and  $\gamma_f = 0^\circ$ , which means that during the transfer the vector normal to the solar sail and the solar rays will always make an angle of  $0^\circ$ , so maximizing the force applied over the spacecraft during the transfer. Case 4 is available in the purple line, where  $\gamma_i = 90^\circ$  and  $\gamma_f = 90^\circ$ , which means that during the transfer the vector normal to the solar sail and the solar rays will always make an angle of  $90^\circ$ , so minimizing the force applied over the spacecraft. Table 4.8 shows the lowest values of  $\Delta v$  found for each solar sail configuration and the corresponding time required by the transfer.

Table 4.8 - Transfers from  $L_2$  to A

solar sail configuration	$\gamma_i$ (deg)	$\gamma_f$ (deg)	lowest $\Delta v$ (m/s)	time (days)
case 1	90	57.35	0.789	244
case 2	71.88	71.88	0.762	245
case 3	0	0	1.822	91
case 4	90	90	0.972	213

SOURCE: Author

#### 4.2.6 Transfer from $L_2$ to AEP C

This transfer is now between the Lagrange point  $L_2$  and the artificial equilibrium point C, shown in Figure 4.1 and 4.2. Similarly with the case from  $L_1$  to A, this transfer goes from  $z = 0$  to a position  $z$  region where the spacecraft can observe one pole of the asteroid.

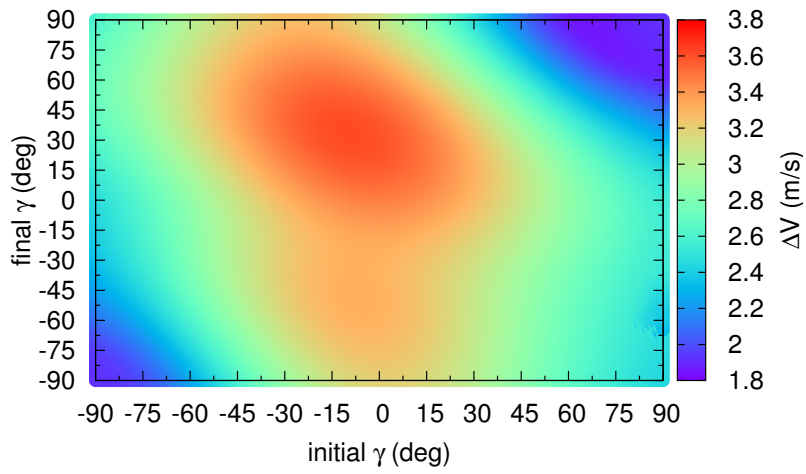
The results found for these points are presented in Figure 4.15. Figure 4.15a shows the  $\Delta V$  as a function of  $\gamma_i$  and  $\gamma_f$ . The values of  $\gamma$  varies according to Equation (4.7) in the range from  $-90^\circ$  to  $90^\circ$ . The best results for this transfer are found in the bottom left and top right of the plot where the lowest values were found. Figure 4.15b shows the time for the minimum  $\Delta V$  found for the respective  $\gamma_i$  and  $\gamma_f$ . For most of the transfers the minimum  $\Delta V$  are found for times between 120 to 160 days. Figure 4.15c shows the results of the four solar sail configuration. Case 1 is the red line, where  $\gamma_i = 90^\circ$  and  $\gamma_f = 70.74^\circ$ , the values of  $\gamma$  that allows the spacecraft to remain in the Lagrange point  $L_2$  and at the equilibrium point C. Case 2 is the green line, where  $\gamma_i = 67.04^\circ$  and  $\gamma_f = 90^\circ$ , the values of  $\gamma$  that results in the lowest fuel consumption, although these values do not let the spacecraft remain in equilibrium neither before nor after the transfer. Attitude maneuvers are required here. Case 3 is the blue line, where  $\gamma_i = 0^\circ$  and  $\gamma_f = 0^\circ$ , which means that during the transfer the vector normal to the solar sail and the solar rays will always make an angle of  $0^\circ$ , so maximizing the force applied over the spacecraft during the transfer. Case 4 is the purple line, where  $\gamma_i = 90^\circ$  and  $\gamma_f = 90^\circ$ , which means that during the transfer the vector normal to the solar sail and the solar rays will always make an angle of  $90^\circ$ , so minimizing the force applied over the spacecraft. Table 4.9 shows the lowest values of  $\Delta v$  found for each solar sail configuration and the corresponding time required by the transfer.

Table 4.9 - Transfers from  $L_2$  to C

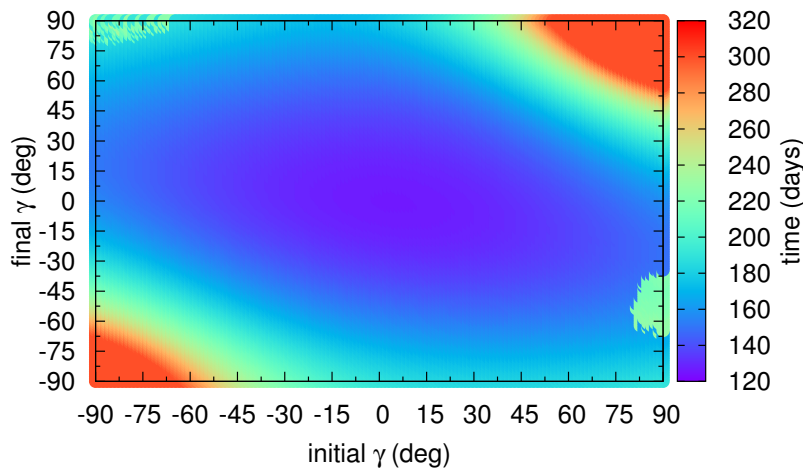
solar sail configuration	$\gamma_i$ (deg)	$\gamma_f$ (deg)	lowest $\Delta v$ (m/s)	time (days)
case 1	90	70.74	1.884	300
case 2	67.04	90	1.853	300
case 3	0	0	3.455	126
case 4	90	90	1.917	300

SOURCE: Author

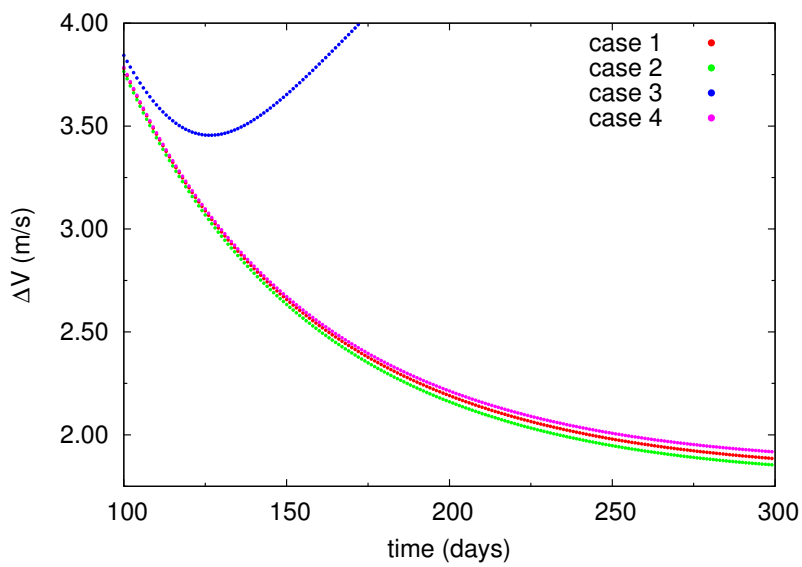
Figure 4.15 - Transfers from L<sub>2</sub> to C.



(a)  $\Delta V$  for linear variation of  $\gamma$ .



(b) Transfer time for linear variation of  $\gamma$ .



(c)  $\Delta V$  as function of time.

SOURCE: Oliveira et al. (2018).

## 5 MAPPING TRAJECTORIES FOR A SPACECRAFT TO HIT AN ASTEROID TO AVOID A COLLISION WITH THE EARTH

The aim of this chapter is find trajectories to send a spacecraft to an asteroid with the objective of hitting it, to change its orbit around the Sun and consequently avoid its collision with the Earth. Several researches considered this problem in the past (ROSS et al., 2001; CARUSI et al., 2002; IZZO, 2005; VASILE; COLOMBO, 2008; ENGLANDER et al., 2009; CASALINO; SIMEONI, 2012; ZUIANI et al., 2012). The idea is to make a general study to find the time of flight and total delta-V required to leave an orbit nearby Earth and hit an asteroid. We chose the asteroid (175706) 1996FG3 (SCHEIRICH et al., 2015; YU et al., 2014), to exemplify the method. A study like this is important because its objective is to minimize the time of flight and increment the velocity to be applied in the Earth, but to maximize the velocity that the spacecraft has when it arrives at the asteroid. Therefore, these trajectories in this work are different from the ones found for scientific mission, which usually come from the search for the minimum consumption of fuel, so minimizing the total velocity variation of the spacecraft.

The time required by the spacecraft to reach its target is very important to modify the orbit of the asteroid, then even trajectories with high fuel consumption may be interesting, since the time of transfer is short, considering the whole mission and the effects in the deviation of the asteroid trajectory. So, the idea is to make mappings that can show the time of transfer, increment of velocity and the velocity of approach, such that the mission designer can choose the best options for each situation.

The dynamical model used is the circular restricted three-body problem (SZEBEHELY, 1967), considering the Sun and the Earth as the main primaries of the system. Besides those gravity forces, the effects of the solar radiation pressure in the trajectory of the spacecraft is also included. This is very important, because some trajectories may be longer, so accumulating those effects during a long time. Those effects may also affect the increment of velocity for launching and the impact velocity. The effects of the solar radiation pressure depends on the area/mass ratio of the spacecraft, so it is possible to increase or decrease those effects by adding or removing panels to the spacecraft, if it is interesting for the mission. However, the main idea is not to use the solar radiation pressure as a control, since they have a very low thrust, which is not adequate for collision avoidance missions, but to measure its effects in the trajectory and the main parameters of the mission.

## 5.1 Methodology

As mentioned before, the restricted three-body problem is the model used in this work, considering the canonical system of units, described in section 2.2. The unit of mass is the total mass of the system, where the mass of Sun ( $M_1$ ) is added to the mass of the Earth ( $M_2$ ) and the spacecraft ( $M_3$ ) is assumed to have a negligible mass. In this system, the non-dimensional mass of the Earth is given by the mass ratio:

$$\mu = \frac{M_2}{M_1 + M_2}, \quad (5.1)$$

while the non-dimensional mass of Sun is given by  $(1 - \mu)$ .

Using in this problem a fixed inertial reference system, where the origin is located in the center of the Sun-Earth system, it is possible to develop the equations of motion. The x-axis is the line connecting  $M_1$  and  $M_2$  and the vertical axis is the line perpendicular to the x-axis. In this system,  $M_1$  and  $M_2$  have positions that are given by:

$$\begin{aligned} \bar{x}_1 &= -\mu r \cos \nu, \\ \bar{y}_1 &= -\mu r \sin \nu, \\ \bar{z}_1 &= 0, \\ \bar{x}_2 &= (1 - \mu)r \cos \nu, \\ \bar{y}_2 &= (1 - \mu)r \sin \nu \\ \bar{z}_2 &= 0. \end{aligned} \quad (5.2)$$

Where  $r$  is the distance between the two primaries, given by:

$$r = \frac{1 - e^2}{1 + e \cos \nu}, \quad (5.3)$$

and  $\nu$  is the true anomaly of  $M_2$ . In the inertial reference system, the equations of motion of the spacecraft are given by:

$$\begin{aligned} \ddot{\bar{x}} &= -\frac{(1 - \mu)(\bar{x} - \bar{x}_1)}{r_1^3} - \frac{\mu(\bar{x} - \bar{x}_2)}{r_2^3}, \\ \ddot{\bar{y}} &= -\frac{(1 - \mu)(\bar{y} - \bar{y}_1)}{r_1^3} - \frac{\mu(\bar{y} - \bar{y}_2)}{r_2^3}, \\ \ddot{\bar{z}} &= -\frac{(1 - \mu)(\bar{z} - \bar{z}_1)}{r_1^3} - \frac{\mu(\bar{z} - \bar{z}_2)}{r_2^3}. \end{aligned} \quad (5.4)$$

Where  $r_1$  and  $r_2$  are the distances from the spacecraft to  $M_1$  and  $M_2$ , respectively,

given by:

$$\begin{aligned} r_1^2 &= (\bar{x} - \bar{x}_1)^2 + (\bar{y} - \bar{y}_1)^2, \\ r_2^2 &= (\bar{x} - \bar{x}_2)^2 + (\bar{y} - \bar{y}_2)^2. \end{aligned} \tag{5.5}$$

Table 5.1 shows the parameters used to calculate the acceleration of the solar radiation pressure in the Sun-Earth system, as described in section 2.1.

Table 5.1 - Parameters of the Sun-Earth system.

$r_s$	<i>variable</i>
$S_r/c$	$4.56 \times 10^{-6} \text{ N/m}^2$
$\mu_{sun}$	$1.327 \times 10^{20} \text{ m}^3/\text{s}^2$
$\mu_{earth}$	$3.986 \times 10^{14} \text{ m}^3/\text{s}^2$
<i>A/m ratio</i>	0, 0.1, 0.5 and 5 $\text{m}^2/\text{kg}$
$C_r$	1.5

SOURCE: Luzum et al. (2011)

Table 5.2 presents the values of the parameters of the Sun-Earth system considering the canonical system of units.

Table 5.2 - Canonical system of units for the Sun-Earth system.

unit of distance	149,596,000 <i>km</i>
unit of time	58.13 <i>days</i>
unit of velocity	29.79 <i>km/s</i>

SOURCE: Prado (2006)

The target of the mission, i.e., the arrival point of the transfer from Earth, is the binary asteroid (175706) 1996FG3 (SCHEIRICH et al., 2015; YU et al., 2014), that was discovered on 1996, March 24 and is an Apollo Family Near Earth Asteroid. This type of asteroid has an orbit that crosses orbit of the Earth around the Sun, however it is more distant from the Sun than the Earth, for most of its orbit. It has a 395 days orbital period tilted at an angle of 2 degrees to the plane of the Solar System, which

takes it in a periapsis of  $0.69 \text{ au}$  from the Sun, slightly inside the orbit of Venus, to an apoapsis of  $1.42 \text{ au}$ , slightly outside the orbit of Mars. It has an eccentricity  $e = 0.349$  and a semi-major axis of about  $1.05 \text{ au}$ .

## 5.2 Results

The main results of this work is to find trajectories of the spacecraft that leave the Earth and intercept the asteroid after some time. The initial date is specified and it is the moment that the spacecraft leaves the Earth. After that, a time of flight is defined, such that it is possible to know the exact location of the asteroid after this time of flight. It means that this is a problem of finding trajectories linking two given points.

It can be formulated as: "Find an orbit (in the three-body problem context) that makes a spacecraft to leave a given point A and goes to another given point B". This is the "Two Point Boundary Value Problem" (TPBVP). If the transfer time is free, there is an infinite number of solutions. The approach used here to find the solutions is to give a time of flight for the transfer as already explained. So, this problem becomes the "Lambert's three-body problem" which can be formulated as: "Find an orbit (in the three-body problem context) that makes a spacecraft to leave a given point A and go to another given point B, arriving there after a specified time of flight". So, by changing the time of flight, it is possible to find a family of transfer orbits, verifying the transfer angle, the variation of velocity required to send the spacecraft to orbit and the relative velocity of impact with the asteroid. The algorithm used to solve this problem is described in section 2.4.

This solution gives the trajectory of the spacecraft, as well as quantities of the fuel consumption, specified by amount of  $\Delta V$  in the entire transfer time, *i.e.*,  $\Delta V_1$  in the launch of the spacecraft and  $\Delta V_2$  in the interception of the spacecraft with the asteroid.

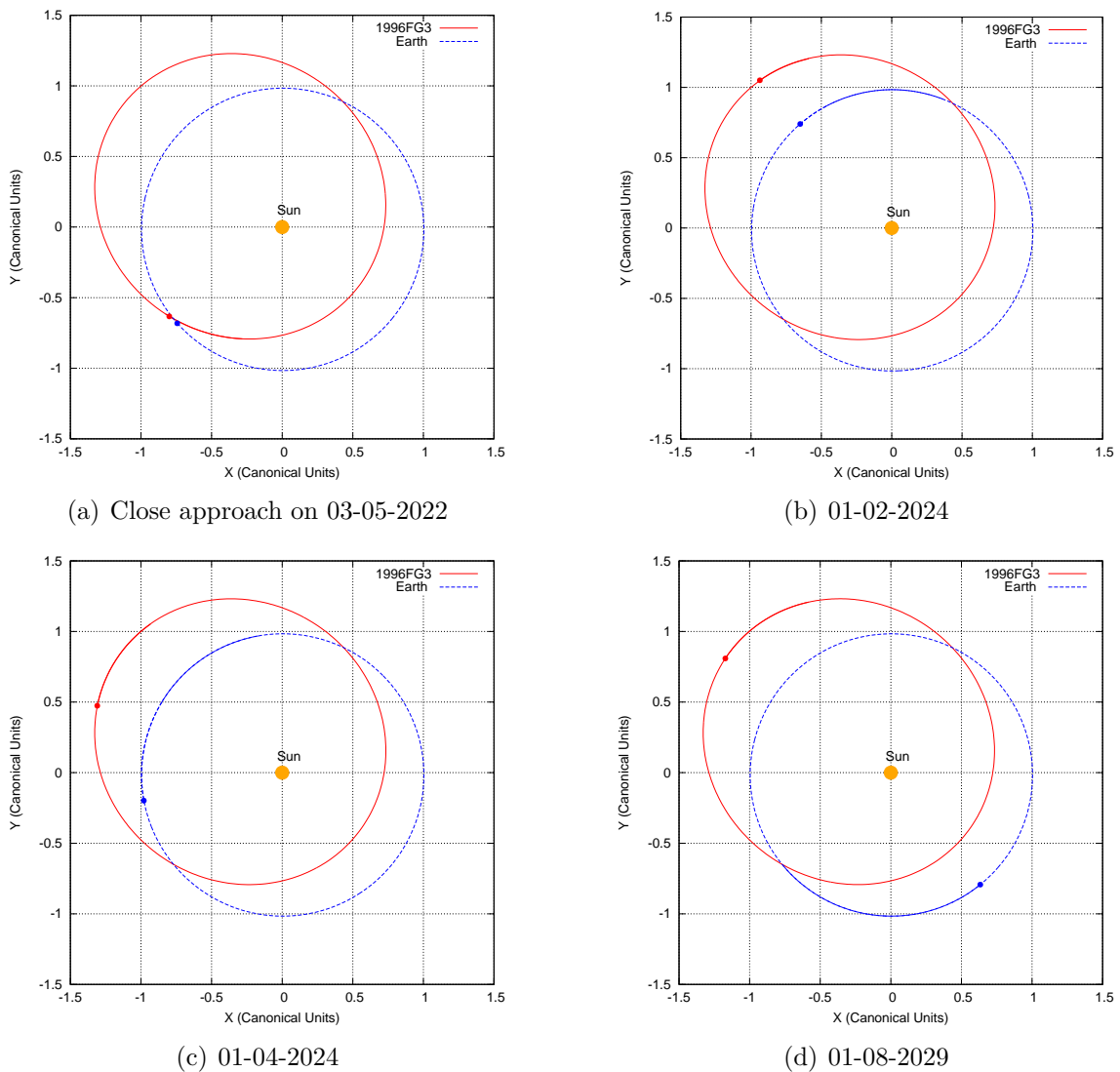
In this work four different dates were proposed to the spacecraft intercepts the asteroid. Table 5.3 presents those dates and the respective distance of approach between the Earth and the asteroid. Figure 5.1 shows the orbits of the Earth and asteroid 1996FG3 in a fixed inertial system, centered in the Sun. It shows the orbit of the Earth (blue) as well as the orbit of the asteroid 1996FG3 (red) around the Sun in those four different dates. Thus, the objective of this work is to find the respective amount of  $\Delta V$  ( $\Delta V_1 + \Delta V_2$ ) necessary to reach the target asteroid considering the different distances between the Earth and the asteroid in these dates.

Table 5.3 - Distances between the Earth and the asteroid 1996FG<sub>3</sub>.

date of interception	distance ( <i>au</i> )	distance ( <i>km</i> )
2022, May 3rd	0.078440837408898	11,734,582
2024, Feb 1st	0.423079604518748	63,291,807
2024, Apr 1st	0.749653805045622	112,146,612
2029, Aug 1st	2.414218261669318	361,161,911

SOURCE: Oliveira et al. (2017a)

Figure 5.1 - Asteroid and Earth orbits in a fixed inertial system fixed in the Sun.

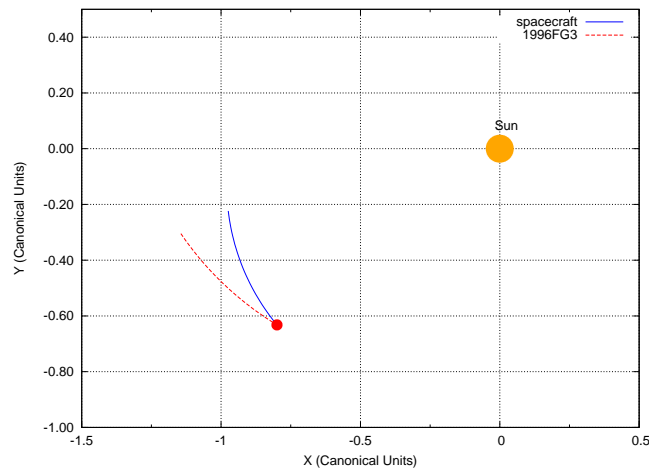


SOURCE: Oliveira et al. (2017a)

The proposed solution to intercept the asteroid is to launch the spacecraft in a range of 360 days, with a 30 days interval window between each possible launch. Thus, the transfer time since the launch of the spacecraft from Earth until its interception with the asteroid covers the range from 30, 60, 120, 150, 180, 210, 240, 270, 300, 330 and 360 days before the previous selected dates in Table 5.3.

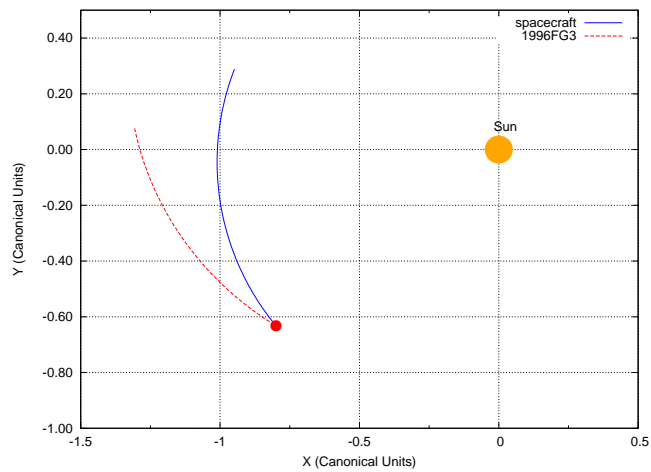
As a result, the trajectories of the asteroid and the spacecraft, since the day it is launched until the collision date of closest approach with the Earth on 2022, May 3rd are presented in Figures 5.2 to 5.13. The red dot indicates the final location of the spacecraft, *i.e.*, the interception with the asteroid in the selected date. The red line is the trajectory of the asteroid since the spacecraft was launched from Earth until it is reached by the spacecraft and the blue line indicates the trajectory of the spacecraft since it was launched from Earth until its collision with the asteroid. As it was mentioned before there are 12 possible transfers trajectories presented in those figures, covering the range of 30 days of the window transfer time.

Figure 5.2 - Trajectories of the asteroid and the spacecraft for a 30 days transfer.



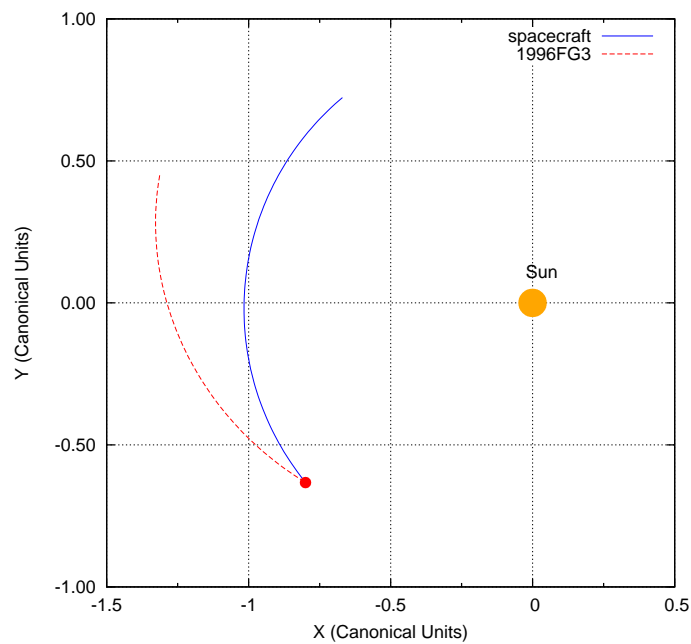
SOURCE: Oliveira et al. (2017a).

Figure 5.3 - Trajectories of the asteroid and the spacecraft for a 60 days transfer.



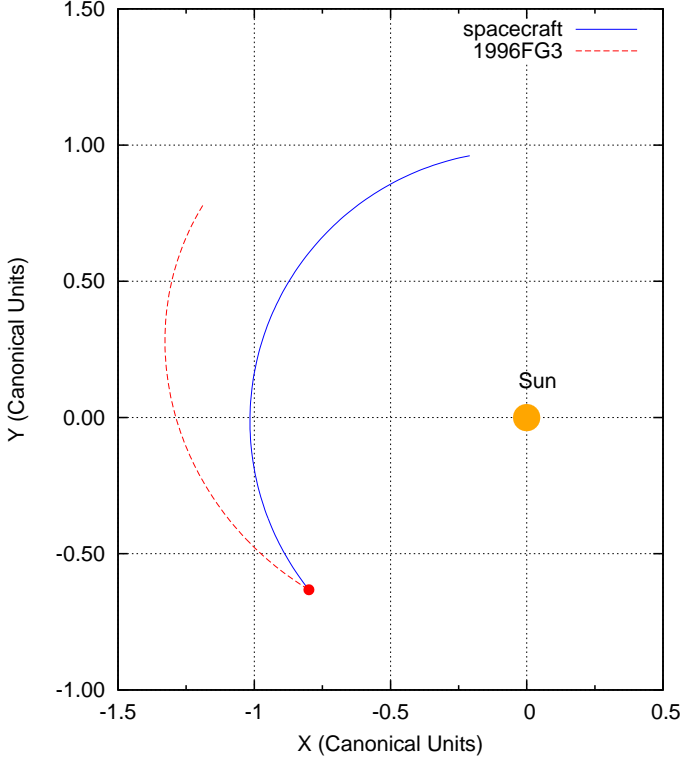
SOURCE: Oliveira et al. (2017a).

Figure 5.4 - Trajectories of the asteroid and the spacecraft for a 90 days transfer.



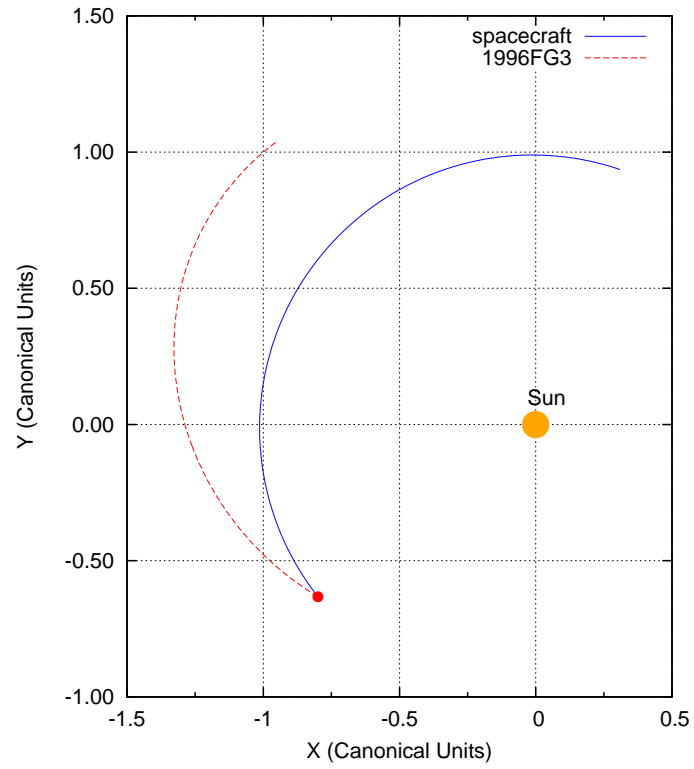
SOURCE: Oliveira et al. (2017a).

Figure 5.5 - Trajectories of the asteroid and the spacecraft for a 120 days transfer.



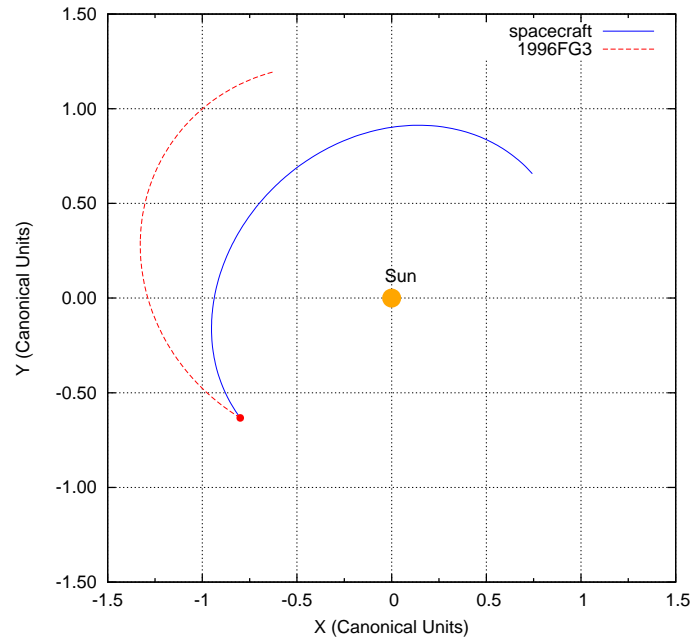
SOURCE: Oliveira et al. (2017a).

Figure 5.6 - Trajectories of the asteroid and the spacecraft for a 150 days transfer.



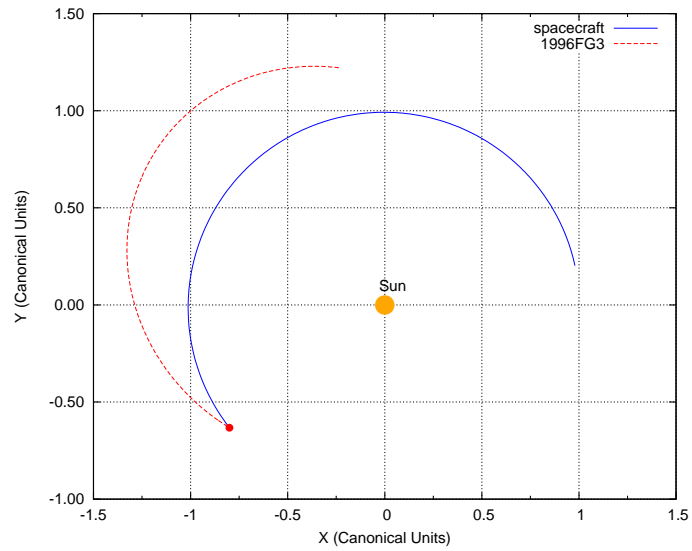
SOURCE: Oliveira et al. (2017a).

Figure 5.7 - Trajectories of the asteroid and the spacecraft for a 180 days transfer.



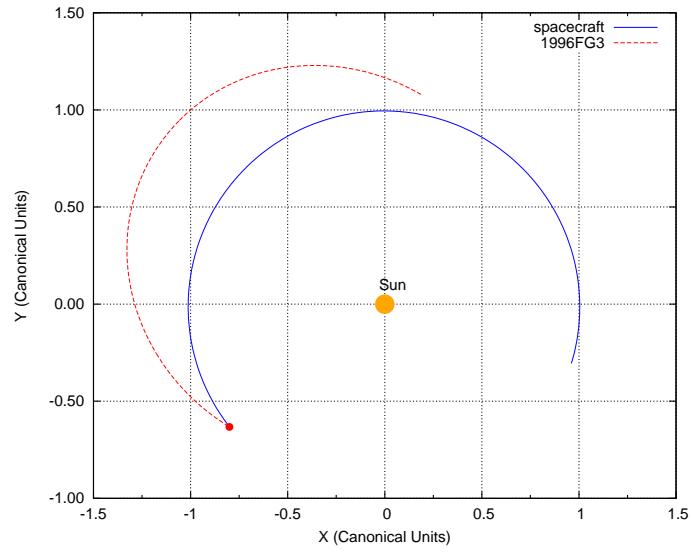
SOURCE: Oliveira et al. (2017a).

Figure 5.8 - Trajectories of the asteroid and the spacecraft for a 210 days transfer.



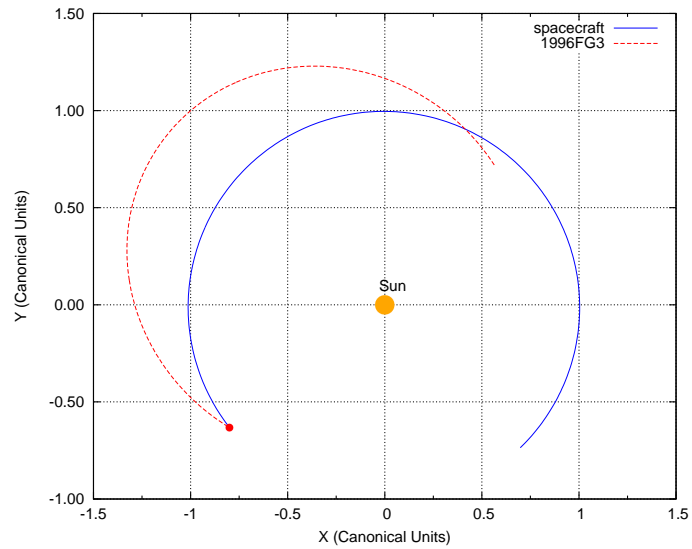
SOURCE: Oliveira et al. (2017a).

Figure 5.9 - Trajectories of the asteroid and the spacecraft for a 240 days transfer.



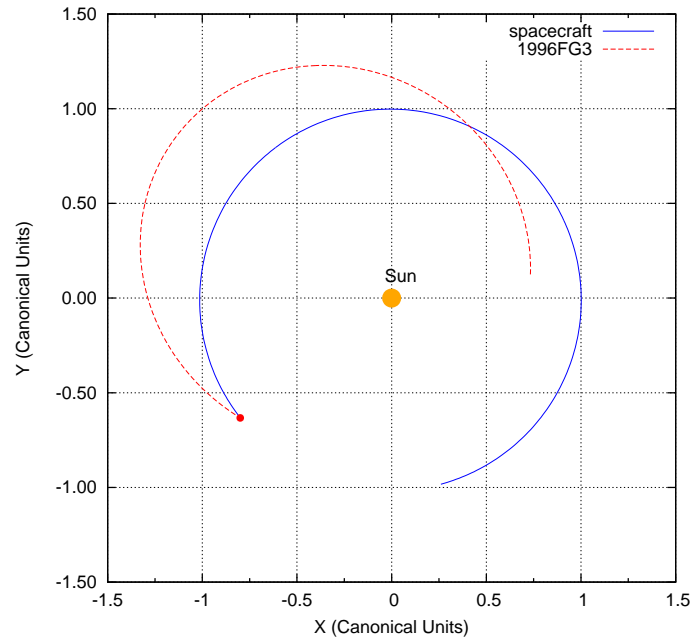
SOURCE: Oliveira et al. (2017a).

Figure 5.10 - Trajectories of the asteroid and the spacecraft for a 270 days transfer.



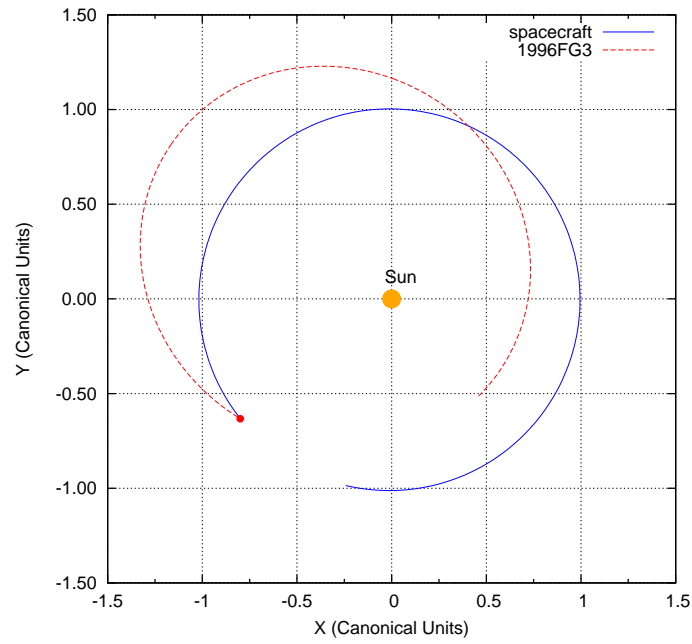
SOURCE: Oliveira et al. (2017a).

Figure 5.11 - Trajectories of the asteroid and the spacecraft for a 300 days transfer.



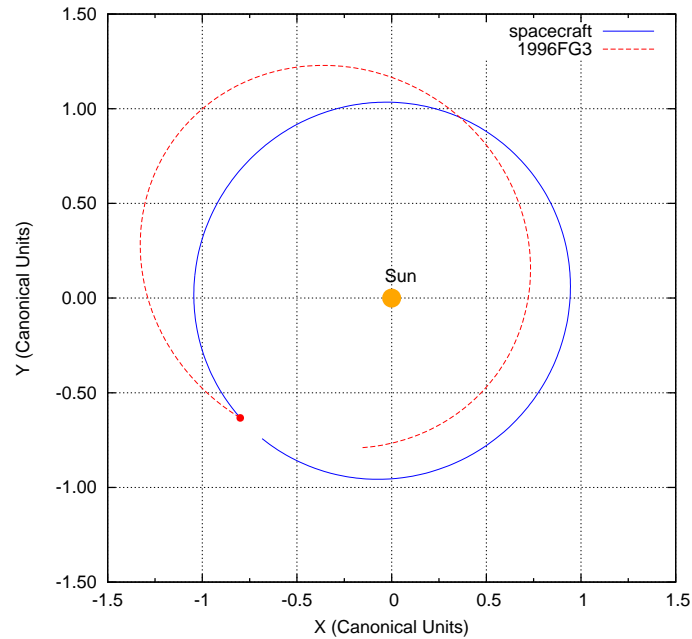
SOURCE: Oliveira et al. (2017a).

Figure 5.12 - Trajectories of the asteroid and the spacecraft for a 330 days transfer.



SOURCE: Oliveira et al. (2017a).

Figure 5.13 - Trajectories of the asteroid and the spacecraft for a 360 days transfer.



SOURCE: Oliveira et al. (2017a).

As a result for the possible transfer times for those four selected dates and distances between the Earth and the target asteroid the Tables 5.4 to 5.10 show these results in terms of the fuel consumption, specified by the  $\Delta V$ .

As was mentioned before a bi-impulsive maneuver, described in section 2.3, is taken at the beginning of transfer in the orbit of the Earth ( $\Delta V_1$ ) and the second impulse,  $\Delta V_2$ , which is the real impact velocity of the spacecraft with the asteroid and that will be used to change its momentum at the end of transfer. It means that the best trajectories are the ones with lower  $\Delta V_1$  and higher  $\Delta V_2$ . However, the final decision on which transfer to use depends on the impulse capacity to send the spacecraft from the Earth, the time required to hit the asteroid and the deflection that will be necessary.

Thus, as a first look, from all solutions found in the simulations, the transfer time of 270 days for the impact date on 2022, May 3rd in Table 5.7, is the best candidate for optimal trajectory, because it has the smaller  $\Delta V_1$  and a large  $\Delta V_2$ . The values are shown in Tables 5.4 to 5.10 and the best candidates are highlighted in green. However, the final choice of what could be the best transfer depends of many conditions as it was commented before.

The variation of the area/mass ratio is only considered for the impact date of 2022, May 3rd. Tables 5.4 to 5.7 shows these results. The values of area/mass used are: 0 m<sup>2</sup>/kg, 0.1 m<sup>2</sup>/kg, 0.5 m<sup>2</sup>/kg and 5 m<sup>2</sup>/kg. This wide range of values are considered to verify the effects of the solar radiation pressure on this type of mission. For all others impact dates the area/mass used is 0 m<sup>2</sup>/kg. The conclusion is that the solar radiation pressure has a minimum effect on these transfers. The values of  $\Delta V_1$  and  $\Delta V_2$  presented in Tables 5.4 to 5.7 show that the change in the  $\Delta V$  are very small and only for a greater value of area/mass (5 m<sup>2</sup>/kg) this change can be noticed.

It is also possible to observe that the values of  $\Delta V_1$  in Tables 5.8 to 5.10 are much higher than those of the Table 5.4. This was expected since the distances that the spacecraft covers are greater. However, it is more reliable to send a mission to impact the asteroid when the distances between the Earth and the target are higher, avoiding any kind of danger to the Earth.

Table 5.4 - Initial and final  $\Delta V$  with  $A/m = 0 \text{ m}^2/\text{kg}$  for transfers between the Earth and the asteroid 1996FG<sub>3</sub> in the approach of 03-05-2022

Transfer time (days)	$\Delta V_1$		$\Delta V_2$	
	canonical units	<i>km/s</i>	canonical units	<i>km/s</i>
30	0.15638	4.658	0.3482	10.372
60	0.08086	2.408	0.3320	9.889
90	0.05540	1.650	0.3392	10.104
120	0.04781	1.424	0.3477	10.355
150	0.06583	1.961	0.3563	10.613
180	0.55739	16.602	0.6346	18.900
210	0.07687	2.290	0.3670	10.930
240	0.04143	1.234	0.3616	10.771
270	0.03450	1.028	0.3600	10.722
300	0.03805	1.133	0.3574	10.644
330	0.05812	1.731	0.3514	10.466
360	0.22779	6.785	0.3531	10.516

SOURCE: Oliveira et al. (2017a)

Table 5.5 - Initial and final  $\Delta V$  with  $A/m = 0.1 \text{ m}^2/\text{kg}$  for transfers between the Earth and the asteroid 1996FG<sub>3</sub> in the approach of 03-05-2022

Transfer time (days)	$\Delta V_1$		$\Delta V_2$	
	canonical units	<i>km/s</i>	canonical units	<i>km/s</i>
30	0.15637	4.657	0.3483	10.373
60	0.08084	2.408	0.3321	9.890
90	0.05537	1.649	0.3393	10.105
120	0.04778	1.423	0.3477	10.357
150	0.65810	19.601	0.3564	10.615
180	0.55738	16.601	0.6346	18.901
210	0.07686	2.289	0.3670	10.930
240	0.04142	1.234	0.3617	10.772
270	0.03449	1.027	0.3600	10.722
300	0.03804	1.133	0.3574	10.644
330	0.05811	1.731	0.3514	10.466
360	0.22778	6.784	0.3531	10.516

SOURCE: Author

Table 5.6 - Initial and final  $\Delta V$  with  $A/m = 0.5 \text{ m}^2/\text{kg}$  for transfers between the Earth and the asteroid 1996FG<sub>3</sub> in the approach of 03-05-2022

Transfer time (days)	$\Delta V_1$		$\Delta V_2$	
	canonical units	<i>km/s</i>	canonical units	<i>km/s</i>
30	0,15632	4,656	0,3484	10,376
60	0,08074	2,405	0,3322	9,896
90	0,05524	1,645	0,3395	10,112
120	0.04767	1.420	0.3479	10.363
150	0.06575	1.958	0.3566	10.620
180	0.55731	16.599	0.6346	18.902
210	0.07683	2.288	0.3671	10.934
240	0.04139	1.233	0.3618	10.775
270	0.03447	1.027	0.3601	10.725
300	0.03802	1.132	0.3574	10.645
330	0.05810	1.730	0.3514	10.467
360	0.22775	6.783	0.3530	10.515

SOURCE: Author

Table 5.7 - Initial and final  $\Delta V$  with  $A/m = 5 \text{ m}^2/\text{kg}$  for transfers between the Earth and the asteroid 1996FG<sub>3</sub> in the approach of 03-05-2022

Transfer time (days)	$\Delta V_1$		$\Delta V_2$	
	canonical units	<i>km/s</i>	canonical units	<i>km/s</i>
30	0.15584	4.642	0.3496	10.412
60	0.07962	2.372	0.3343	9.957
90	0.05383	1.603	0.3419	10.182
120	0.04646	1.384	0.3502	10.432
150	0.06510	1.939	0.3586	10.681
180	0.55656	16.577	0.6351	18.915
210	0.07655	2.280	0.3685	10.976
240	0.04115	1.226	0.3629	10.808
270	0.03433	1.022	0.3609	10.749
300	0.03796	1.131	0.3579	10.660
330	0.05805	1.729	0.3516	10.471
360	0.22737	6.772	0.3528	10.507

SOURCE: Author

Table 5.8 - Initial and final  $\Delta V$  with  $A/m = 0 \text{ m}^2/\text{kg}$  for transfers between the Earth and the asteroid 1996FG<sub>3</sub> in the approach of 01-02-2024

Transfer time (days)	$\Delta V_1$		$\Delta V_2$	
	canonical units	<i>km/s</i>	canonical units	<i>km/s</i>
30	0.772	22.987	0.917	27.304
60	0.362	10.793	0.579	17.247
90	0.275	8.194	0.450	13.406
120	0.259	7.713	0.355	10.560
150	0.254	7.571	0.271	8.077
180	0.951	28.340	0.697	20.772
210	0.254	7.565	0.121	3.603
240	0.265	7.908	0.059	1.762
270	0.296	8.808	0.068	2.020
300	0.368	10.949	0.168	5.003
330	0.566	16.873	0.364	10.845
360	1.505	44.814	1.086	32.344

SOURCE: Oliveira et al. (2017a)

Table 5.9 - Initial and final  $\Delta V$  with  $A/m = 0 \text{ m}^2/\text{kg}$  for transfers between the Earth and the asteroid 1996FG<sub>3</sub> in the approach of 01-04-2024

Transfer time (days)	$\Delta V_1$		$\Delta V_2$	
	canonical units	<i>km/s</i>	canonical units	<i>km/s</i>
30	1.451	43.205	1.035	30.836
60	0.676	20.120	0.359	10.679
90	0.371	11.044	0.243	7.223
120	0.201	5.994	0.249	7.423
150	0.115	3.420	0.256	7.634
180	0.106	3.149	0.249	7.423
210	0.999	29.744	0.754	22.454
240	0.155	4.626	0.188	5.595
270	0.185	5.505	0.144	4.281
300	0.232	6.919	0.088	2.623
330	0.316	9.415	0.044	1.325
360	0.515	15.336	0.196	5.835

SOURCE: Oliveira et al. (2017a)

Table 5.10 - Initial and final  $\Delta V$  with  $A/m = 0 \text{ m}^2/\text{kg}$  for transfers between the Earth and the asteroid 1996FG<sub>3</sub> in the approach of 01-08-2029

Transfer time (days)	$\Delta V_1$		$\Delta V_2$	
	canonical units	<i>km/s</i>	canonical units	<i>km/s</i>
30	4.907	146.158	4.556	135.695
60	2.817	83.902	2.276	67.776
90	2.166	64.505	1.545	46.019
120	1.797	53.523	1.171	34.885
150	1.507	44.899	0.922	27.450
180	1.247	37.139	0.729	21.705
210	1.006	29.961	0.572	17.040
240	0.788	23.462	0.447	13.303
270	0.598	17.797	0.351	10.461
300	0.438	13.043	0.284	8.466
330	0.311	9.268	0.245	7.301
360	2.064	61.464	1.450	43.183

SOURCE: Oliveira et al. (2017a)

Considering the launching of a spacecraft from the Earth, at different dates, so that its trajectory is tangential to that of the Earth, the study in question shows the simulation of possibility of approaching with the asteroid 1996FG3 in a date predicted by JPL Small Body Database Browser which was considered to be 2022, May 3rd.

The general goal is to choose the best date choice where there is lower  $\Delta V$  at launch a maximum  $\Delta V$  at the time of interception. But, detailed decisions depends on the constraints of the mission related to the available increment of velocity and time of transfer.

## 6 CONCLUSIONS

The effects of the solar radiation pressure using bi-impulsive transfer between the Lagrangian points and the Lagrangian points and the primaries were studied in the Earth-Moon, Sun-Earth and in systems of asteroids. The results indicated that the solar radiation pressure modifies the trajectory of the spacecraft, modifying the energy required for the transfers. When the transfers involved large bodies such as the Sun, the Earth and Moon, the effects are small, in terms of the global effect of finding transfers with minimum energy. As shown in a previous work, [Oliveira et al. \(2016\)](#), the effects of the solar radiation pressure on transfers realized in the Sun-Earth system has a minimal effect. Even in those cases, the initial flight path angles are different for a given energy, so the initial data for the minimum are different.

However, when considering smaller bodies, like asteroid systems, the importance of the solar radiation pressure increases, and the locations and values of the best transfers are different which indicates that the force due to solar radiation pressure has a great effect in systems of small bodies, when compared to systems of larger bodies. The effects of the distance Sun-asteroid and the initial position of the Sun show the importance in considering the effects of the solar radiation pressure. The differences in the variation of velocity between the many situations are larger and there are several cases where the solar radiation pressure decreases or increases the variation of velocity required for the transfer. The results show that the solar radiation pressure has strong effects in the dynamics of these transfers. It was found that the solar radiation pressure changes the trajectories performed by the spacecraft, modifying the energy required for the transfers which is an indication that the spacecraft would not reach the aimed target. Therefore, the solar radiation pressure can be used also to reduce the magnitude of the increment of velocities required. Thus, it is possible to choose the right moment to perform the maneuver, such that the magnitudes of the impulses to be applied can be minimized, which is a type of indirect control.

In other problem, considering the orbit of a spacecraft in the Sun-Ida system, new points of equilibrium were found with the addition of a solar sail. Those points, called artificial equilibrium points (AEP), allows a spacecraft to park closer to the body, so improving the data coming from a mission. It was also possible to find points that are out of the plane of the primaries, so allowing the observations of the poles of the asteroid. This is very important, because it gives the whole picture of the surface of the celestial body. There are many different forms to make the transfer between several AEPs, using different configurations of the solar sail during the

trip, varying the  $\gamma$  angle. The results show that it is possible to make these transfers between the new equilibrium points to consume less fuel, which can improve the mission time and even make new maneuvers around the target body. On the other hand, the results also show that missions with longer duration are also an option. These possibilities offer a large range of locations for the spacecraft, which give more applications to a mission.

In the last problem, focused in finding trajectories to send a spacecraft to an asteroid with the objective of hitting it, to change its orbit around the Sun and consequently avoid its collision with the Earth, it was possible to observe that there were different increment of velocity at launch that result also in different collision velocities with the asteroid. It depends on the chosen launching dates and transfer time. It was also shown that the area/mass ratio does not have a great impact in this type of mission because only for high values of area/mass, small changes in the values of  $\Delta V$  can be noticed. A more advanced investigation of this study should lead to the definition of an asteroid "angle of attack" of the spacecraft, as well as the moment of that crash, with a good margin of safety, in order to modify its translational momentum to avoid a collision course with the Earth.

## REFERENCES

- ALIASI, G.; MENGALI, G.; QUARTA, A. A. Artificial equilibrium points for a generalized sail in the circular restricted three-body problem. **Celestial Mechanics and Dynamical Astronomy**, v. 110, n. 4, p. 343–368, 2011. 80
- \_\_\_\_\_. Artificial equilibrium points for a generalized sail in the elliptic restricted three-body problem. **Celestial Mechanics and Dynamical Astronomy**, v. 114, n. 1-2, p. 181–200, 2012. 80
- ALMEIDA, A. K. de; PRADO, A. F. B. A.; YOKOYAMA T. AND SANCHEZ, D. M. Spacecraft motion around artificial equilibrium points. **Nonlinear Dynamics**, v. 91, n. 3, p. 1473–1489, 2018. 80, 82
- ARAUJO, R.; WINTER, O. C.; PRADO, A. F. B. A. Stable retrograde orbits around the triple system 2001 sn263. **Monthly Notices of the Royal Astronomical Society**, v. 449, n. 4, p. 4404–4414, 2015. 20, 42, 45
- ARAUJO, R.; WINTER, O. C.; PRADO, A. F. B. A.; SUKHANOV, A. Stability regions around the components of the triple system 2001 sn263. **Monthly Notices of the Royal Astronomical Society**, v. 423, n. 4, p. 3058–3073, 2012. 20, 42, 43, 44, 45
- BELTON, M.; CHAPMAN, C.; THOMAS, P.; DAVIES, M.; GREENBERG, R.; KLAASEN, K.; BYRNES, D.; D’AMARIO, L.; SYNNOTT, S.; JOHNSON, T. Bulk density of asteroid 243 ida from the orbit of its satellite dactyl. **Nature**, v. 374, n. 6525, p. 785–788, 1995. 79
- BELTON, M. J.; CHAPMAN, C. R.; KLAASEN, K. P.; HARCH, A. P.; THOMAS, P. C.; VEVERKA, J.; MCEWEN, A. S.; PAPPALARDO, R. T. Galileo’s encounter with 243 ida: An overview of the imaging experiment. **Icarus**, v. 120, n. 1, p. 1–19, 1996. 79
- BOND, V. R.; SPONAUGLE, S. J.; FRAIETTA, M. F.; EVERETT, S. F. Cislunar libration point as a transportation node for lunar exploration. **AAS Paper**, p. 91–103, 1991. 19
- BROUCKE, R. Traveling between the lagrange points and the moon. **Journal of Guidance, Control and Dynamics**, v. 2, n. 4, p. 257–263, 1979. 1, 18, 20, 85

CABETTE, R. E. S.; PRADO, A. F. B. A. Transfer orbits to/from the lagrangian points in the restricted four-body problem. **Acta Astronautica**, v. 63, n. 11, p. 1221–1232, 2008. 1, 20, 85

CARUSI, A.; VALSECCHI, G. B.; D'ABRAMO, G.; BOATTINI, A. Deflecting neos in route of collision with the earth. **Icarus**, v. 159, n. 2, p. 417–422, 2002. 1, 107

CASALINO, L.; SIMEONI, F. Indirect optimization of asteroid deflection missions with electric propulsion. **Journal of Guidance, Control, and Dynamics**, v. 35, n. 2, p. 423–433, 2012. 107

CHAMBERLIN, A.; YEOMANS, D. Jpl small-body database browser. **Jet Propulsion Laboratory: Solar System Dynamics**, 2017. Disponível em: <<http://ssd.jpl.nasa.gov/sbdb.cgi>>. 82, 83

CURTIS, H. D. **Orbital mechanics for engineering students**. Boston: Butterworth-Heinemann, 2013. 14

DANDOURAS, I.; PIRARD, B.; PRADO, J. High performance solar sails for linear trajectories and heliostationary missions. **Advances in Space Research**, v. 34, n. 1, p. 198–203, 2004. 80

ENGLANDER, J. A.; CONWAY, B. A.; WALL, B. J. Optimal strategies found using genetic algorithms for deflecting hazardous near-earth objects. In: IEEE CONGRESS ON EVOLUTIONARY COMPUTATION. **Proceedings...** Trondheim, Norway: IEEE, 2009. p. 2309–2315. 107

FARQUHAR, R. W. Future missions for libration-point satellites. **Astronautics Aeronautics**, v. 7, 1969. 19

FARRÉS, A.; JORBA, À. A dynamical system approach for the station keeping of a solar sail. **The Journal of the Astronautical Sciences**, v. 56, n. 2, p. 199–230, 2008. 80

FORWARD, R. L. Statite-a spacecraft that does not orbit. **Journal of Spacecraft and Rockets**, v. 28, n. 5, p. 606–611, 1991. 80

GAL-EDD, J.; CHEUVRONT, A. The osiris-rex asteroid sample return mission operations design. In: IEEE AEROSPACE CONFERENCE, 2015. **Proceedings...** Big Sky, Montana: IEEE, 2015. p. 1–9. 1, 8

- GLASSMEIER, K.-H.; BOEHNHARDT, H.; KOSCHNY, D.; KÜHRT, E.; RICHTER, I. The rosetta mission: flying towards the origin of the solar system. **Space Science Reviews**, v. 128, n. 1-4, p. 1–21, 2007. 1, 9
- IZZO, D. On the deflection of potentially hazardous objects. In: AAS/AIAA SPACE FLIGHT MECHANICS CONFERENCE, 15., 2015. **Proceedings...** Copper Mountain, Colorado: AAS/AIAA, 2005. p. 05–141. 1, 107
- JÚNIOR, A. K. A.; PRADO, A. F. B. A.; SANCHEZ, D. M.; YOKOYAMA, T. Searching for artificial equilibrium points to place satellites "above and below" l3 in the sun-earth system. **Revista Mexicana de Astronomia y Astrofisica**, v. 53, p. 349–359, 2017. 80, 82
- KAWAGUCHI, J. A solar power sail mission for a jovian orbiter and trojan asteroid flybys. In: INTERNATIONAL ASTRONAUTICAL CONGRESS. **Proceedings...** Vancouver, Canada: AIAA, 2004. 1, 9
- KAWAGUCHI, J.; KUNINAKA, H.; FUJIWARA, A.; UESUGI, T. Muses-c, its launch and early orbit operations. **Acta Astronautica**, v. 59, n. 8, p. 669–678, 2006. 1, 3, 4
- KOPP, G.; LEAN, J. L. A new, lower value of total solar irradiance: evidence and climate significance. **Geophysical Research Letters**, v. 38, n. 1, 2011. 12
- LO, M.; WILLIAMS, B.; BOLLMAN, W.; HAN, D.; HAHN, Y.; BELL, J.; HIRST, E.; CORWIN, R.; HONG, P.; HOWELL, K. Genesis mission design. In: AIAA/AAS ASTRODYNAMICS SPECIALIST CONFERENCE AND EXHIBIT. **Proceedings...** Boston, Massachusetts: AIAA, 1998. p. 4468. 2, 53
- LUZUM, B.; CAPITAINE, N.; FIENGA, A.; FOLKNER, W.; FUKUSHIMA, T.; HILTON, J.; HOHENKERK, C.; KRASINSKY, G.; PETIT, G.; PITJEVA, E. The iau 2009 system of astronomical constants: the report of the iau working group on numerical standards for fundamental astronomy. **Celestial Mechanics and Dynamical Astronomy**, v. 110, n. 4, p. 293–304, 2011. 12, 22, 33, 45, 54, 83, 109
- MAZANEK, D. D.; BROHPY, J. R.; MERRILL, R. G. Asteroid retrieval mission concept-trailblazing our future in space and helping to protect us from earth impactors. In: IAA PLANETARY DEFENSE CONFERENCE, 3., 2013. **Proceedings...** Flagstaff, Arizona, USA: IAA, 2013. 1, 8
- MCINNES, C. R. **Solar sailing: technology, dynamics and mission applications**. Berlin: Springer-Verlag, 2004. 82

\_\_\_\_\_. Space-based geoengineering: challenges and requirements. **Proceedings of the Institution of Mechanical Engineers, Part C: Journal of Mechanical Engineering Science**, v. 224, n. 3, p. 571–580, 2010. 80

MICHEL, P.; BARUCCI, M. A.; CHENG, A.; BÖHNHARDT, H.; BRUCATO, J. R.; DOTTO, E.; EHRENFREUND, P.; FRANCHI, I.; GREEN, S.; LARA, L.-M. Marcopolo-r: Near-earth asteroid sample return mission selected for the assessment study phase of the esa program cosmic vision. **Acta Astronautica**, v. 93, p. 530–538, 2014. 1, 53

MORI, O.; SAWADA, H.; HANAOKA, F.; KAWAGUCHI, J.; SHIRASAWA, Y.; SUGITA, M.; MIYAZAKI, Y.; SAKAMOTO, H.; FUNASE, R. Development of deployment system for small size solar sail mission. **Transactions of the Japan Society for Aeronautical and Space Sciences, Space Technology Japan**, v. 7, n. ists26, p. Pd\_87–Pd\_94, 2009. 9

MORIMOTO, M. Y.; YAMAKAWA, H.; UESUGI, K. Artificial equilibrium points in the low-thrust restricted three-body problem. **Journal of Guidance, Control, and Dynamics**, v. 30, n. 5, p. 1563–1568, 2007. 80

OLIVEIRA, G. M. C.; GOMES, V. M.; PRADO, A. F. B. A.; SANCHEZ, D. M. Transfers between the lagrangian points and the primaries considering radiation pressure. **Advances in the Astronautical Sciences**, v. 158, p. 1513–1530, 2016. 18, 34, 35, 36, 37, 38, 39, 40, 41, 42, 44, 46, 47, 48, 49, 50, 51, 52, 85

OLIVEIRA, G. M. C.; JUNIOR, A. K. A.; PRADO, A. F. B. A. Determining locations and transfers of artificial equilibrium points in a double asteroid system. **Advances in the Astronautical Sciences**, v. 162, p. 3885–3900, 2018. 18, 79, 81, 84, 90, 93, 97, 100, 103, 106

OLIVEIRA, G. M. C.; PRADO, A. F. B. A.; SANCHEZ, D. M.; GOMES, V. M. Traveling between the earth-moon lagrangian points and the earth. In: INTERNATIONAL CONFERENCE ON SPACE OPERATIONS, 14., 2016. **Proceedings...** Daejeon, Korea, 2016. p. 2558. 1, 18, 19, 24, 25, 26, 27, 28, 29, 30, 31, 32, 85, 125

OLIVEIRA, G. M. C.; PRADO, A. F. B. A.; SANCHEZ, D. M.; NASCIMENTO, J. M.; GOMES, V. M. Mapping trajectories for a spacecraft to hit an asteroid to avoid a collision with the earth. **Advances in the Astronautical Sciences**, v. 161, p. 249–265, 2017. 18, 111, 112, 113, 114, 115, 116, 117, 118, 119, 120, 122, 123

- OLIVEIRA, G. M. C.; PRADO, A. F. B. A.; SANCHEZ, D. M.; GOMES, V. M. Orbital transfers in an asteroid system considering the solar radiation pressure. **Astrophysics and Space Science**, v. 362, n. 10, p. 187, 2017. [15](#), [18](#), [21](#), [57](#), [58](#), [59](#), [60](#), [61](#), [62](#), [63](#), [64](#), [65](#), [66](#), [67](#), [68](#), [69](#), [70](#), [72](#), [73](#), [74](#), [75](#), [76](#), [77](#), [85](#)
- O'SHAUGHNESSY, D. J.; MCADAMS, J. V.; BEDINI, P. D.; CALLOWAY, A. B.; WILLIAMS, K. E.; PAGE, B. R. Messenger's use of solar sailing for cost and risk reduction. **Acta Astronautica**, v. 93, p. 483–489, 2014. [3](#), [80](#)
- O'SHAUGHNESSY, D. J.; MCADAMS, J. V.; WILLIAMS, K. E.; PAGE, B. R. Fire sail: Messenger's use of solar radiation pressure for accurate mercury flybys. **Advances in the Astronautical Sciences**, v. 133, n. Part I, 2009. [80](#)
- PRADO, A. F. B. A. Traveling between the lagrangian points and the earth. **Acta Astronautica**, v. 39, n. 7, p. 483–486, 1996. [1](#), [18](#), [20](#), [85](#)
- \_\_\_\_\_. Orbital maneuvers between the lagrangian points and the primaries in the earth-sun system. **Journal of the Brazilian Society of Mechanical Sciences and Engineering**, v. 28, n. 2, p. 131–139, 2006. [18](#), [20](#), [85](#), [109](#)
- PRADO, A. F. B. A.; BROUCKE, R. Transfer orbits in restricted problem. **Journal of Guidance, Control, and Dynamics**, v. 18, n. 3, p. 593–598, 1995. [18](#)
- \_\_\_\_\_. Transfer orbits in the earth-moon system using a regularized model. **Journal of Guidance, Control, and Dynamics**, v. 19, n. 4, p. 929–933, 1996. [18](#)
- PRESS, W. H.; FLANNERY, B. P.; TEUKOLSKY, S. A.; VETTERLING, W. T. **Numerical recipes: the art of scientific computing**. 3. ed. New York, NY, USA: Cambridge University Press, 2007. [16](#), [17](#)
- PROCKTER, L.; MURCHIE, S.; CHENG, A.; KRIMIGIS, S.; FARQUHAR, R.; SANTO, A.; TROMBKA, J. The near shoemaker mission to asteroid 433 eros. **Acta Astronautica**, v. 51, n. 1, p. 491–500, 2002. [1](#)
- RAYMAN, M. D.; FRASCHETTI, T. C.; RAYMOND, C. A.; RUSSELL, C. T. Dawn: a mission in development for exploration of main belt asteroids vesta and ceres. **Acta Astronautica**, v. 58, n. 11, p. 605–616, 2006. [1](#)
- ROSS, I. M.; PARK, S.-Y.; PORTER, S. D. V. Gravitational effects of earth in optimizing? v for deflecting earth-crossing asteroids. **Journal of Spacecraft and Rockets**, v. 38, n. 5, p. 759–764, 2001. [107](#)

- SALAZAR, F. J. T.; MCINNES, C. R.; WINTER, O. C. Intervening in earth's climate system through space-based solar reflectors. **Advances in Space Research**, v. 58, n. 1, p. 17 – 29, 2016. ISSN 0273-1177. 80
- SANTOS, L. B. T. dos. **Pontos lagrangianos: aplicação para o asteroide 2001SN263**, Dissertation (Mestrado em Engenharia e Tecnologia Espaciais/Mecânica Espacial e Controle) - Instituto Nacional de Pesquisas Espaciais, São José dos Campos, Brazil, 2013. 18, 85
- SANTOS, W. G.; PRADO, A. F. B. A.; OLIVEIRA, G. M. C.; SANTOS, L. B. T. Analysis of impulsive maneuvers to keep orbits around the asteroid 2001sn263. **Astrophysics and Space Science**, v. 363, n. 1, p. 14, Dec 2017. ISSN 1572-946X. 18, 85
- SCHEIRICH, P.; PRAVEC, P.; JACOBSON, S.; ĎURECH, J.; KUŠNIRÁK, P.; HORNOCH, K.; MOTTOLA, S.; MOMMERT, M.; HELLMICH, S.; PRAY, D. The binary near-earth asteroid (175706) 1996fg3 - an observational constraint on its orbital evolution. **Icarus**, v. 245, p. 56–63, 2015. 20, 53, 54, 55, 107, 109
- SIMONELLI, D. P.; VEVERKA, J.; THOMAS, P. C.; HELFENSTEIN, P.; CARCICH, B. T.; BELTON, M. J. Ida lightcurves: consistency with galileo shape and photometric models. **Icarus**, v. 120, n. 1, p. 38–47, 1996. 79
- STRANGE, N.; LANDAU, D.; MCELRATH, T.; LANTOINE, G.; LAM, T. **Overview of mission design for NASA asteroid redirect robotic mission concept**, Pasadena, CA: Jet Propulsion Laboratory, National Aeronautics and Space Administration, 2013. 1, 8
- SUKHANOV, A.; VELHO, H. d. C.; MACAU, E.; WINTER, O. The aster project: flight to a near-earth asteroid. **Cosmic Research**, v. 48, n. 5, p. 443–450, 2010. 1, 42
- SYMON, K. R. **Mechanics**. 3. ed. [S.l.]: Addison-Wesley Publishing Company, 1971. 82
- SZEBEHELY, V. **Theory of orbits**. New York: Academic Press, 1967. 13, 14, 19, 80, 85, 107
- TSUDA, Y.; MORI, O.; FUNASE, R.; SAWADA, H.; YAMAMOTO, T.; SAIKI, T.; ENDO, T.; YONEKURA, K.; HOSHINO, H.; KAWAGUCHI, J. Achievement of ikaros - japanese deep space solar sail demonstration mission. **Acta Astronautica**, v. 82, n. 2, p. 183–188, 2013. 1, 4, 5, 6, 7

- TSUDA, Y.; YOSHIKAWA, M.; ABE, M.; MINAMINO, H.; NAKAZAWA, S. System design of the hayabusa 2 - asteroid sample return mission to 1999 ju3. **Acta Astronautica**, v. 91, p. 356–362, 2013. [7](#), [8](#), [80](#)
- VALLADO, D. A. **Fundamentals of astrodynamics and applications**. El Segundo, California and Dordrecht, The Netherlands: [s.n.], 2001. [12](#)
- VASILE, M.; COLOMBO, C. Optimal impact strategies for asteroid deflection. **Journal of Guidance, Control, and Dynamics**, v. 31, n. 4, p. 858–872, 2008. [107](#)
- WOLTERS, S. D.; ROZITIS, B.; DUDDY, S. R.; LOWRY, S. C.; GREEN, S. F.; SNODGRASS, C.; HAINAUT, O. R.; WEISSMAN, P. Physical characterization of low delta-v asteroid (175706) 1996fg3. **Monthly Notices of the Royal Astronomical Society**, v. 418, n. 2, p. 1246–1257, 2011. [20](#), [53](#), [54](#), [55](#)
- YANG, H.; GONG, S.; BAOYIN, H. Two-impulse transfer orbits connecting equilibrium points of irregular-shaped asteroids. **Astrophysics and Space Science**, v. 357, n. 1, p. 66, 2015. [1](#), [18](#)
- YOSHIKAWA, M.; FUJIWARA, A.; KAWAGUCHI, J. Hayabusa and its adventure around the tiny asteroid itokawa. **Proceedings of the International Astronomical Union**, v. 2, n. 14, p. 323–324, 2006. [3](#)
- YU, L.; JI, J.; WANG, S. Shape, thermal and surface properties determination of a candidate spacecraft target asteroid (175706) 1996fg3. **Monthly Notices of the Royal Astronomical Society**, v. 439, n. 4, p. 3357–3370, 2014. [107](#), [109](#)
- ZUIANI, F.; VASILE, M.; GIBBINGS, A. Evidence-based robust design of deflection actions for near earth objects. **Celestial Mechanics and Dynamical Astronomy**, v. 114, n. 1-2, p. 107–136, 2012. [107](#)



## PUBLICAÇÕES TÉCNICO-CIENTÍFICAS EDITADAS PELO INPE

### **Teses e Dissertações (TDI)**

Teses e Dissertações apresentadas nos Cursos de Pós-Graduação do INPE.

### **Manuais Técnicos (MAN)**

São publicações de caráter técnico que incluem normas, procedimentos, instruções e orientações.

### **Notas Técnico-Científicas (NTC)**

Incluem resultados preliminares de pesquisa, descrição de equipamentos, descrição e ou documentação de programas de computador, descrição de sistemas e experimentos, apresentação de testes, dados, atlas, e documentação de projetos de engenharia.

### **Relatórios de Pesquisa (RPQ)**

Reportam resultados ou progressos de pesquisas tanto de natureza técnica quanto científica, cujo nível seja compatível com o de uma publicação em periódico nacional ou internacional.

### **Propostas e Relatórios de Projetos (PRP)**

São propostas de projetos técnico-científicos e relatórios de acompanhamento de projetos, atividades e convênios.

### **Publicações Didáticas (PUD)**

Incluem apostilas, notas de aula e manuais didáticos.

### **Publicações Seriadas**

São os seriados técnico-científicos: boletins, periódicos, anuários e anais de eventos (simpósios e congressos). Constam destas publicações o Internacional Standard Serial Number (ISSN), que é um código único e definitivo para identificação de títulos de seriados.

### **Programas de Computador (PDC)**

São a seqüência de instruções ou códigos, expressos em uma linguagem de programação compilada ou interpretada, a ser executada por um computador para alcançar um determinado objetivo. Aceitam-se tanto programas fonte quanto os executáveis.

### **Pré-publicações (PRE)**

Todos os artigos publicados em periódicos, anais e como capítulos de livros.